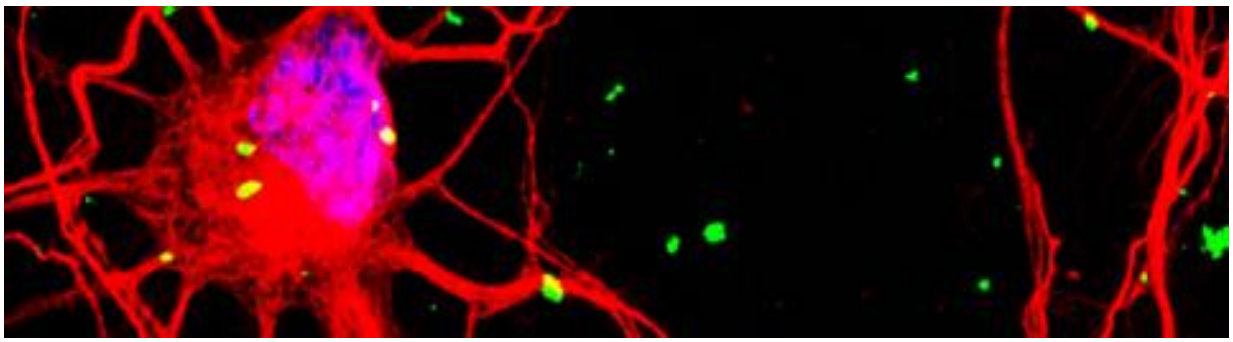

Corso di Dottorato in Neuroscienze
Curriculum Neuroscienze e Neurotecnologie
Ciclo XXXI

Titolo: “Sensory information processing in mouse barrel cortex”

Autore: Stefano Varani
Supervisor: Tommaso Fellin

ISTITUTO ITALIANO DI TECNOLOGIA

UNIVERSITÀ DEGLI STUDI DI GENOVA

Table of Contents

1 Introduction

1.1 Somatosensation

We depend on our senses to perceive and to consciously interact with the environment. As humans, we have at our disposal a wide array of sensory systems to build our representation of the world: visual, olfactory, somatosensory, gustatory, vestibular and auditory. In particular, somatosensation grants us the ability to detect, discriminate, and recognize objects through touch. Moreover, it also allows us to feel our body movement and position in space (proprioception), to perceive temperature (thermoception) and to inform us of possible harmful stimuli (nociception) (Carey, Lamp, & Turville, 2016; Lumpkin & Bautista, 2005; Reed-Geaghan & Maricich, 2011; Taylor et al., 2016).

To design a study investigating sensory perception, it is important to define and distinguish two key processes: the *encoding* of information related to the stimulus into brain circuits, and the *decoding* of the stimulus information to instruct a behavioural choice (e.g., a motor command). In the act of encoding, the physical properties of the stimulus are transduced into electrical impulses in the nerve cells of both the peripheral and the central nervous system in the form of precise patterns of neuronal activity (Delmas, Hao, & Rodat-Despoix, 2011; Hao, Bonnet, Amsalem, Ruel, & Delmas, 2014). These are then integrated and interpreted (decoding process) to perform a behavioural choice (Abraira & Ginty, 2013; Panzeri, Harvey, Piasini, Latham, & Fellin, 2017). How the brain generates sensations based on these processes remains to be fully understood.

Touch sensation is possible thanks to specialized sensory receptors that are present at one end of primary sensory neurons that densely innervate the skin (Oaklander & Siegel, 2005). A mechanical stimulus elicits the opening of sodium channels present in those structures to determine a depolarization in the neuronal membrane, which may lead to action potential (AP) firing activity (Oaklander & Siegel, 2005). Primary sensory neurons usually have bifurcated axons. One branch extends to the periphery and innervates the skin, and the other branch extends towards the central nervous system to reach the spinal cord (Figure 1) (Delmas et al., 2011; Lumpkin, Marshall, & Nelson, 2010). Thus, primary sensory neurons transduce a mechanical stimulus into electrical impulses and convey the signal towards the central nervous system. Sensory neurons encode stimuli by generating distinct patterns of APs. The AP discharge increases in conjunction with the

stimulus intensity until a plateau of maximal activity is reached (Oaklander & Siegel, 2005). If the stimulus is not able to excite the receptor above a certain level and sufficiently depolarize the membrane above the threshold for AP firing, the cell remains silent. The spatial area that is able to elicit APs is distinctive for each sensory neuron and define the receptive field of the cell(Goodwin & Wheat, 2008). Moreover, primary sensory neuron afferents can be categorized as rapidly or slowly adapting (Zucker & Welker, 1969). In the presence of a constant stimulus, the first class responds only to the stimulus on- and off-set, and the latter instead slowly decreases its firing activity over the course of the stimulus (Figure 1) (Delmas et al., 2011; Lumpkin et al., 2010). All these features add up to build a distinctive profile of AP firing for each neuron that allows single cells to encode the different properties of the position, frequency and amplitude of the stimulus (Zucker & Welker, 1969). Sensory receptors are the first element of a more complex system that generates the sense of touch. Before reaching the neocortex, the information extracted from the sensor is relayed to other stations of the somatosensory pathway, namely, the brainstem and the thalamus (Diamond, von Heimendahl, Knutsen, Kleinfeld, & Ahissar, 2008). Both of these regions actively participate in shaping the sensory signal that finally arrives in the neocortex (Delmas et al., 2011).

Evolutionarily, the neocortex is the most recent mammalian brain structure to emerge. The different areas that constitute the neocortex are involved in many brain functions, such as sensory perception, motor command, and cognition, among others. Somatosensory information reaches the neocortex in a precise area called the primary somatosensory cortex (S1) (Diamond & Arabzadeh, 2013). This area is anatomically and functionally divided into six horizontal layers, from I to VI, with each layer having a distinctive role (Douglas & Martin, 2004). S1 together with the primary sensory neurons, brainstem and thalamus is thus responsible for translation of the physical characteristics of the sensory stimulus in specific brain activity patterns (encoding process). From S1, information then spreads both at cortical and subcortical levels to secondary sensory cortices, motor cortices, other associative areas and higher order nuclei. In these areas, electrical signals are integrated and elaborated to guide an appropriate behavioural response (decoding process) (Panzeri et al., 2017). Because of these processes, it is possible for humans and other mammals to precisely distinguish and recognize, among others, gentle touches, vibrations, textures, and objects.

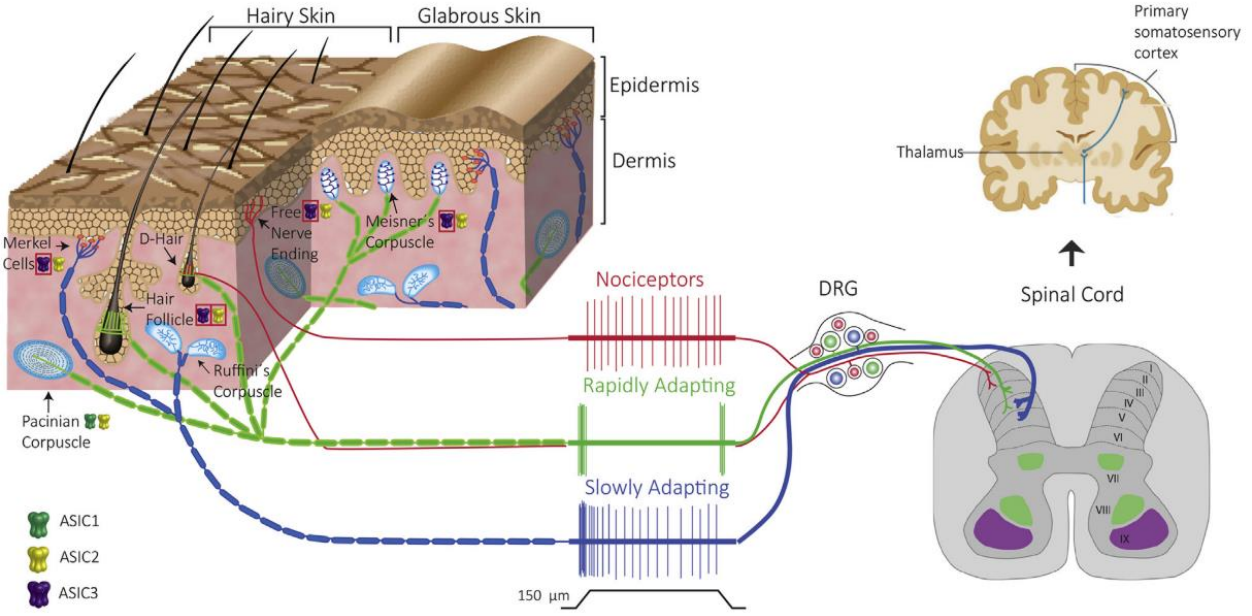

Figure 1. **Somatosensation: from sensory afferents end organs to the cerebral cortex**. Schematics of the somatosensation signalling pathway, representing the variability of end organs and spike activity of dorsal root ganglia primary neurons. Adapted from (Omerbašić, Schuhmacher, Bernal Sierra, Smith, & Lewin, 2015).

1.2 The rodent whisker system

Rodents have been widely used as a model for several practical and technical reasons. They are small and docile and are therefore easy to handle and house. Their life cycle is very short compared with humans (approximately 2-3 years), reaching adulthood in approximately 10 weeks, and they reproduce rapidly. Thus, is possible to test several generations in a relatively short amount of time. Moreover, they are mammals and thus present some characteristics that are similar to humans both at physiological and genetic levels, giving them an edge versus other simpler model organisms, such as insects, fish or worms. The genome of mice can be manipulated and analysed easily; the whole genome has been sequenced and published (Waterston et al., 2002), leading to the availability of a wide selection of mouse lines. Moreover, individuals of a mouse line are almost genetically identical, removing genetic variability in the interpretation of results. Although there are differences between the human and rodent brain, e.g., the latter lacks gyrification, the invasiveness of the majority of techniques used in brain physiology makes rodents the perfect surrogate for this area of study.

The whisker somatosensory system of rodents has been extensively used as a model for studying sensory processing due to its behavioural relevance and precisely organized modular structure (Diamond et al., 2008; Feldmeyer et al., 2013). Indeed, dark, narrow burrows are the natural habitat of wild mice and rats; in this context, vision is limited, whereas touch perception, coming from vibrissae, represents the major sense through which rodents collect information from the nearby environment (Diamond et al., 2008). Vibrissae are tactile hairs that are conserved among most mammals, excluding humans. They are longer and ticker than common hairs and are generated from well-innervated follicles. Facial (mystacial) vibrissae, also called whiskers, extending from the snout of the animal, grant tactile sensation that extends to the proximity of the head. To gather knowledge about the environment, rodents move their vibrissae rhythmically back and forth at a frequency centred approximately 5-20 Hz in a process called “whisking” (Figure 2) (Knutsen & Ahissar, 2009; Nikbakht, Tafreshiha, Zoccolan, & Diamond, 2018). The rodent whisker system can discriminate several physical properties of the whisker deflection, such as amplitude, direction, frequency, speed and acceleration (Randy M. Bruno, Khatri, Land, & Simons, 2003; C. C. H. Petersen, 2007; Shipley, 1974; Stuttgen, Ruter, & Schwarz, 2006; Temereanca & Simons, 2003; Zucker & Welker, 1969), with high spatial and temporal resolution, allowing the animals to detect and localize objects and discriminate between different objects or textures and, therefore, navigate the surrounding environment using their whiskers (Randy M. Bruno et al., 2003; C. C. H. Petersen, 2007; Shipley, 1974; Stuttgen et al., 2006; Temereanca & Simons, 2003; Zucker & Welker, 1969).

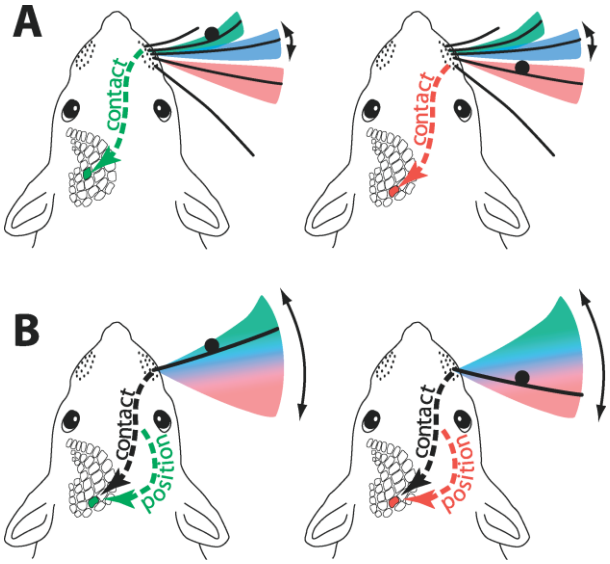

Figure 2. **Whisker system sensory information.** Cartoons representing a rodent using its vibrissae to localize an object. The position of an object can be encoded by both the identity of the whisker contacting it (**A**) and the timing of the contact event during the whisking activity (**B**). Adapted from (Mehta, Whitmer, Figueroa, Williams, & Kleinfeld, 2007).

Mice and rats have a set of roughly ~30-35 whiskers on each side of the snout and share the same follicle arrangement (Diamond & Arabzadeh, 2013; Nikbakht et al., 2018). Facial vibrissae are usually arranged in five horizontal rows, designated A to E, and different numbered arcs. In this array, each individual whisker can be identified univocally by a letter and a number (Diamond & Arabzadeh, 2013; Diamond et al., 2008). The first arc, the most posterior, is an exception to this rule and is labelled with Greek letters from alpha to delta. Then, from caudal to rostral, each arc is identified by a number and each row by a letter, specifically the most dorsal is labelled "A" and the most ventral is labelled "E". This disposition is present on both side of an animal's snout in a specular manner and is identical in all animals (Figure 3) (Diamond et al., 2008; Knutsen & Ahissar, 2009). Whiskers are generated in large follicles that are densely innervated with various types of sensory neuron afferents. When the vibrissa contacts an object, the resulting mechanical force on the follicle is detected by the mechanoreceptors that populated the follicle itself (Diamond & Arabzadeh, 2013). Moreover, thanks to the contraction of muscles present in the whisker pad, rodents can vary the position of the vibrissae (with respect to the snout) to control the receptive field of whisker sensation.

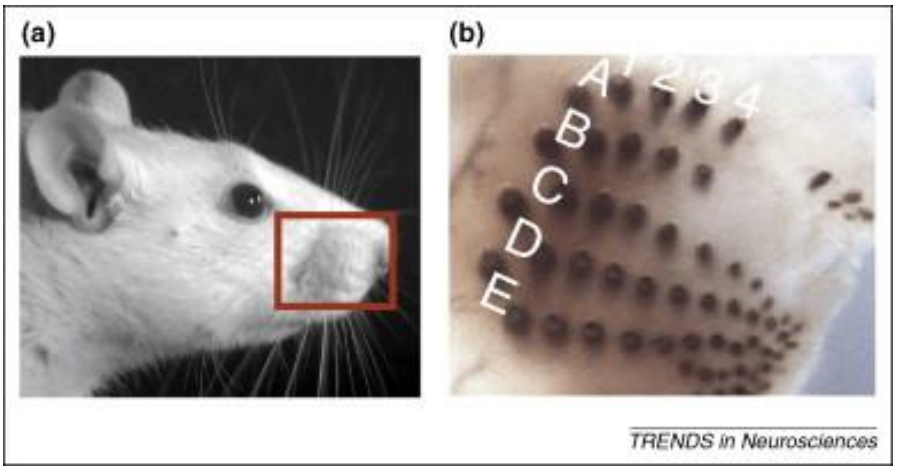

Figure 3. **The rodent whisker arrangement. a**) The whisker pad on the snout of a rat. **b**) Magnification of the whisker pad with the organization of rows and arcs. Follicles on the left of the letters are labelled with Greek letters: from top to bottom α, β, ɣ and δ. Adapted from (Knutsen & Ahissar, 2009)

To understand how the rodent whisker somatosensory system permits animals to efficiently interact with the environment, it is important to identify the elements of the system, which consist of their roles and how they connect and interact with each other (Sehara & Kawasaki, 2011). In fact, at every station, the signal can be modulated and divided into different pathways that relay complementary information.

The whisker system ascending pathway starts in the periphery (Figure 4) (Diamond et al., 2008), where each whisker follicle is innervated by a multitude of mechanoreceptors (50-200) (Welker & Van der Loos, 1986). The somata of those neurons are clustered in a region called the trigeminal ganglion. As is common along the whole pathway, here the cell bodies are somatotopically arranged as whisker rows in the snout of the animal: neurons innervating the whiskers in row A are more dorsal than those innervating row B, and so on (Feldmeyer et al., 2013). In the absence of a stimulus, sensory neurons are silent; when excited, they can encode different properties of the stimulus, such as the velocity and orientation of the mechanical stimulus, as well as the position of the whisker (Arabzadeh, Zorzin, & Diamond, 2005; L. M. Jones, Depireux, Simons, & Keller, 2004; Shoykhet, Doherty, & Simons, 2000). The trigeminal ganglion neuron, in general, reports information from only one whisker with fast adapting AP firing (Aronoff et al., 2010; C. C. H. Petersen, 2003). Moreover, due to the inertia and interaction with the air itself, sensory neurons in the ganglia are able to encode when the animal is whisking even without touching anything (free whisking). Projections from the trigeminal neurons bifurcate and make excitatory glutamatergic synapses in two nuclei in the brainstem trigeminal complex: the principal trigeminal

nucleus (PrV) and the spinal trigeminal nucleus (SpV) (Figure 5) (Bale & Petersen, 2009; Feldmeyer et al., 2013; C. C. H. Petersen, 2003).

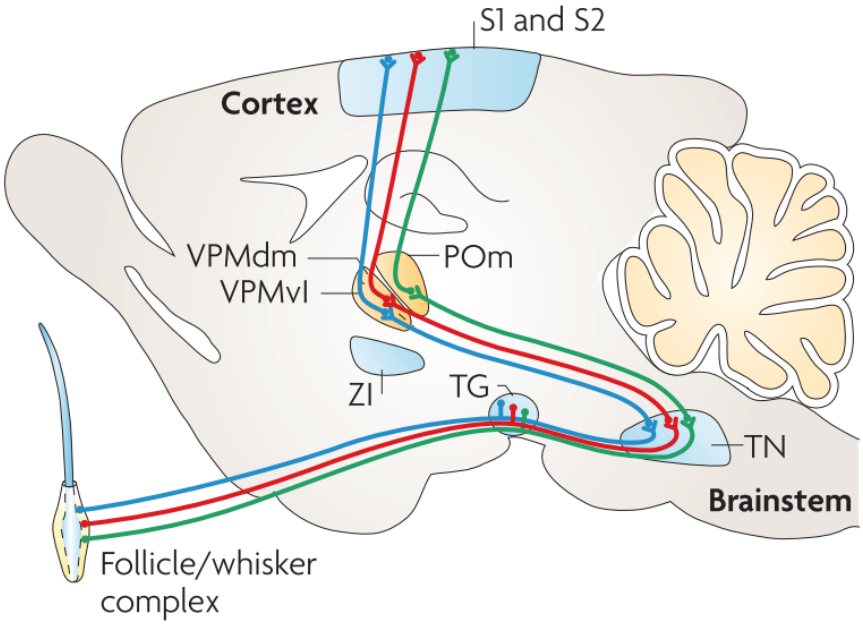

Figure 4. **Anatomy of the whisker system.** Inputs generated in the follicles travel through different stations before reaching designate areas in the cortex. Different colours represent distinct ascending pathways. Adapted from (Diamond et al., 2008).

Neurons in the brainstem refine the tactile information they receive from the sensory afferents: they are able to adapt the response to a stimulus, integrate signals coming from different whiskers and infer direction selectivity (Feldmeyer et al., 2013; Minnery, Bruno, & Simons, 2003). Each cell of the PrV is contacted mostly by sensory neurons that innervate a single whisker, leading to a single whisker receptive field. The PrV neurons are arranged in a somatotopic disposition, where cells that receive information from the same vibrissa are in proximity. These clusters, visible by cytochrome oxidase stain, are called barrelettes (Ma, 1991). Cells of the PrV form the so called lemniscal sensory pathway that innervates mostly the dorsomedial part of the ventral posterior medial nucleus of the thalamus (dmVPM) of the contralateral hemisphere.

Neurons in the SpV are also organized in barrelettes, but they receive signals from more than one vibrissae, building a multi-whisker receptive field. From this nucleus originates both the paralemniscal pathway, which contacts the contralateral posterior medial nucleus of the thalamus (POm), and the extralemniscal pathway, which innervates the ventrolateral part of the VPM (vlVPM) (Figure 5) (Feldmeyer et al., 2013; R. S. Petersen, Panzeri, & Maravall, 2009).

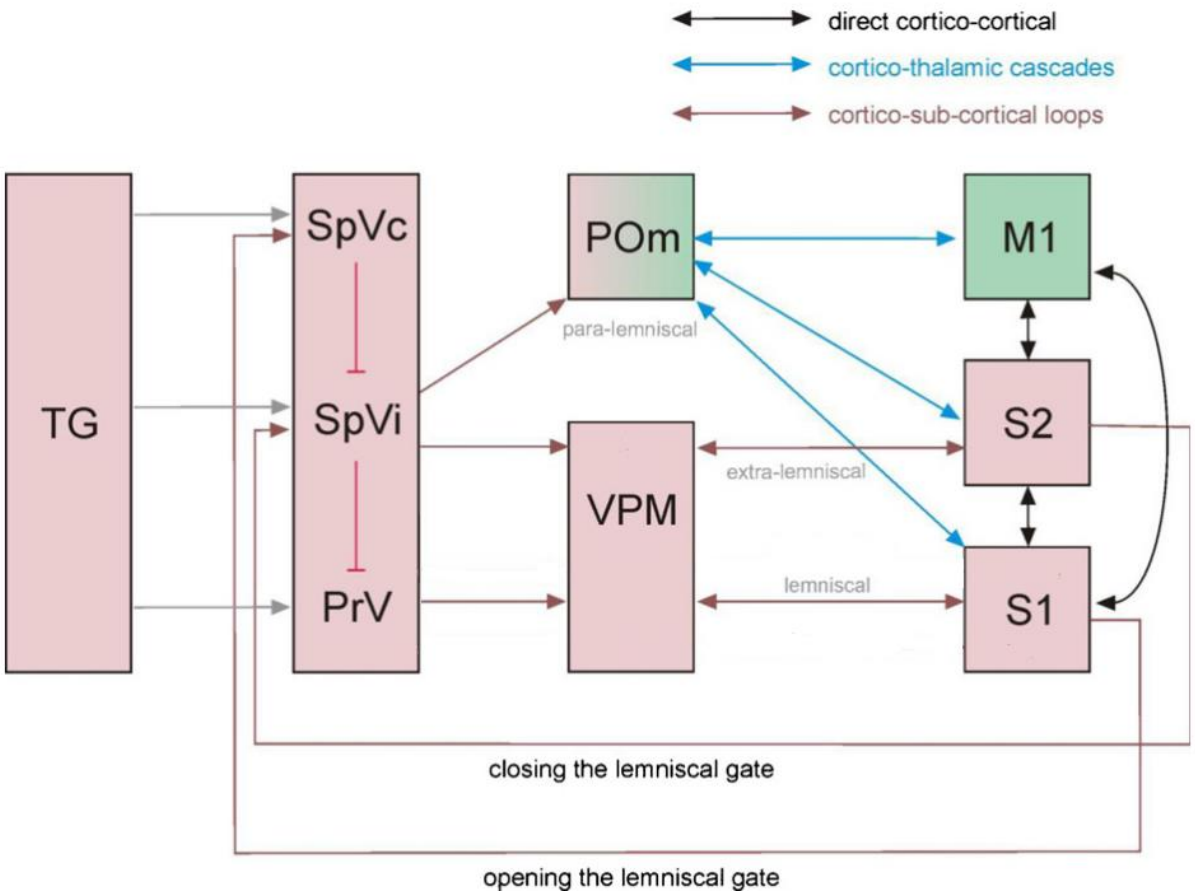

Figure 5**. Schematic representation of the rodent whisker system.** Primary sensory neurons in the trigeminal ganglion (TG) encode whisker sensation into a neuronal signal that it is transmitted to the trigeminal brainstem complex (TN). This complex includes the principal nucleus (PrV) and the spinal sub-nuclei (interpolaris SpVi; caudalis SpVc). From here, the ascending pathways divide into lemniscal extra-lemniscal, and paralemniscal. The lemniscal pathway arises from PrV barrelettes transporting single whisker (principal whisker) information to barreloids in the ventral posterior nucleus (VPM) first and then to barrels in the primary somatosensory cortex (S1). The extra-lemniscal pathway conveys multi-whisker neuronal signals, it arises from the SpVi and reaches the secondary somatosensory cortex (S2) through the ventro-lateral portion of the VPM. The paralemniscal pathway also starts from the SpVi and carries multi-whisker signals. It first reaches the POm and from there contacts S1, S2 and the motor cortex (M1). Adapted from (Feldmeyer et al., 2013).

The thalamus is a common station in sensory pathways. It has been demonstrated to be not only a relay station, as was initially hypothesized, but also an active member in shaping the sensory information. Moreover, there are recurrent interactions between the thalamus and cortex creating thalamo-cortical loops. Thalamic nuclei can be classified as first order, the principal driver inputs of which arise directly from subcortical structures, and high order, if they also receive driver inputs from the cortex (Bickford, 2016). The nuclei principally involved in whisker somatosensation

are VPM and POm (Figure 4 and Figure 5). They participate in distinct pathways and do not communicate directly, suggesting that they accomplish different functions (Feldmeyer et al., 2013). However, they both receive inhibition from the reticular nucleus and zona incerta and feedback from layer V and VI of the barrel cortex (C.-S. Lin, Nicolelis, Schneider, & Chapin, 1990). The VPM is a first order nucleus that is contacted by both the lemniscal and extralemniscal pathways, although the afferents relative to each of them are spatially separated (Figure 5). The lemniscal pathway contacts the thalamus in the dorsomedial part of the VPM (dmVPM). Here, the topographical organization of the neuron somata reflects the clusterization in PrV forming barrelloids: there is a complete correspondence between barrelloids and the whisker map in the snout of the animal (Figure 6). For the majority of the neurons in the lemniscal pathway, information is derived mostly from a single principal whisker, and the response latency is very short (from 5 to 10 ms) (Feldmeyer et al., 2013). Along this pathway, cells respond to both the movement of the whiskers and the interaction with an object (touch). Moreover, these cells are tuned for physical properties of the stimulus such as direction and velocity (Ito, 1988; Timofeeva, Mérette, Émond, Lavallée, & Deschênes, 2003). The principal targets of dmVPM axons are the cells inside the barrels in layer IV of the whisker area of S1 (wS1); however there are also direct projections in layer V, VI and deep layer III (Figure 7) (Constantinople & Bruno, 2013; Lübke & Feldmeyer, 2007). The axons of dmVPM neurons within individual barreloids project somatotopically to wS1 in layer IV to form discrete clusters called barrels for the typical “barrel” form, which is easily visible in stained slices. For this reason, the wS1 is also called the “barrel cortex”. These barrels present a somatotopic representation of the whisker disposition on the mystacial pad (Figure 6) (Woolsey & Van der Loos, 1970). Cells in the ventral part of the VPM (vlVPM), by contrast, participate in the extra-lemniscal pathway, which conveys information preferentially about touch (Figure 5) (Feldmeyer et al., 2013). Those cells receive inputs from more than one whisker and, as a consequence, are not somatotopically organized (Pierret, Lavallée, & Deschênes, 2000). Neurons in the vlVPM project to both the wS1 and secondary somatosensory cortex (S2). In wS1, they form synapses with cells in the septa of layer IV as well as basal layer III and layer IV. In S2, they are connected with layer IV and VI. The other thalamus nucleus, POm, is classified as a higher order nucleus, but nevertheless, it participates in the paralemniscal ascending pathway receiving information directly from the SpV (Figure 5) (Feldmeyer et al., 2013). In contrast to dmVPM neurons, POm cells have multi-whisker receptive fields and lack a somatotopic arrangement of the somata. Moreover, POm neurons respond to whisker deflection

with longer latencies, and in the wS1, their projection pattern is mostly complementary to the cell of the dmVPM (Figure 7). Indeed, the paralemniscal pathway enters wS1 mostly in layer IV septa as well as in layer I, II/III and layer V. In addition to S1, POm connects bidirectionally with S2 and the primary motor cortex (M1) (Feldmeyer et al., 2013). Although there are still controversies, it is believed that the paralemniscal pathway conveys information that is more related to whisker movements (Feldmeyer et al., 2013).

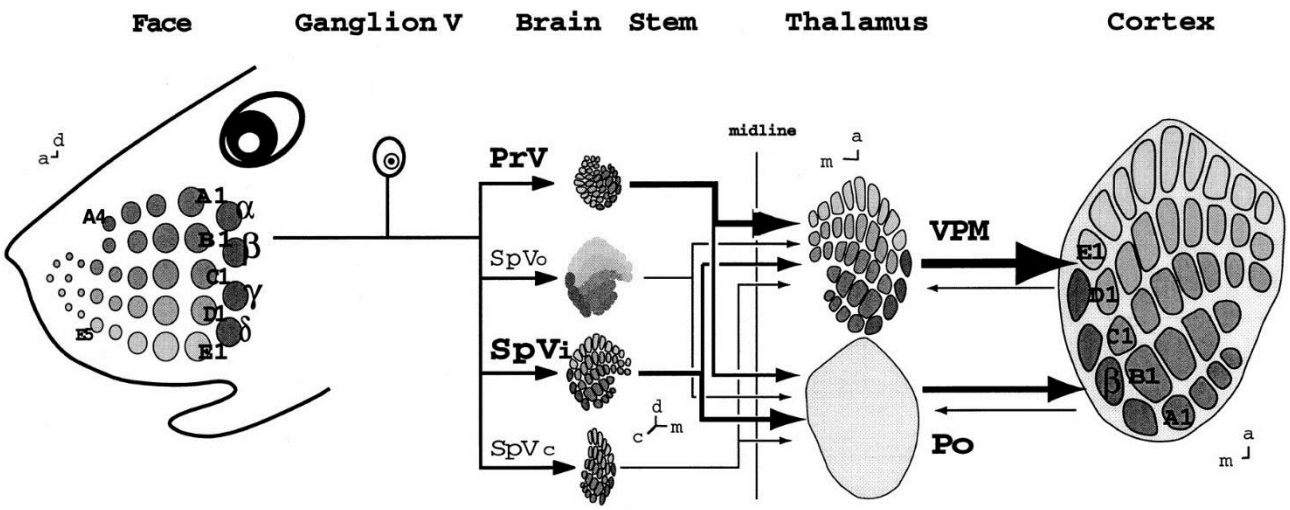

Figure 6. **From whiskers to barrels.** Cartoon summarizing the somatic representation of the whiskers at each stage of the vibrissa somatosensory system. Each whisker is represented by a barrelette in the brainstem, a barrelloid in the thalamus and a barrel in the cortex. Adapted from (Yuste & Simons, 1997).

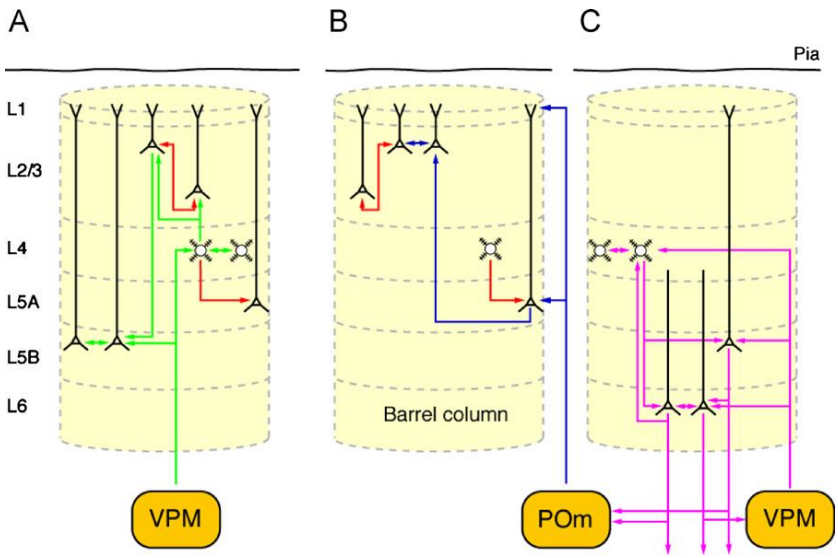

Figure 7. **Thalamocortical projections in the barrel cortex.** Adapted from (Lübke & Feldmeyer, 2007)

The final destination of all three ascending pathways are the somatosensory areas in the neocortex. Here sensory areas are highly organized, both anatomically and functionally. Based on the morphology and localization of different neurons, six layers have been identified. Layer IV of S1, also named the granular layer, is the major target of the thalamo-cortical projection. In the area receiving whisker tactile inputs, neurons inherit the somatotopic organization from the lemniscal pathway to form barrel-like clusters called barrels. These structures are interrupted by zones that receive multi-whisker information from the POm and the vlVPM, called septa. Extending this organization vertically across layers results in barrel columns: functional elements of the somatosensory pathway. Neurons inside a barrel column are highly connected, transmitting information from one layer to the other (see Section 1.3 for a detailed description). In a simplified view of the columnar network, sensory inputs entering the cortex in layer IV are relayed to superficial layers II/III, which integrate them with other inputs from different ascending pathways and send the resulting information to infragranular layer V and VI. Infragranular layers represent the major output of S1 projecting towards both cortical and subcortical areas.

The principal targets of cortico-cortical projections are the ipsilateral S2, ipsilateral M1 and contralateral S1. For a comprehensive list see (Mao et al., 2011). S2 is a higher order area with respect to S1, and the two somatosensory areas are strongly interconnected, creating a cortico-cortical loop between the two (Carvell & Simons, 1987). Both of them participate in the formation of sensory perception, and the difference in response time is very short (Aronoff et al., 2010). It has been suggested that S2 is involved in the integration of multi-whisker inputs and in choice-related responses. (Zuo et al., 2015) It has been reported that spike timing of neurons of both S1 and S2 is more informative about texture stimuli properties and animal decisions with respect to the spike rate. Multi-area imaging during a discrimination task in head-restrained mice showed coordinated activity in S1 and S2 during goal-directed motor behaviours and sensory processing (Chen, Voigt, Javadzadeh, Krueppel, & Helmchen, 2016). Another study confirmed the role of S2 projections to S1 in choice-related activity and that a large response in S2 can predict successful trials with respect to missed trials (Kwon, Yang, Minamisawa, & O'Connor, 2016).

The primary motor cortex is an area in the neocortex involved in the animal motor activities. The interaction of S1 with M1 it is believed to be implicated in the motor behaviour related to tactile information (Petrof, Viaene, & Sherman, 2015). In M1, layer II/III and layer Va are the major

recipients of input coming from the S1 (Mao et al., 2011). In contrast, M1 pyramidal neurons project preferentially to layer I, layer V and IV. There are also reciprocal connections between S2 and M1, creating a framework for an orchestrated recruitment of these areas during tactile sensory perception (Suter & Shepherd, 2015).

The deep layers of the primary somatosensory cortex project back to the ipsilateral thalamic nuclei of the ascending pathway to create a thalamo-cortico-thalamic loop (Diamond & Arabzadeh, 2013). Moreover, the cortex projects to the thalamic reticular nucleus, forming inhibitory connections with both the VPM and POm (Lam & Sherman, 2010). Feedback projections in the whisker sensory system are also present between S1 and the spinal trigeminal nuclei. In addition, from S1 originate several subcortical projections that innervate nuclei related to motor response generation and refinement. One major target of both supragranular and infragranular layers axons is the striatum in the basal ganglia, which has been shown to have both anatomical and functional maps (Diamond & Arabzadeh, 2013). Moreover, direct connections have also been documented in the superior colliculus and in the pons (Aronoff et al., 2010).

1.3 The whisker primary somatosensory cortex

The information associated with whisker perception reaches the cerebral cortex in a precise primary somatosensory sensory area (wS1), which is also called the barrel cortex, as mentioned above (Figure 8). The name is derived from a specialized cyto-organization in layer IV, the barrel field (Figure 8, red). Barrels that are considered the major thalamocortical recipients receive the axonal projection from the VPM with a precise somatotopic organization, in which each mystacial whisker is mainly represented by its own barrel (Simons & Carvell, 1989a; Veinante & Deschênes, 1999).

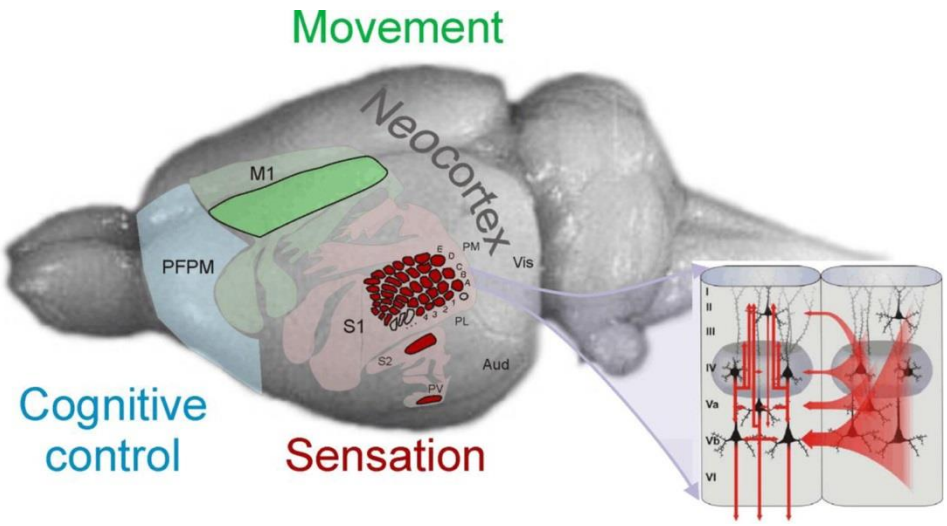

Figure 8. **The primary somatosensory cortex.** Representation of the mouse brain showing principal neocortex brain areas with their correlated functions. Area principally involved in whisker somatosensation are highlighted. On the right, a schematic of the barrel functional column is depicted. Adapted from (Feldmeyer et al., 2013).

The barrel cortex is part of the neocortex, the evolutionarily youngest brain structure. It is composed of two main classes of neurons: glutamatergic excitatory neurons that account for the 80% of cortical neurons, and GABA (γ-aminobutyric acid)-ergic inhibitory cells (interneurons) that represent the remaining 20%. The ratio between excitatory and inhibitory neurons varies depending on the cortical area and species (Douglas & Martin, 2004). The neocortex is generally organized in six horizontal laminae (or layers) (Douglas & Martin, 2004) that can be distinguished based on their different cell densities and on the distinct shape of the cell somata and dendrites that characterize the neurons in each layer (Figure 9) (Narayanan, Udvary, & Oberlaender, 2017). This arrangement is a direct consequence of the radial migration of neurons generated in the cortical ventricular zone during development (Dehay & Kennedy, 2007). The layers are sequentially numbered from I to VI going deeper from the most dorsal part of the brain.

The laminar structure of neocortex is similar between different areas, as described below. From the pial surface, the most superficial layer (layer I) presents very few primary GABAergic cells and is composed mostly of axons and dendrites ascending from the lower layers II/III and V. Proceeding down, layers II and III show several morphological and functional similarities and in mice are difficult to distinguish and, thus, are usually considered one layer, layer II/III. Excitatory layer II/III pyramidal neurons project either horizontally to other layer II/III pyramidal cells or vertically to neurons in layer V. Extensive callosal long-range axonal projections are present, which

reach the opposite hemisphere. Layer IV is the main target of the thalamo-cortical projections and is particularly developed in the barrel cortex. The most represented population therein are glutamatergic spiny stellate cells that form extensive local connections and send their inputs preferentially to superficial layer II/III. As previously stated, histological staining of neurons with cytochrome oxidase reveals in three dimensions a tightly packed assembly of cells in the wS1 that are shaped like barrels intermingled with zones of low cell density called septa (Woolsey & Van der Loos, 1970). In layer V, there are large pyramidal neurons that send their axonal projections both to cortical and subcortical areas (such as the contralateral hemisphere, thalamus, striatum and several other extra-cortical structures), making this one of the main output layers (Brown and Hestrin 2009; Hattox and Nelson 2007;Feldmeyer 2012). However, they also project intracortically to layer II/III and layer V/VI (Lefort, Tomm, Floyd Sarria, & Petersen, 2009; Shepherd, Stepanyants, Bureau, Chklovskii, & Svoboda, 2005). There are two morphologically distinct classes of neurons in layer V: upper layer Va neurons with a slender-tufted apical dendritic arborization, and lower thick-tufted layer Vb neurons. In the barrel cortex, thick-tufted neurons respond more reliably to whisker deflection with respect to the other group, which seems to show greater recruitment during whisker movement (de Kock, Bruno, Spors, & Sakmann, 2007; de Kock & Sakmann, 2009). The deepest layer, layer VI, is composed of pyramidal neurons that primarily contact subcortical areas such as the thalamic nuclei. Since layer V and VI neurons of the barrel cortex project to the VPM and POm, they are believed to be involved in the cortico-thalamic feedback pathway of the whisker sensory pathway.

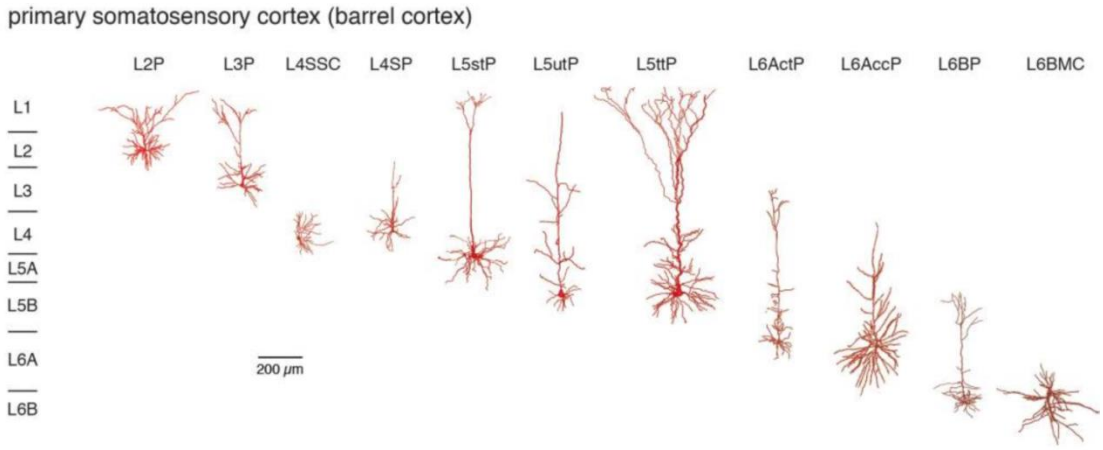

Figure 9. **Excitatory neurons of the rodent primary somatosensory cortex.** Simplified representation of the morphology of principal cells in the barrel cortex from layer II to VI; the variety of neurons actually present in the brain is wider. Different grades of red represent distinct somatodendritic domains; bright red for superficial and dark red for deep layers. Apart from layer IV spiny stellate neurons and layer VIb multipolar cells, neurons in the barrel cortex show a pyramidal morphology. Adapted from (Radnikow & Feldmeyer, 2018).

In addition to the horizontal laminar organization, the barrel cortex, such as other sensory areas of the neocortex, is vertically organized into groups of synaptically interconnected cells that form functional "columns" with similar physiological and functional properties (Figure 10). Neurons belonging to a column can either make short range intracolumnar or long range transcolumnar synapses, whether or not the projections remain inside the column. In addition, since a column extends across all layers, connections can be intralaminar or translaminar. Most of the connections in the barrel cortex are both intracortical and intralaminar connections between interconnected neurons, granting the possibility for recurrent excitation but also feedback inhibition and disinhibition when interneurons are involved (Figure 10) (Lübke & Feldmeyer, 2007).

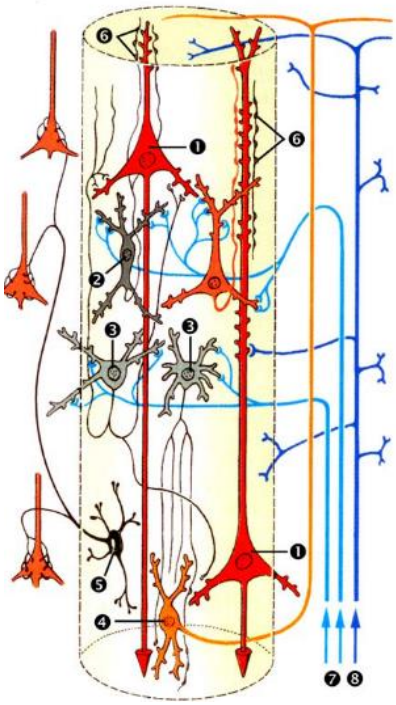

Figure 10. **The functional barrel column.** Representation of a simplified cortical column, including excitatory and inhibitory neurons. Pyramidal neurons are represented by number **1** (red cells); **3** corresponds to layer IV spiny stellate cells (light grey); **2**, **4** and **6** identify interneurons; and **7** and **8** specify fibres (blue) arising from other brain region (e.g., thalamus). Adapted from (Lübke & Feldmeyer, 2007).

The barrel cortex is one of the most used models to study columnar microcircuits: here, the barrel-related columns are relatively easy to visualize forming a structure that processes the sensory information preferentially of a single principal whisker. In contrast, septa-related columns, the

ones that extend vertically from the septa in layer IV, receive mostly ascending multi-whisker information from the POm and vlVPM. Septa neurons are less responsive to whisker stimulation with respect to cells in the barrels, but they are recruited by rhythmic whisker movements (at least in rats) (Sehara & Kawasaki, 2011). Although the barrel column organization seems preserved across rodents, mouse septa columns are less pronounced with respect to rats, which may underlie some differences (Feldmeyer et al., 2013).

Within a single barrel column, the preferential flow of synaptic inputs has similarities with other sensory cortices (e.g., visual cortex in cats), leading to the hypothesis of a conserved "canonical" neocortical microcircuit for the sensory process in the neocortex. Within a column, sensory information enters layer IV and then reaches the supragranular layer II/III before being relayed to infragranular layers V and VI (Armstrong-James, Fox, & Das-Gupta, 1992; Douglas & Martin, 2004; Feldmeyer, 2012; Gilbert & Wiesel, 1979; Oberlaender et al., 2012). The latter are considered among the major outputs and contact targets outside the column, reaching both cortical and subcortical regions for higher order level processing (Feldmeyer, 2012). Indeed, translaminar excitatory connections support this theory: connections between layer IV to layer II/III and layer II/III to layer V are dominant with respect to those in the opposite direction (Lübke & Feldmeyer, 2007). However, in parallel with this scheme, infragranular layers have also been shown to receive sensory inputs directly from the VPM, with latencies comparable to the canonical pathway, and the whisker-elicited response in layer V persists after reduction of the layer II/III spiking activity during whisker stimulation (Armstrong-James et al., 1992; Chmielowska, Carvell, & Simons, 1989; Constantinople & Bruno, 2013; de Kock et al., 2007). Moreover, the paralemniscal ascending projection from the POm also directly contacts layer V, although with longer latencies (Lübke & Feldmeyer, 2007). Taken together, these evidences suggest that layer V is a distinct sensory signal processing unit in the barrel column that may perform in parallel to the canonical pathway. Thus, electrophysiological studies have demonstrated functional connectivity from layer V to superficial layers (Lefort et al., 2009; Shepherd et al., 2005) and that optogenetic modulation of a fraction of layer V pyramidal neurons can influence layer II/III spontaneous activity (Beltramo et al., 2013).

Somatotopic representations of whiskers in the barrel cortex and the neurons in barrel-related columns present a whisker identity preference (i.e., neurons respond preferentially to the principal whisker). Barrel cortex neurons encode specific physical properties of the whisker deflection: amplitude, speed, acceleration, frequency and direction (Arabzadeh, Petersen, &

Diamond, 2003; Simons, 1978; Wilent & Contreras, 2005). At each station in the sensory ascending pathway, neurons encode different features of the stimulus. Subcortical neurons tend to represent the stimulus properties more faithfully and directly, e.g., they increase their response in a linear manner with respect to the increment of deflection (Bale, Davies, Freeman, Ince, & Petersen, 2013; Maravall, Alenda, Bale, & Petersen, 2013). In contrast, it is believed that cortical neurons respond to a variation with respect to a background level (Maravall, Petersen, Fairhall, Arabzadeh, & Diamond, 2007). This phenomenon suggests that the cortex is able to represent the firing activity of more complex stimuli. It is important to notice that what has been said is true if considered at population level, but single neurons show high variability in their response. There are cells inside a barrel that exhibit a better response to the surrounding whisker with respect to the principal one (Clancy, Schnepel, Rao, & Feldman, 2015; Takashi R. Sato, Gray, Mainen, & Svoboda, 2007). In addition, the spike activity of two nearby cells can vary greatly in response to different properties of the stimulus. This characteristic is usually referred to as salt and pepper functional organization. Direction tuning is the ability of a neuron to vary its response according to the angular direction of the whisker stimulation in the plane orthogonal to the whisker follicle (Brecht & Sakmann, 2002; Wilent & Contreras, 2005)(Figure 11). The majority of neurons of the trigeminal ganglion show a directional preference (Kwegyir-Afful, Marella, & Simons, 2008), and this characteristic is transferred to cells via both the lemniscal and the paralemniscal pathways down to S1. In the barrel cortex, directional selectivity has been shown to emerge via a difference in timing between excitation and inhibition (Wilent & Contreras, 2005). An angular tuning preference map, where cell with similar tuning are close together and arranged in an organized manner, has been shown in the VPM (Timofeeva et al., 2003), although the presence of a similar map in the barrel cortex is still disputed (Andermann & Moore, 2006; Kerr et al., 2007).

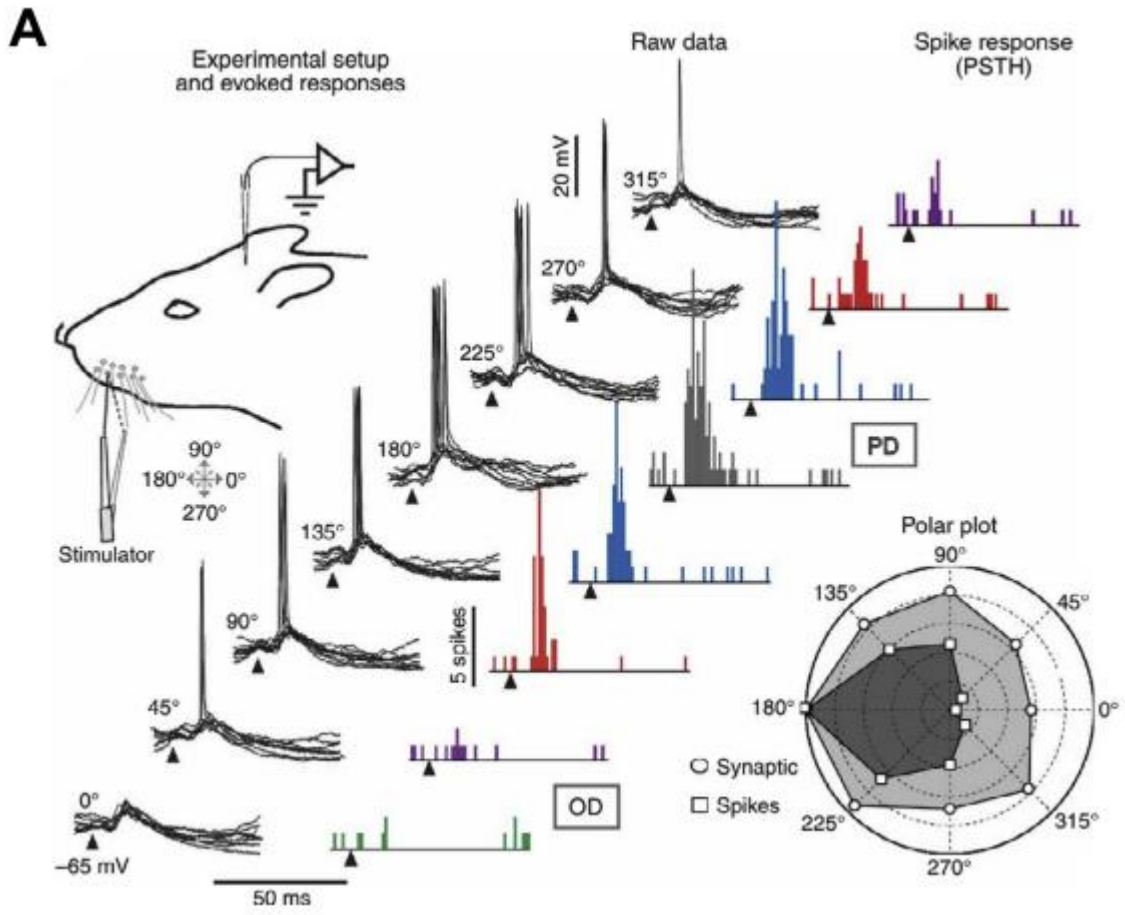

Figure 11. **Angular direction selectivity. A)** Intracellular recording from a neuron of the barrel cortex layer IV in an anaesthetized rat during whisker stimulation in 8 different directions. Eight traces are shown for each direction; the arrow indicates the stimulus onset. From the raw data, a peristimulus time histogram is built, highlighting the preferred direction (PD) and opposite direction (OD). A polar plot is derived from the average responses. Adapted from (Wilent & Contreras, 2005).

Neurons in the neocortex form a heterogeneous cell class, the members of which are characterized by different functional properties, morphologies, specific locations and genetic identities. As already mentioned above, more than 80% of the cells in the barrel cortex are glutamatergic excitatory neurons or principal cells, which are localized across all the layer excluding layer I (Lefort et al., 2009). The remaining cells are GABA-ergic cells, also known as interneurons, which are present in all layers (Druga, 2009). For the correct functionality of cortical networks, there must be a fine balance between excitatory and inhibitory forces. Among principal cells, based on morphology and localization, two main class are identified in the somatosensory cortex: pyramidal neurons and spiny stellate cells. Although the boundary between these two classes can be blurry, the former have a conic cell body from which several basal dendrites branch

out at the base and a singular long and thick apical dendrite extends from the top towards the superficial layers. The size of the soma varies across layers, with deep layer cells being the largest. Moreover, they usually have only one axon that can project far from the cell body. Based on the location of the axonal target, pyramidal neurons are divided into three non-overlapping classes: intratelencephalic, with post-synaptic targets inside the cerebrum, cortico-thalamic cells that preferentially contact the ipsilateral thalamus and pyramidal tract cells that contact, among others (cortex, striatum and thalamus), subcerebral areas (brainstem, spinal cord and midbrain) (K. D. Harris & Shepherd, 2015). In contrast, spiny stellate or granular cells are star-shaped with short axons, and their soma is smaller than pyramidal neurons. They tend to make strong local synaptic connections with recurrent contacts between each other. Stellate cells are the most represented principal neuron within layer IV.

The barrel cortical circuits described above mainly deal with the flow of excitatory information across layers. However, as already mentioned, 20% of neocortical neurons are GABAergic inhibitory cells. Interneurons are present in each layer and are usually characterized by local axonal projections (Druga, 2009). However, there are many cases of interneurons providing interlaminar inhibition, such as, for example, layer V and VI interneurons, which have an axon spanning across most layers (Bortone at al 2014; Buchanan et al 2012). Three main non-overlapping classes that together represent the vast majority of neocortical interneurons have emerged based on genetic markers: one class that expresses a calcium binding protein, parvalbumin (PV); one that expresses the neuropeptide somatostatin (Sst); and one that expresses receptor 5-hydroxytryptamine 3a (5HT3aR) (Figure 12) (Rudy, Fishell, Lee, & Hjerling-Leffler, 2011). These classes are not evenly distributed across the different layers in the barrel cortex. 5HT3aR is mostly represented in the superficial layers, whether Sst and PV populate the deeper layers, with the latter being especially concentrated in layer IV (Figure 13) (Rudy et al., 2011).

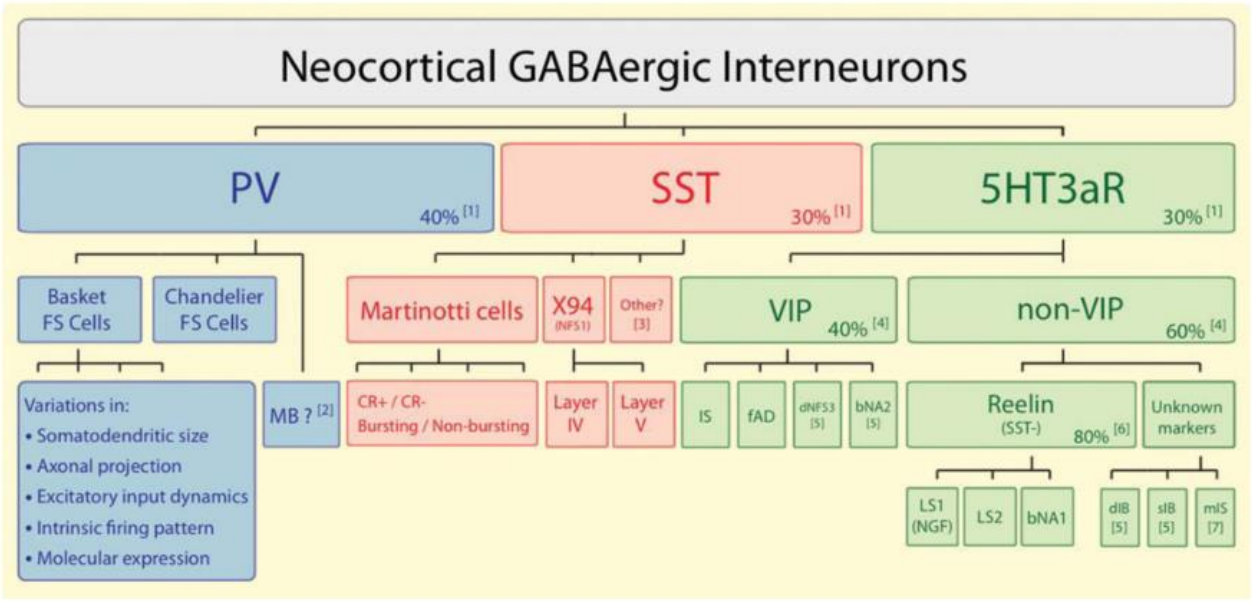

Figure 12. **Genetically identified classes of interneurons in the neocortex.** The three genetically distinct classes of interneurons that together account for nearly the totality of GABAergic neurons in the somatosensory cortex. Adapted from (Rudy et al., 2011).

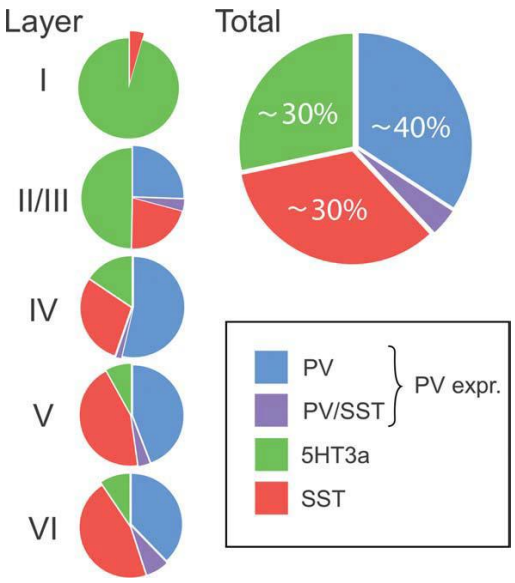

Figure 13. **Proportion of the three groups of GABAergic interneurons in the barrel cortex.** Distribution of the three non-overlapping classes of interneuron in the S1 barrel cortex across layers (left) or total (right). Adapted from (Rudy et al., 2011)

1.3.1 Parvalbumin interneurons

Parvalbumin-positive cells represent the largest group among cortical interneurons, accounting for almost 40% of the total cortical inhibitory population. Almost all PV interneurons are fast spiking cells characterized by a high firing rate and a small spike frequency adaptation marked after hyperpolarization following each spike (Cauli et al., 1997; Kawaguchi & Kubota, 1997). PV interneurons are able to strongly inhibit and therefore control the firing activity of postsynaptic cells. In the whisker tactile system, layer IV PV receive dense innervation from the VPM and administer feedforward inhibition, shaping the cortical representation of the stimulus (Moore, Carlen, Knoblich, & Cardin, 2010). Due to their precise timing, they create a narrow window for post-synaptic potential summation and AP generation (Rudy et al., 2011). Based on morphology, two main subclasses of PV are being observed, basket cells and chandelier cells. The former form inhibitory axosomatic synapses, surrounding the cell body of the post-synaptic cells with their axon (Markram et al., 2004). They represent the main source of inhibition at the level of local circuitry. Chandelier cells, by contrast, form axo-axonic synapses that target the axon initial segment of local pyramidal neurons. This group of cells is much smaller than the previous one, and their function is not yet well understood. There is evidence that depending on the resting potential of the post-synaptic cells, the release of GABA at the axon initial segment may be excitatory instead of inhibitory (Rudy et al., 2011). Both basket and chandelier cells are fast spiking, although they show slightly different electrophysiological properties. There is indeed a third PV-positive group, which was discovered in (Blatow et al., 2003) populating the superficial layers of the mouse cortex and exhibiting distinct firing activity from fast spiking cells. Members of this group respond to stimulation with an initial burst of APs, followed by a prolonged after-hyperpolarization. For this reason, they are called multipolar bursting, and in contrast to the other PV interneurons, they target dendritic branches (Blatow et al., 2003; Kubota et al., 2011).

1.4 Layer IV in rodent somatosensation

Although the VPM projects to several cortical layers (III, IV, V and VI), layer IV has been viewed as a key member of the transmission of the sensory information to the cortex (Chmielowska et al., 1989; Koralek, Jensen, & Killackey, 1988; Lu & Lin, 1993; Lübke & Feldmeyer, 2007). In the

lemniscal pathway, layer IV is the principal recipient driving thalamic input, leading to the belief that it is the entry point of the whisker tactile information. The main targets of the ascending pathway are both excitatory spiny neurons and GABAergic interneurons. The projections that innervate layer IV are somatotopically arranged as the whiskers on the contralateral side of the snout of the rodent (E. G. Jones & Diamond, 1995). This input organization is extended to the whole barrel column through the transmission of the signal that emerges from layer IV to the other layers (Aronoff et al., 2010). Indeed, excitatory neurons in layer IV are able to respond to whisker stimulation with a short latency, having one of the fastest responses among the whole cortical column. Each synapse from the VPM is able to elicit a rather weak depolarization in layer IV excitatory neurons (~1 mV); however, the thalamocortical inputs are strongly convergent, with a single layer IV cell receiving from approximately 85 thalamic projections. Moreover, thalamic inputs have high temporal synchronicity (Lübke & Feldmeyer, 2007).

In layer IV, spiny excitatory neurons can be further divided into two main populations: spiny stellate cells, the most represented group, and star pyramidal neurons. Both of these classes are the starting block of the intracortical signal processing preferentially contacting pyramidal cells in layer II/III and other spiny neurons in layer IV; however, axon collaterals extend all across the barrel cortex, from layer I down to layer VI (Lübke, Egger, Sakmann, & Feldmeyer, 2000). Moreover, in both classes, both regular firing and intrinsically bursting cells have been observed (Feldmeyer, Egger, Lübke, & Sakmann, 1999; Schubert, Kötter, Zilles, Luhmann, & Staiger, 2003) (Figure 14).

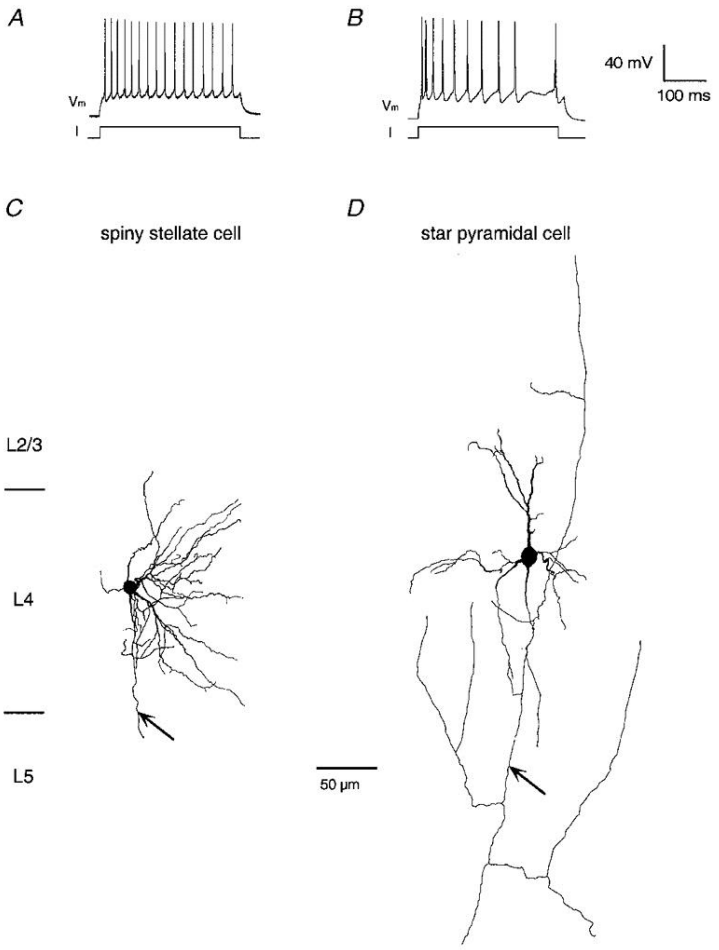

Figure 14. **Barrel cortex layer IV spiny neurons. A**) Representative action potential firing pattern of a regular spiking spiny stellate neuron. **B**) Same as in **A** but for a star pyramidal neuron. **C**) Morphological reconstructions of a spiny stellate cell, axonal projections are not shown entirely. **D**) Same as **C** but for a pyramidal cell. Adapted from (Feldmeyer et al., 1999).

Spiny stellate cells in layer IV extend their dendrites preferentially towards the centre of the barrel in which their soma is located, with relatively small horizontal and vertical extension. Indeed, the majority of the spiny stellate dendritic domain remains inside the barrel and forms a strong synapse with either the thalamocortical long projection or axon collateral of another spiny stellate cell in the same barrel (Lübke et al., 2000). The majority of inhibitory inputs also originate from interneurons inside the same barrel, although some inhibition also arises from the lower layer III and layer V (Schubert et al., 2003). Spiny stellate neurons on average form 3.4 connections between each other, with a strong excitatory drive that is able, in some pair of cells, to elicit an AP in the postsynaptic neuron (Feldmeyer et al., 1999). The recurrent connections between layer IV spiny neurons are approximately 20-30% of the total synapses, and this high reciprocal interaction has been proposed to function as an amplifier of the signal incoming from the thalamus; however,

this hypothesis is still debated (R. M. Bruno & Sakmann, 2006; Carpenter, 1892; Douglas, Koch, Mahowald, Martin, & Suarez, 1995; Lübke & Feldmeyer, 2007)(Figure 15).

Regarding axonal projections, spiny stellate neurons contact all cortical laminae inside the home cortical column. The principal axon branches in several collaterals innervate extensively layer IV and II/III. The principal axon branches in several collaterals innervate extensively layer IV and II/III. These layers account for more than 75% of the total synaptic boutons found in (Lübke et al., 2000); layer II/III showed the highest density of boutons across all layers. The other targets of spiny stellate projections are layer V and VI, albeit the synaptic boutons therein are in very fewer number. These observations support the idea that the sensory stimulus in layer IV is strongly relayed to more superficial layers (Lübke et al., 2000).

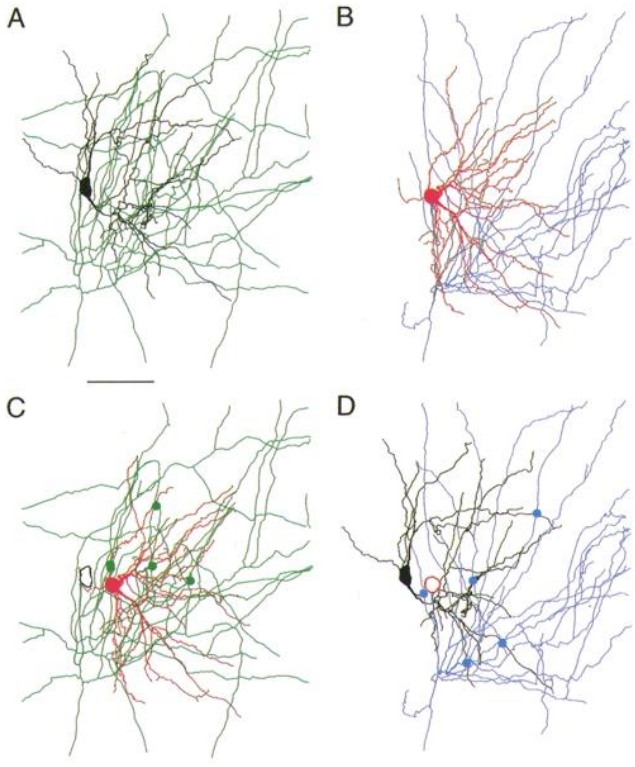

Figure 15. **Barrel cortex spiny stellate neurons are recurrently connected.** Two reciprocally connected neurons were reconstructed in three dimensions. One cell is drawn in black with a green axon **A**), while the other is drawn in red with a blue axon **B**). **C**) Putative synapses between the axon of the cell in **A** (green) and the dendrites of the cell in **B** (red) are represented by green dots. **D**) Similar to **C**, blue dots represent putative synaptic contacts between the blue axon of the cell in **B** and the black dendrites of the cell in **A**. Scale bar 50 µm. Adapted from (Feldmeyer et al., 1999).

The second class of excitatory neurons, star pyramidal cells, which account for approximately 20% of the total, shares many features with spiny stellate neurons. The soma and dendritic arborization are confined inside the barrel, but in addition they have an apical dendrite without a terminal tuft that usually reaches the superficial layers. Moreover, they differ from the other class because they never show asymmetric dendritic organization (Lübke et al., 2000). This class shares strong intra-barrel connectivity, with no differences in synaptic strength, and inhibitory drive mostly from layer IV, layer III and V (Schubert et al., 2003). In addition, star pyramidal neurons show excitatory post synaptic potential (EPSP) layers in the same column, mostly layer Vb and IV, and spiny cells from surrounding barrels. Layer IV pyramidal neurons seem to participate in translaminar and transcolumnar circuits (Schubert et al., 2003). Similar to spiny stellate neurons, the star pyramidal axon extends through all cortical layers of a singular columns, although they contact mostly layer IV and layer II/III. In comparison to spiny stellate cells, the axonal collateral of star pyramidal neuron is less dense and forms fewer synaptic boutons. Moreover, in superficial layers, it extends beyond the border of the principal barrel contacting the surrounding columns (Lübke et al., 2000).
Whisker deflection leads to an excitatory response that usually anticipates a strong and diffuse inhibitory wave. Whisker-evoked spikes in layer IV are modulated by a strong feedforward inhibition that filter the sensory input coming from the thalamus in a time-dependent manner (Bale & Maravall, 2018). Moreover, it has been suggested that layer IV interneurons are able to separate and refine the touch with respect to the whisker active movement inputs to excitatory neurons (Estebanez, Férézou, Ego-Stengel, & Shulz, 2018). Feedforward inhibition is involved in the relay of tactile information from layer IV to layer II/III spiny neurons and, indeed, is able to contact with high efficacy different types of interneurons in the superficial layer (Feldmeyer et al., 2013).

Thalamic projections contact several types of interneurons in the granular layer (Sermet et al., 2018). Among them, PV interneurons receives strong synapses with a shorter latency that undergo depression after repeated stimulation (Beierlein, Gibson, & Connors, 2003). Thalamic projections to fast spiking interneurons lead to feedforward inhibition that in spiny neurons contrast EPSP with a delay of approximately 1-2 ms with respect to excitatory drives. This feature creates a small window of opportunity for excitatory cells, promoting fast and synchronous EPSP summation despite slow, highly variable inputs. The majority of PV interneurons in layer IV have thick axonal arborization that remain confined inside the home barrel, forming extensive connections with principal cells of the same layer. This phenomenon suggests that PV interneurons in the granular

layer are not able to directly inhibit the surrounding barrels (Koelbl, Helmstaedter, Lübke, & Feldmeyer, 2015). In contrast to spiny neurons, layer IV fast spiking neurons increase their firing rate during whisking even in the absence of touch. This activation reduces the firing activity of spiny neurons during whisker movements, increasing their ability to respond selectively to touch events (Yu, Gutnisky, Hires, & Svoboda, 2016). Moreover, fast spiking neurons have larger receptive fields and are less direction-tuned with respect to regular spiking neurons (Randy M. Bruno & Simons, 2002).

Additionally, Sst and 5HT3aR are directly contacted by the thalamus, although their response is weaker with respect to PV-positive interneurons. Among GABAergic interneurons of the rodent neocortex, Sst-expressing cells represent one of the largest cell populations, second only to PV interneurons. It has been shown that in layer IV of the mouse S1, the majority of Sst interneurons belong to a subclass (X94) that has specific characteristics (Xu, Jeong, Tremblay, & Rudy, 2013). Their axon projections are confined mostly in layer IV and are able to fire at a higher frequency with respect to the remaining Sst interneurons. Albeit these cells are weakly driven by thalamic projections, they receive facilitating excitatory inputs from principal cells during repeated sensory stimulations. Strikingly, inhibition of Sst in layer IV leads to a decrease in firing activity in spiny neurons. This phenomenon has been explained as a disinhibition effect that arises from the strong connections between X94 and PV neurons in layer IV (Xu et al., 2013).

Whisker sensory information flow from the granular to the supragranular layer is unidirectional and mostly intracolumnar. There is a high connectivity across layers, but at the level of a singular synapse, the efficiency is relatively low, requiring the simultaneous activation of approximately 50 spiny neurons to elicit AP firing in a superficial pyramidal cell. It has been suggested that the low synaptic efficacy is employed to gate the lateral spread of sensory information within layer II/III (Lübke & Feldmeyer, 2007).

Despite the amount of anatomical and functional evidence available, a fine understanding of the role of layer IV in the whisker sensory perception is still missing, especially considering that the canonical pathway is being challenged by the emergence of new possible circuits.

In anaesthetized animals, the spontaneous activity of spiny neurons is characterized by a low firing frequency (0.58 ± 0.36 Hz in juxtasomal recording) (de Kock et al., 2007) and typical bistable slow subthreshold dynamics where the membrane potential during up states is 10-20 mV more

depolarized than during down states. In the same preparation, at the subthreshold level, all cells in layer IV have a multi-whisker receptive field, although the response increases upon stimulation of the principal whisker. However, while cells with a soma inside a barrel show a much stronger response to the principal whisker with respect to the surrounding vibrissae, septa-related cells have a more homogeneous and broader response across different whiskers. Moreover, the barrel cell response has a shortened latency (Brecht & Sakmann, 2002).

At the suprathreshold level, barrel spiny neurons respond almost exclusively to the principal whisker, narrowing their receptive field, while neurons in the septa usually fail to generate an action potential regardless of the whisker stimulated (Brecht & Sakmann, 2002; de Kock et al., 2007) (Figure 16). Among the different layers, the granular layer is one of the fastest to respond to principal whisker stimulation (de Kock et al., 2007).

In anaesthetized animals, a shared feature among all neurons in layer IV is a selectivity for the angular direction of whisker stimulation. This phenomenon has been shown both at suprathreshold (Randy M. Bruno & Simons, 2002; Simons & Carvell, 1989b) and subthreshold levels (Brecht & Sakmann, 2002). It has been proposed that this feature emerges from convergent co-tuned inputs from thalamocortical projections (Randy M. Bruno et al., 2003). Moreover, it has been shown that direction selectivity can emerge from a different timing of the window of opportunity between excitatory and inhibitory inputs. For the preferred direction, excitatory inputs anticipate inhibition by a larger margin with respect to the other direction, leading to an increased response (Wilent & Contreras, 2005).

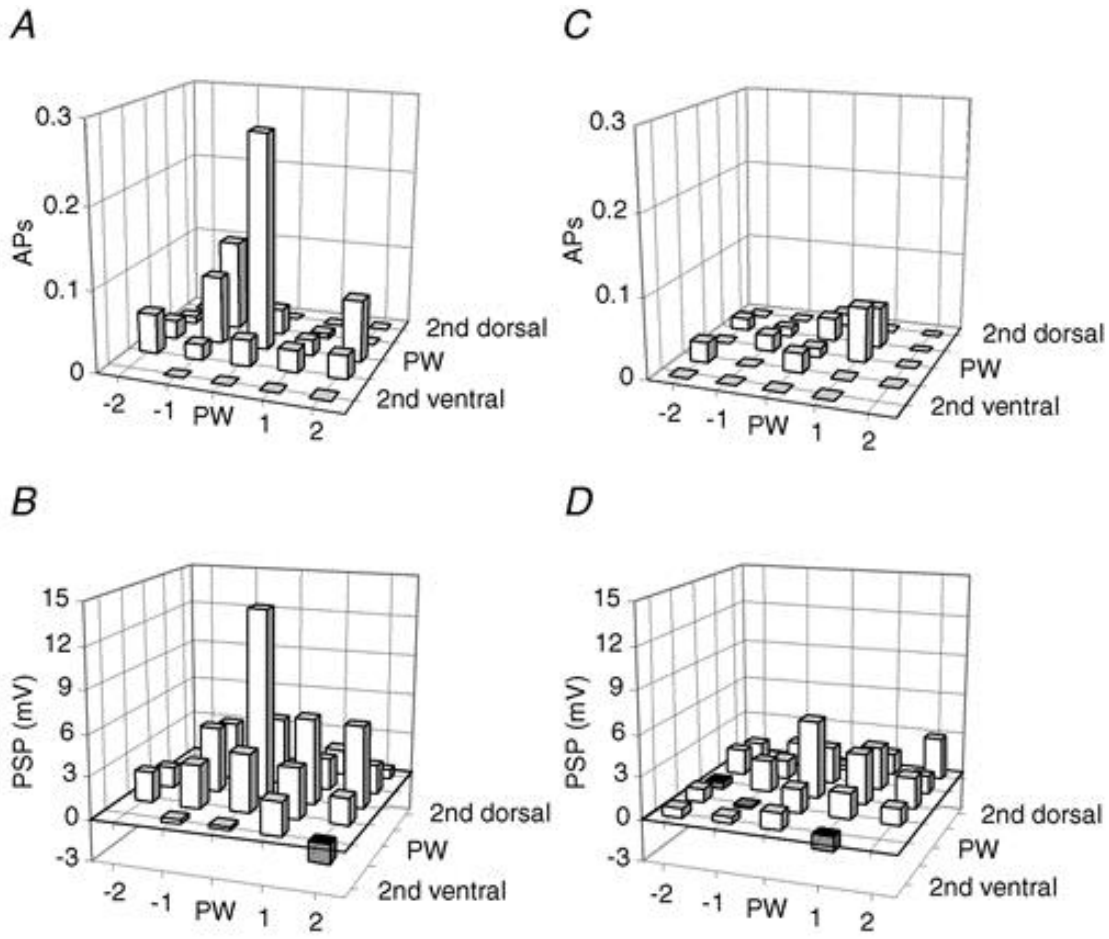

Figure 16. **Supra and subthreshold receptive field of layer IV cell in the rat barrel cortex**. **A**) Average action potentials elicited by a single whisker deflection in layer IV cells inside a barrel. The response for different whiskers are shown. **B**) As in A but showing the membrane potential dynamics. **C/D**) As in **A** and **B** respectively but recorded in a cell with the soma located in a septa. Adapted from (Brecht & Sakmann, 2002).

In a series of experiments, O'Connor and colleagues investigated the activity of the layer IV somatosensory cortex in head-restrained awake mice trained to report the location of an object in a go/no-go task using either a single whisker row or a single whisker. The mice had to either lick (go) or withhold lick (no-go) in response to a pole that could be presented in a target position out of two possible location (O'Connor, Clack, et al., 2010) (Figure 17). First, they ensured the involvement of the barrel cortex in the task by injecting muscimol, a strong GABA receptor antagonist. Indeed, mouse performance dropped to chance level during barrel inactivation. Similar results were observed by creating a lesion in the area relative to the whiskers used for the task (O'Connor, Clack, et al., 2010). In the same preparation, recordings were obtained from excitatory cells from different layers with the loose-seal juxtasomal technique. Together with layer V, layer IV

showed the highest firing activity during the task (mean 11.96 ± 16.50 Hz). In addition, these layers showed that the majority of neurons modulate their firing activity differently in relation to go or no-go trials (O'Connor, Peron, Huber, & Svoboda, 2010).

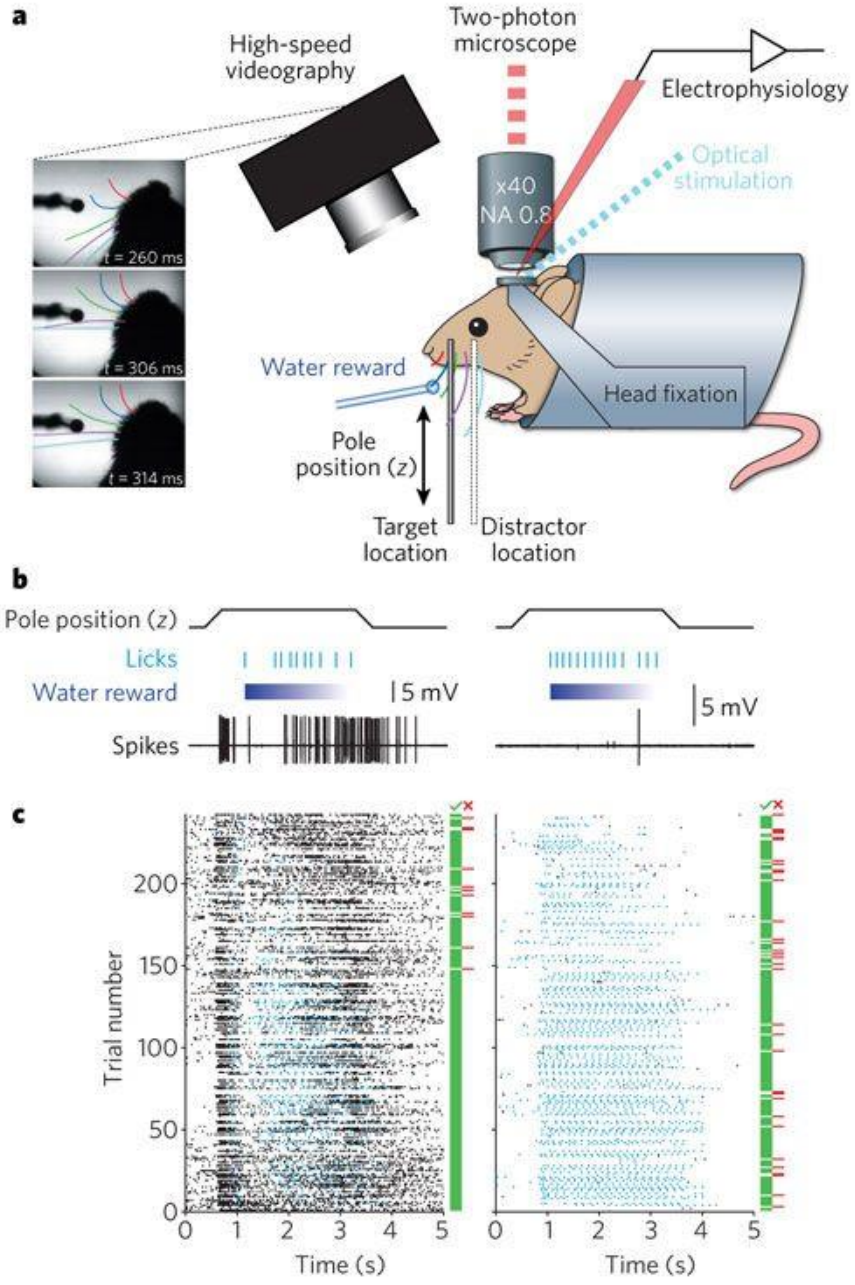

Figure 17. **Head fixed whisker object localization task in a mouse**. **a**) Setup for recording the activity of neurons during an object localization task. This configuration allows electrophysiological recording and/or imaging coupled with optical stimulation. A high speed camera is used to record whisking activity weather and a lick detector is used to score the animal choice. **b**) Two examples of neuronal spiking activity during trials showing licking events, pole presentation and water reward availability. **c**) Raster plots recorded from two cells in repeated trials (242). Both action potentials (black marks) and lick events (blue marks) are represented. Each green or red bar represents a correct or incorrect trial respectively. Adapted from (O'Connor, Huber, & Svoboda, 2009).

Moreover, in another study, the researchers investigated the coding strategy used by mice to distinguish the location of an object with a single whisker. Due to the whisking activity performed by the mice during the task, the go position led to greater touch and a larger number of spikes than the no-go position. Although layer IV cells that are responsive to pole touch have short latencies (8.7 ms) and small jitter across trials (5 ms), the evidence suggested that the animals rely more on the number of layer IV spikes elicited (spike count) rather than at what time the spike are generated (spike timing). During detection trials, optogenetic activation of layer IV principal cells is able to evoke illusory touch in trained mice, leading them to believe that the pole is in the go position in no-go trials. This effect is specific for neurons in the barrel corresponding to the trained whisker. In agreement with this finding, inhibiting the firing activity of layer IV neurons shifts the animal towards the no-go response (O'Connor et al., 2013).

A more detailed analysis of the firing activity of layer IV using same task in (O'Connor et al., 2013) has demonstrated that these cells show low firing during the baseline period (0.73 Hz) and that the firing increases in the sample epoch (1.91 Hz). During touch events, layer IV cells in the principal barrel respond with strong and temporal precise spikes. In contrast, neurons in the surrounding barrels have weaker and more irregular activity. Moreover, the firing rate of layer IV neurons is low during epochs of both whisking (0.67 Hz) and non-whisking (0.23 Hz), showing no significant differences between the two at the population level, suggesting that most of the layer IV excitatory cells spikes during this discrimination task encode for touch events rather than the whisking phase. Thus, looking only at the spiking activity of layer IV excitatory cells, it is possible to infer with good accuracy when touch events occur. This possibility is true for neurons of the principal barrel, whereas the same is not possible for the surrounding barrels (Andrew Hires, Gutnisky, Yu, O'Connor, & Svoboda, 2015).

Selective inhibition of layer IV principal cells in awake mice leads to a decrease in the suprathreshold sensory response of regular spiking layer II/III units, in agreement with predictions based on the conventional model of cortical sensory information flow. However, there is an increase in layer V suprathreshold stimulus-evoked activity. Layer IV principal cell activity has been shown to directly contact fast spiking inhibitory neurons in layer V, driving synaptic inhibition in the infragranular layer. This microcircuit is able to sharpen the sensory tuning in layer V (Pluta et al., 2015).

1.5 Layer II/III in rodent somatosensation

Layer II/III performs the role of a central hub of the cortex. Here, the whisker sensory lemniscal and paralemniscal pathways combine to generate refined sensory information that will be relayed to other cortical and subcortical regions (Lübke & Feldmeyer, 2007). Indeed, a single whisker sensory signal that arrives in layer II/III from layer IV is integrated herein with inputs from surrounding barrel columns. Sensory information is then distributed vertically within the barrel column but also across the barrel cortex and to other cortical regions by local and long-range axon collaterals of layer II/III pyramidal cells (Lübke & Feldmeyer, 2007). Layer II/III principal cells contact mostly other neurons in the same layer and infragranular neurons in layer V (Feldmeyer et al., 2013; Lübke & Feldmeyer, 2007; C. C. H. Petersen, 2007). The connectivity between supragranular layer pyramidal cells is higher for local connections and decrease along with the distance between the neurons; presynaptic activity usually elicits a low amplitude EPSP. For connections between layer II/III principal cells, axons descending to the infragranular layer form a low synaptic strength and low synaptic efficacy contact with layer Vb pyramidal neurons.

Layer II/III also receives multi-whisker information from the paralemniscal pathway through projections from layer Va principal cells preferentially contacting layer II/III cells located in the barrel septa (Bureau, Von Paul, & Svoboda, 2006; Shepherd et al., 2005). Thus, the presence of two functionally distinct populations of layer II/III pyramidal neurons has been proposed, with one receiving mostly information about whisking and touch-related information through the VPM and one receiving mostly whisking only input from the POm (Lübke & Feldmeyer, 2007).

In addition, there is a bidirectional connection between the barrel cortex layer II/III and other cortical areas, in particular S2 and M1 (Chen, Carta, Soldado-Magraner, Schneider, & Helmchen, 2013; Chen et al., 2015; Feldmeyer et al., 2013; Helmchen, Gilad, & Chen, 2018) (Figure 18). Information arising from M1 carry the motor context while S2 is more involved in choice-related signalling (Helmchen et al., 2018).

Electrophysiological and calcium imaging recordings in both anaesthetized and awake mice have permitted studies of the layer II/III response during both passive or active whisker stimulation during task performance (see Petersen & Crochet 2013 for a detailed review) . All these studies are useful to understand the role of layer II/III in the processing of sensory information. Intracellular membrane potential recordings in both anaesthetized and awake head-restrained rodents have

shown that layer II/III pyramidal neurons present large subthreshold responses to whisker stimulation (Brecht, Roth, & Sakmann, 2003; Crochet & Petersen, 2006; Crochet, Poulet, Kremer, & Petersen, 2011; Poulet & Petersen, 2008; Sachidhanandam, Sreenivasan, Kyriakatos, Kremer, & Petersen, 2013). Indeed, juxtasomal recordings have demonstrated that the layer II/III suprathreshold response to whisker stimulation is low compared with the deeper layers in both anaesthetized and awake head-restrained animals during passive whisker stimulation or while performing an object location task (de Kock et al., 2007; O'Connor, Clack, et al., 2010). In particular, the sensory-evoked spiking activity of layer II/III excitatory neurons was found to be intermingled, and moreover, most of the spikes were generated in a small subset of highly active cells, while the majority of cells remained silent (Crochet et al., 2011; O'Connor, Peron, et al., 2010). Indeed, the mean AP firing rate of layer II/III neurons for active whisking against a pole during an object location task was 3.0 Hz, while the median firing rate was approximately 0.2 Hz, the lowest found across layers (excluding layer I) (O'Connor, Peron, et al., 2010). Similar results during active touch were also found in whole-cells recordings (Crochet et al., 2011).

Thanks to the improvement of imaging techniques, it was possible to monitor the activity in 75% of superficial barrel cortical neurons in awake mice during an object location (Peron et al., 2015). This imaging study revealed the presence of distinct subclasses of layer II/III responsive neurons: indeed, layer II/III principal neurons showed activity related to behavioural aspects such as whisking and touch. The number of touch-responsive cells decreased in the surrounding columns, while that of whisking-responsive cells was unchanged. However, neurons from different subclasses were spatially intermingled. Similar results were also found during a texture discrimination task (Chen et al., 2013).

This sparse and intermingled distribution of layer II/III neurons that are responsive to different tactile features seems to indicate the presence of differently tuned cells (C. C. H. Petersen & Crochet, 2013). Indeed, the spatial organization of layer II/III neurons based on a preference for the directions of the whisker deflections was observed in rodents: neurons with a similar angular preference appeared to be spatially clustered within a single barrel column (Andermann & Moore, 2006; Kremer, Leger, Goodman, Brette, & Bourdieu, 2011). This preference map seems to appear late during postnatal development since it was not present in immature animals (Kerr et al., 2007; Kremer et al., 2011). A recent two-photon imaging study has shown that orientation-specific

neuronal responses in layer II/III are organized in a locally heterogeneous salt and pepper distribution (Kwon, Tsytsarev, Erzurumlu, & O'Connor, 2018).

The advent of retrograde tracers has permitted the study of the functional properties of layer II/III excitatory neurons based on their projecting targets (Helmchen et al., 2018). Barrel cortex layer II/III pyramidal cells project to either M1 or S2 to form two populations with little overlap, and in behaving animals, they seems to have different properties (Chen et al., 2013). These two classes, S1-S2 and S1-M1 projection neurons, present different intrinsic electrophysiological (Yamashita et al., 2013) and different functional responses during behavioural tasks (Chen et al., 2013). Both classes present touch-responsive neurons but whisking-responsive cells are absent in the S2 projecting neurons. M1 projecting neurons have a multi-whisker receptive field, and their activity is strongly associated with whisker stick-slips events (Chen et al., 2013; T. R. Sato & Svoboda, 2010). In passive deflection preparation, they have a strong and fast response that adapts rapidly after repetition of the stimulus (Yamashita et al., 2013). It is hypothesized that they are involved mostly in touch detection, object localization and, along with neurons in M1, in the generation of a whisking strategy when the animal touches a novel object (Bale & Maravall, 2018). In contrast, layer II/III cells projecting to S2 seem to have narrowed receptive fields and to show a prolonged depolarization in response to whisker stimulation (Clancy et al., 2015; T. R. Sato & Svoboda, 2010). In opposition to the other population, their activity is sustained upon continuous interaction with an object and, in the awake whisker detection task, to correlate with the animal's choice (Chen et al., 2013; Kwon et al., 2016). Therefore, they are likely to play a role in object feature discrimination (Bale & Maravall, 2018).

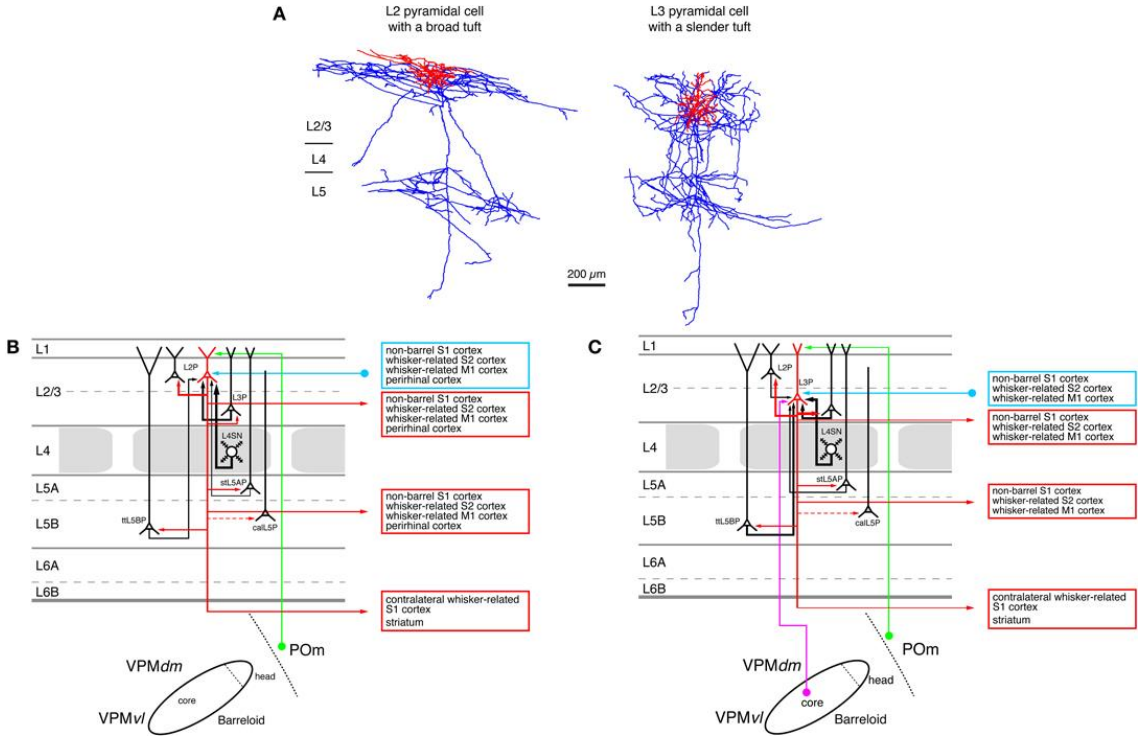

Figure 18. **Excitatory connections of layer II/III principal cells in the rat barrel cortex. A**) Morphological reconstruction of two pyramidal cells in barrel cortex layer II/III, one located in the upper part (left) and the other in the lower part of the layer (right). Dendrites are coloured in red, while axons are in blue. **B**) Simplified schematics of the excitatory input and output of a layer II pyramidal cells. **C**) Same as in **B** but for a pyramidal cell in layer III. Adapted from (Feldmeyer, 2012).

Moreover, in primary visual cortex it has been shown that cholinergic and adrenergic inputs, which vary with the arousal level of the animal, can strongly influence layer II/III neurons (Polack, Friedman, & Golshani, 2013). Therefore, the whisker stimulus response in superficial layers is influenced by and, in turn, influences the activity of an extended portion of the neocortex, integrating not only sensory-related but also contextual information (Quiquempoix et al., 2018).

The low spiking response of layer II/III excitatory neurons to whisker stimulation was hypothesized to be due to inhibition within layer II/III (C. C. H. Petersen & Crochet, 2013). Indeed, in a single barrel, there are approximately 1,800 principal cells in layer II/III, and approximately 15% of the neurons in -layer II/III are GABAergic (Lefort et al., 2009; Peron, Freeman, Iyer, Guo, & Svoboda, 2015). Across interneurons, the largest group is represented by 5HT3aR-expressing cells, whereas PV and Sst cells account for approximately 30% and 20%, respectively. PV-expressing cells show the highest firing rate during quiet wakefulness, followed, in order, by Sst and 5HT3aR-expressing neurons; however, all of them are well above layer II/III principal neurons (Gentet, Avermann,

Matyas, Staiger, & Petersen, 2010; Gentet et al., 2012). During whisking, PV and Sst firing is reduced, whereas 5HT3aR-expressing neuron firing increases. It is known that M1 neurons strongly innervate VIP interneurons, to a greater extent than other type of cell in the barrel cortex, and therefore M1 activation during whisking behaviour can explain the different activity between classes of interneurons. Furthermore, 5HT3aR-expressing cells strongly inhibit Sst neurons, which may be the reason for the opposite behaviours during whisking between the two, albeit this is not true for PV. It has been suggested that the low and sparse firing rate of pyramidal neurons in superficial layers in response to whisker stimulation is due to a strong activation of inhibitory neurons. Indeed, whisker stimulation increases the firing rate of both PV and 5HT3aR neurons, leading to much higher AP firing than in pyramidal neurons (C. C. H. Petersen & Crochet, 2013). In visual cortex, Sst show a different behaviour that is distinct from the other class, as they seem to receive little excitatory input from layer IV (Adesnik, Bruns, Taniguchi, Huang, & Scanziani, 2012). Moreover, the connection between principal cells and interneurons in superficial layers is dense and strong (Holmgren, Harkany, Svennenfors, & Zilberter, 2003). While there is an approximately 17% probability of finding a connection between pyramidal cells with EPSP of approximately 0.4 mV, pyramidal cells connect with PV interneurons with a much higher probability (58%) and an average EPSP of 0.8 mV. The values for pyramidal to 5HT3aR-expressing cells are, respectively, 24% and 0.4 mV (Avermann, Tomm, Mateo, Gerstner, & Petersen, 2012). The main targets for superficial PV cells are excitatory cells and other PV interneurons, with a connectivity rate of 60% and 55%, respectively (Avermann et al., 2012). The connections between PV and principal cells in both directions are faster than between layer II/III pyramidal cells (C. C. H. Petersen & Crochet, 2013). Principal neurons in L II/III contact Sst interneurons with a probability of 29%, with each synapse generating a low amplitude EPSP (Kapfer, Glickfeld, Atallah, & Scanziani, 2007). However, facilitation of responses in excitatory synapses to Sst-expressing cells has been shown during high frequency stimulation of principal cells (C. C. H. Petersen & Crochet, 2013) (Figure 19).

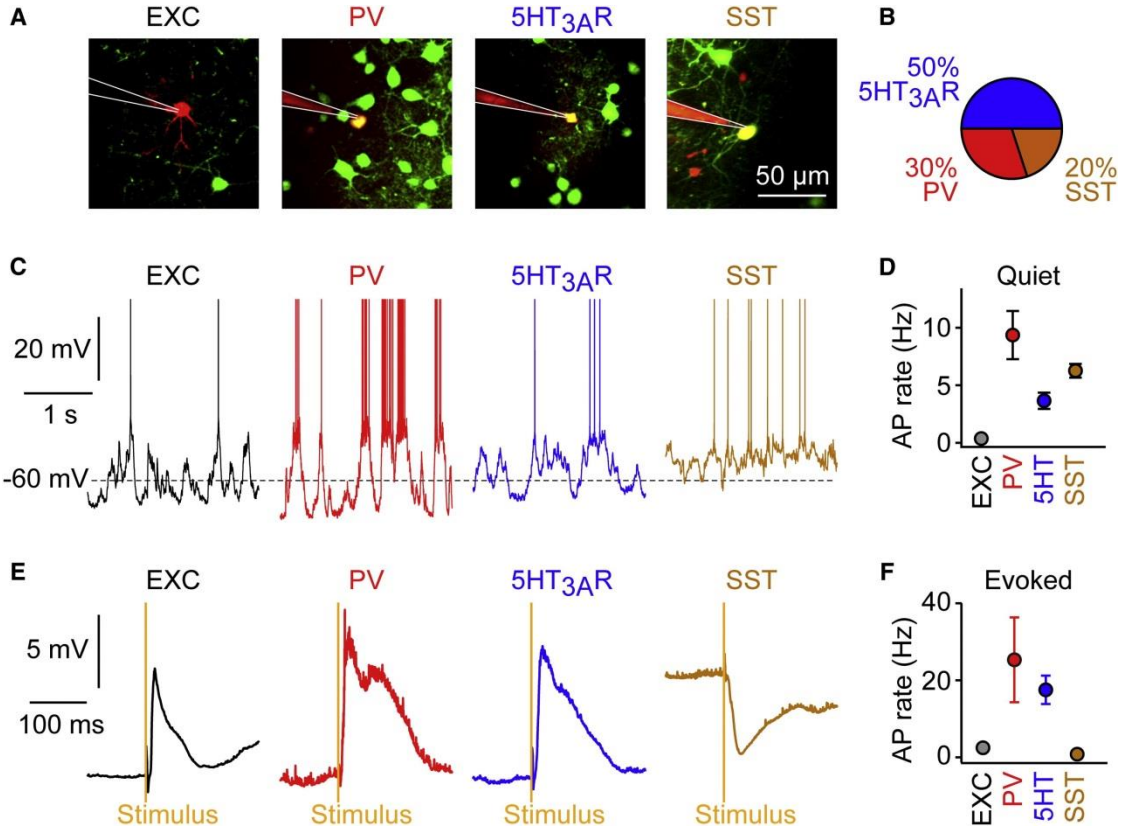

Figure 19. **Activity of layer II/III neuron subtypes in awake head-restrained mice. A**) Two-photon targeted patch-clamp recordings in both excitatory and inhibitory cells of the mouse barrel cortex layer II/III. **B**) Approximate fractions of the genetically identified subpopulation of GABAergic interneurons in the layer II/III mouse barrel cortex. **C**) Representative trace of spontaneous activity recorded in the whole cell configuration for each cell type represented in **A** during quiet wakefulness. **D**) Quantification of the average firing rate during quiet wakefulness. **E**) Average of the evoked postsynaptic potential during passive whisker deflection. **F**) Quantification of the average firing rate evoked by whisker deflection at 50 ms after the stimulus. Adapted from (C. C. H. Petersen & Crochet, 2013).

1.6 Genetic tagging of specific cortical layers

The cerebral cortex forms a complex and accurate network of myriads of connections between a wide variety of neurons. These connections are highly organized in a way that there is specificity for brain area, layers, columns and cell type. Moreover, at the level of the single cell, there is even greater complexity that must still be better understood to justify the observed anatomical evidence. To dissect the cortical network organization, it is fundamental to target and investigate specific subpopulations of neurons, which are the basic components of neural circuits. This goal can be achieved by linking neurons to molecules that allow either to monitoring or manipulating the cells and their activities. Fluorescent proteins are the most used reporters to tag *in vivo*

neurons of interest. Fluorescent reporters offer high sensitivity with low invasiveness and can be visualized almost instantaneously. Moreover, molecules with different wavelength of emission can be used simultaneously, thus increasing the power of the technique (Kremers, Gilbert, Cranfill, Davidson, & Piston, 2011). To achieve selectivity, however, it is fundamental to be able to target specific subpopulations of cells.

One possibility is to use in utero electroporation, which is able to target cortical neurons of a specific layer *in vivo*. This technique exploits the sequential layer-by-layer development of the mammalian neocortex. In utero electroporation consists of the intrauterine injection of plasmid solution, containing the sequence for the tag of interest, in embryos, while short pulses of current are applied. The electric field disrupts the continuity of the cell membrane, allowing the plasmids to enter the progenitor cells. Performing this technique at different developmental stages results in differently marked layers. Due to constraints in manipulating early embryos, this technique has mostly been used to target superficial layer II/III (Adesnik et al., 2012; Beltramo et al., 2013; Petreanu, Huber, Sobczyk, & Svoboda, 2007; Saito & Nakatsuji, 2001).

Currently, advances in molecular genetics allow the insertion of DNA with high fidelity in subpopulations of cells with site-specific recombinase technology. Cre and Flp are the most used recombinase, and they share the same working paradigm consisting of three stages: cleavage, exchange and ligation. The proteins recognize pairs of specific DNA sequences, namely, loxP for Cre and FRT for Flp, and recombine DNA between the two target sequences (Figure 20). Different configurations of the recognition sites can be used to achieve excision, integration or inversion of a segment flanked by target sequences (Branda & Dymecki, 2004). By expressing DNA coding for the recombinases under a cell-specific promoter, it is possible to affect specific neuronal populations.

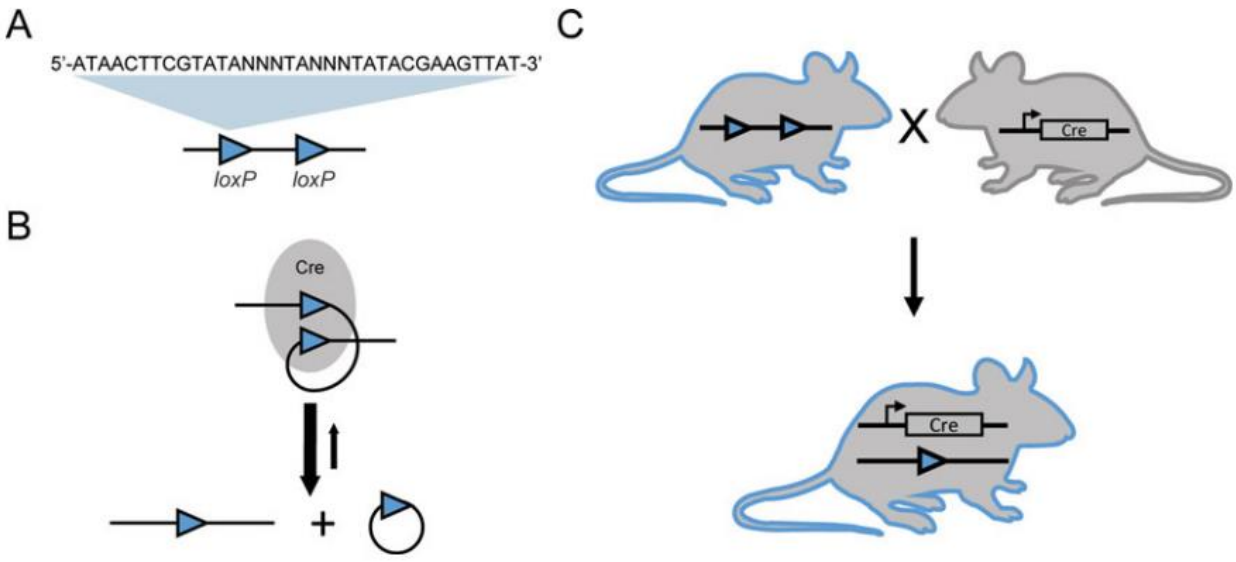

Figure 20. **The Cre-loxP expression system. A**) Amino acid sequence of the loxP motif. **B**) Cre-recombinase recognizes two contiguous loxP sequences and excises the intervening DNA. Based on the orientation of the loxP sequences, different outcomes can occur, either insertion/excision or inversion. In the presented case, the reaction is reversible because two identical loxP sequences are used, resulting in a functional sequence after the Cre activity. **C**) Breeding protocol for generating filial mice with a specific excision of DNA. If a stop codon is targeted, the downstream gene is expressed. Adapted from (McLellan, Rosenthal, & Pinto, 2017).

When the recombinase DNA sequence is expressed in the germline, the mutation is passed down to filial generations to create transgenic mouse lines. The protein sequence can be integrated in the animal genome either randomly or in a targeted way (knock in). In the former modality, the integrated sequence also include a promoter that will regulate the expression of the recombinase. However, the method cannot control the site of insertion and the number of inserted copies, which may create a different profile of expression with respect to the endogenous promoter. In the knock-in techniques, in contrast, the sequence is integrated downstream of the endogenous promoter, resulting in concurrent production of the promoter and recombinase transcripts. This strategy increases the selectivity of the method but may disturb the expression of the endogenous gene. Recently, many mouse lines expressing recombinase with cell specificity have been developed and characterized, while new lines are being generated (Gerfen, Paletzki, & Heintz, 2013; Gong et al., 2007; J. A. Harris et al., 2014; Madisen et al., 2010; Taniguchi et al., 2011) (Figure 21). The breeding of different Cre-lines with reporter lines expressing reporter genes conditionally is a common method that allows easy, high specificity labelling with the advantage of relatively homogeneous expression of the reporter. Moreover, Cre-lines are used in combination

with techniques of transfection of Cre-dependent DNA sequences, e.g., injections of recombinant viral vectors, which allows for even more spatial and temporal selectivity.

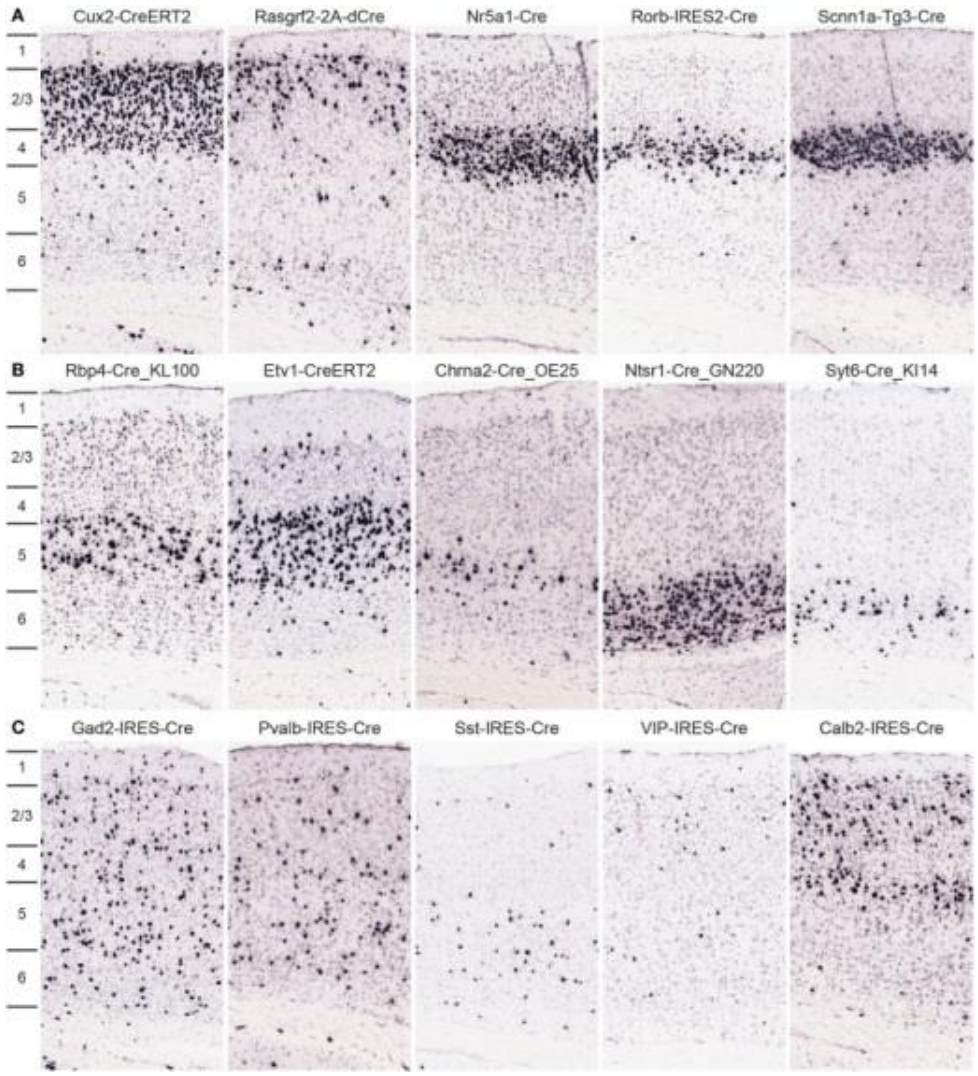

Figure 21. **Cre-lines allow the targeting of genetically identified subpopulations of neurons and interneurons**. **A/B**) Representative images of the conditional expression of tdTomato in different mouse lines expressing Cre recombinase selectively in distinct cortical layers. From top left to bottom right: Cux2-CreERT2 and Rasgrf2-2A-dCre expressing Cre-recombinase preferentially in layer II; Nr5a1-Cre, Rorb-IRES2-Cre and Scnn1a-Tg3-Cre expression in layer IV; Rbp4-Cre_KL100, Etv1-CreERT2 and Chrna2-Cre_OE25 targeting layer V; Ntsr1-Cre_GN220, Syt6-Cre_KI14 for layer VI. **C**) Same as in **A/B** in different mouse lines where the Cre-coded sequence is under interneuron marker promoters: Gad2-IRES-Cre, Pvalb-IRES-Cre, Sst-IRES-Cre, VIP-IRES-Cre and Calb2-IRES-Cre. Adapted from (J. A. Harris et al., 2014).

1.7 Optically targeted recordings

Single cell electrophysiological recordings are powerful methods to understand neuronal properties, as they provide direct information about both suprathreshold and subthreshold cell activity. Moreover, they are extensively used in all preparations, from cell cultures to *in vivo* animal behaviour studies. *In vivo*, both whole-cell and juxtasomal recordings are mostly performed in a "blind" configuration, where the pipette is inserted and advanced in the tissue without *a priori* control of the cell type recorded. Thus, cells that are scarcely present in the medium or particularly difficult to approach due to a small size or other morphological features may be less represented in the recordings. The neocortex contains a wide range of anatomically, genetically and functionally distinct neuronal population (Lodato & Arlotta, 2015). Moreover, even if different cell types have distinct observable characteristics during electrophysiological recordings, to obtain accurate information about the location, morphology and identity, the targeted cells need to be reconstructed *a posteriori*. This is usually achieved by filling the cell with biochemical tracers that will be immunostained and analysed after fixation of the tissue. These procedures may require a waiting period of days after the experiment has been performed. Techniques that tag a fluorescent molecule to specific subpopulations of cells overcome this problem, allowing the direct identification of the cells of interest. Moreover, they allow the targeting of cells based on different properties, which has been essential for the advancement of neurophysiological studies. It has become possible to target axons to identify cells based on their projection profiles or to express fluorochromes under a specific promotor to mark genetically identified subpopulations. It is also possible to observe wide spread fluorescence across cells and to select a small group based on their activity. Mouse lines are available that already express fluorescent markers selectively in different population of cells, or alternatively, it is possible to induce selective expression using the site-specific recombinase system (discussed in the previous chapter).

Optically, the rodent brain is an electron-dense highly scattering medium (W Denk & Svoboda, 1997), meaning that light is unable to penetrate it with enough power to excite a fluorochrome and allow it to be visualized. Light scattering, however, is inversely proportional to the light wavelength: short wavelengths scatter more than longer wavelengths. Therefore, red-shifted light is favoured for imaging at greater depths of the intact brain, but longer wavelengths have lower energy. Thus, a fluorophore needs more than one photon to be excited by longer wavelengths. Two-photon excitation was first described by Goeppert-Mayer in 1931 (Göppert-Mayer, 1931) and

observed by Kayser with the introduction of the first high-power lasers in 1961 (Kaiser & Garrett, 1961). It was finally applied to microscopy in 1990 (Winfried Denk, Strickler, Watt, & Webb, 1990) and is one of the most advanced technique to visualize deep structures in the brain *in vivo*. Mode-locked laser sources that emit high-peak power ultrashort pulses (~140 fs duration) with a fast repetition rate (~80 MHz) are required for two-photon excitation because the absorption of two photons must occur almost simultaneously (10-15 s) to sum their energy (Dal Maschio, Beltramo, De Stasi, & Fellin, 2012) (Figure 22). An advantage of two-photon excitation is that a significant absorption probability is reached only in the focal plane where the light is focused, reducing out-of-focus fluorescence and endowing two-photon microscopy with an intrinsic "confocal nature". Since excitation occurs only in the focal plane, this technique reduces the out-of-focus photobleaching and photodamage present in single-photon microscopy (Svoboda & Yasuda, 2006). Even if the peak power of the laser source is high, the average power is low due to the short pulses, further reducing additional photodamage (Dal Maschio et al., 2012).

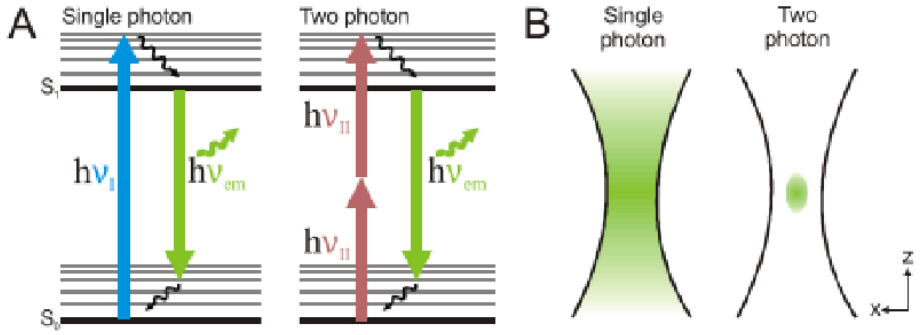

Figure 22. **Principle of two-photon excitation. A**) A simplified Jablonski diagram showing the transitions of an electron through two energy levels following the absorption of either a single or two photons. **B**) Difference in the excitation volume of single and two-photon excitation. Single-photon excitation shows a strong out-of-focus contribution, while two-photon absorption is confined to the focal plane. Adapted from (Dal Maschio et al., 2012).

Overall, this approach extends the deep fluorescence imaging from approximately 100-200 µm of single-photon imaging up to approximately 1000-µm deep with sufficient spatial resolution to visualize even subcellular structures such as dendrites and axons.

In two-photon targeted recordings, electrodes are usually filled with a fluorescent dye to visualize them. This procedure allows for a fine control of the position of the pipette with respect to the cell, increasing the success rate and making it possible to choose where to record from, such as

the soma, dendrites or axon of the targeted cell (Häusser & Margrie, 2014). In this regard, two-photon imaging has been combined with synthetic dyes, transgenic animals, viral vectors or shadow patching to visualize both the recording pipette and the targeted cells (Komai, Denk, Osten, Brecht, & Margrie, 2006; Tao, Zhang, Xiong, & Zhou, 2015) (Figure 23). Briefly, in the shadow patching method, a fluorescent dye, which is unable to pass the cellular membrane, is perfused into the medium, lighting up the extracellular space and making the neuron visible as a negative contrast image with respect to a bright background. This process obviates the necessity for the pre-labelling of neurons (Kitamura, Judkewitz, Kano, Denk, & Häusser, 2008).

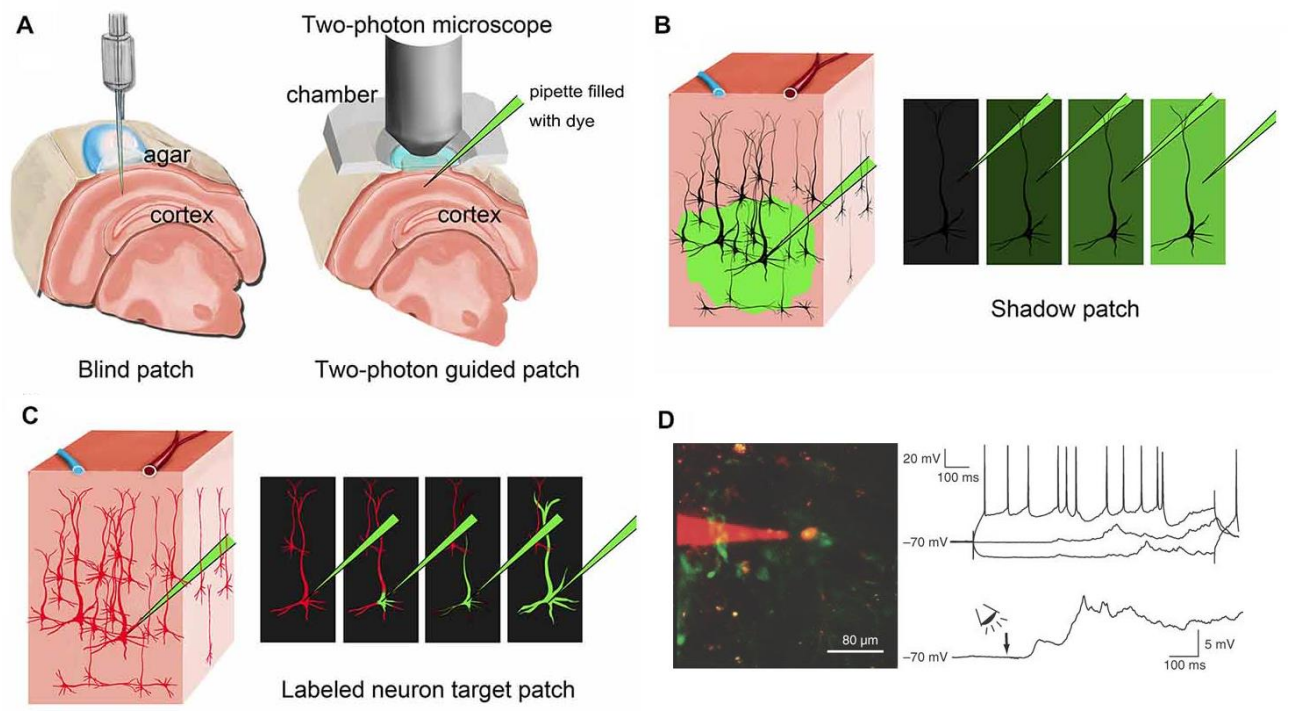

Figure 23. **Two-photon guided electrophysiological recordings. A**) Cartoon of the setup configuration for the blind (left) and two-photon-guided (right) patch clamp recordings. **B**) Schematic of the shadow patch method targeting unlabelled neurons. **C**) Schematic of visually guided whole-cell recordings targeting a genetically identified population of neurons. **D**) Left, image of a successful visually guided whole-cell recording. The green GFP-expressing neuron is turned yellow by the red fluorescent dye filled in the cell. . Right, firing activity of the recorded cell during current injection (top) and the sensory stimulus (bottom). **A-C** adapted from (Tao et al., 2015), **D** adapted from (Komai et al., 2006).

Two-photon targeted recordings have been used *in vivo* for reporting the activity of specific cell types, such as genetically identified principal cells or interneurons.

1.8 Optogenetic manipulations

Investigation of the role and involvement of specific populations of neurons in any network activity, e.g., sensory perception or behaviour, requires the ability to modulate cells with a high level of temporal precision and cellular selectivity, leaving unselected cells unaffected. Pharmacological approaches used in the past have lacked the temporal control to achieve this goal, in which electrical stimulation usually extends its effect over a broader area without cellular selectivity.

Optogenetics is a technique that allows bi-directional manipulation in a selected subpopulation of neurons with millisecond temporal precision and relatively low invasiveness *in vivo.* It was developed by the Deisseroth lab in 2005, and it combines both optical and genetic methods to achieve spatial and temporal selectivity, hence the name (Boyden, Zhang, Bamberg, Nagel, & Deisseroth, 2005). The technique exploit tree principal components: proteins that are able to generate electrical activity rapidly in response to light, molecular techniques that grant the specificity of expression of those proteins in genetically identified classes of neurons, and optical systems to shine light in distinct brain areas.

Opsins can modulate neuron membrane potential in response to light. They belong to the class of seven-transmembrane receptors and are linked to retinal, a chromophore that grants them light sensitivity. Retinal, in fact, after exposition to photons, goes through isomerization that cause conformational changes in the opsin (Chow, Han, Bernstein, Monahan, & Boyden, 2011). This family is divided in two class, type I and type II. Type II opsins are used by animals and are members of the G-coupled protein receptors, sharing with them the slow dynamics of their working pathway. Type I, or microbial opsins, can be found in algae, fungi and prokaryotes and are either light-activated ion channels or ion pumps. Therefore, they are able to swiftly modulate the ionic concentration inside the cell membrane potential, granting rapid control of neuronal activity (Zhang et al., 2011). Even if Type I opsins are not endogenous in the *animalia*, each opsin is encoded by a single short gene (less than 1 kb), allowing the expression of the protein in mammalian neurons using many transfection techniques. Moreover, retinal is already present in neurons in sufficient amounts for the opsin to function (Deisseroth et al., 2006; Zhang, Wang, Boyden, & Deisseroth, 2006). There are different opsins available in nature, each with particular ion selectivity and absorption spectra, and new forms are being discovered or engineered

(Cosentino et al., 2015; Gradinaru, Thompson, & Deisseroth, 2008; J. Y. Lin, Knutsen, Muller, Kleinfeld, & Tsien, 2013; Zhang et al., 2008). This variety allows for either depolarization or hyperpolarization of the neuron membrane potential with specific temporal dynamics and photocurrent amplitudes. Opsins with sufficient spectral separation and sensitivity allow the independent activation of different cell populations (Prigge et al., 2012). The most used type I opsins in optogenetics are the excitatory channelrhodopsins (ChRs) and the inhibitory halorhodopsin (NpHR) and bacteriorhodopsin (BR) (Boyden, 2011) (Figure 24).

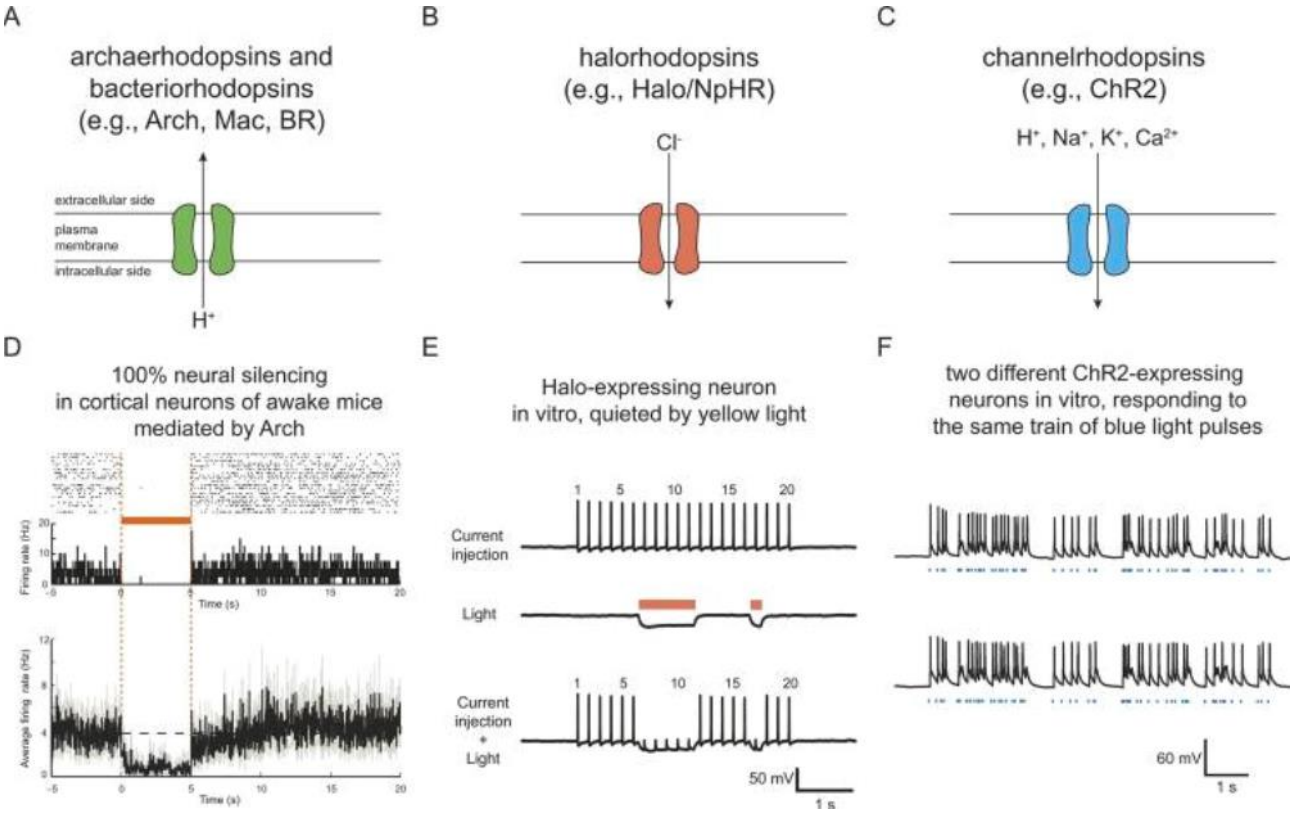

Figure 24. **Classes of type I microbial opsins. A-C**) Representation of the working principle of the most used classes of opsins in optogenetics: bacteriorhodopsins (**A**), halorhodopsins (**B**), and channelrhodopsin (**C**). **D**) In response to light (orange bar) bacteriorhodopsins is able to suppress the spiking activity of neurons. **E**) Same as in **D** but in halorhodopsins expressing neurons. **F**) Contrary to the inhibitory opsins, channelrhodopsin is able to evoke reliable action potential generation in response to light (blue bar). Adapted from (Boyden, 2011).

Channelrhodopsins are non-specific light-gated inwardly rectifying cation channels that were discovered in unicellular algae. In these organisms, channelrhodopsins couple light sensory information to flagellar motion. When stimulated with light, this channel allows passive diffusion

of H^+, Na^+, K^+, and Ca^{++} ions through the cell membrane down the electrochemical equilibrium. Channelrhodopsin 2 (ChR2) was the opsin used in the first published work and is currently extensively used in every optogenetic laboratory (Boyden et al., 2005; Gradinaru et al., 2007; Zhang et al., 2007). ChR2 along with a proton-permeable channel, ChR1, were discovered in a unicellular green alga, *Chlamydomonas reinhardtii* (Nagel et al., 2003). The absorption spectra of ChR2 is approximately 480 nm, and short pulses of blue light are able to elicit a current up to 1000 pA and AP firing in ChR2-expressing neurons (Deisseroth et al., 2006). C1V1 is a variant excitatory opsin that has the advantages of working with a longer wavelength with respect to ChR2 (Yizhar, Fenno, Davidson, Mogri, & Deisseroth, 2011). It is a chimeric product of ChR1 and a channelrhodopsin found in *V. carteri* (VChR1). VChR1 is activated by longer wavelengths with respect to ChR2 but is unable to induce a strong photocurrent (Zhang et al., 2008). To improve its conductance, it has been combined with ChR1. Moreover, the coding sequence of ChR2 has been engineered to modify the performance of the opsin, widely extending the range of applications of this tool, e.g. it is now possible to choose between channels with faster closing kinetics than the native protein (from ~10 to ~4 ms) or kinetics that are so slow they require up to 30 minutes to close unless yellow light is administered (Yizhar et al., 2011). By engineering the ChRs channel to conduct mostly Cl^- ions it is possible to convert ChRs from depolarizing to mostly hyperpolarizing opsins, although these proteins show some limitations (such as limited light sensibility and small retained cation conductance) (Berndt, Lee, Ramakrishnan, & Deisseroth, 2014; Wietek et al., 2014). However, in 2015 (Govorunova, Sineshchekov, Janz, Liu, & Spudich, 2015) presented two natural light-gated anion channel rhodopsins with high performances and fast kinetics, resulting in a valuable tool for photosuppression of neuronal action potentials (Forli et al., 2018; Govorunova et al., 2015; Mardinly, Oldenburg, & Pégard, 2018).

In contrast to ChRs, both NpHR and BR are active electrogenic pumps that are used to silence neuronal activity. In particular, NpHR is a chloride pump that transports Cl^- ions into the cytoplasm in response to stimulation with yellow light (~580 nm) and is indeed able to efficiently suppress the generation of an AP (Zhang et al., 2007). This protein was discovered in the archaea *Natronomas pharaonis* and over the years has been improved to the version that is now commonly used (eNPHR2.0 or eNPHR3.0). When first tested, NpHR used to accumulate in the endoplasmic reticulum or Golgi apparatus due to problems with the membrane trafficking system (Gradinaru et al., 2008). In the latest version, this problem has been resolved by the co-expression of Kir 2.1 ER export and neurite trafficking motifs, improving membrane localization (Gradinaru et

al., 2010). Moreover, the enhanced version shows increments in the generated photocurrent and reliable photoinhibition of firing activity in different types of neuronal populations.

The last main class of microbial opsin used in optogenetics comprises the bacteriorhodopsins, which, similarly to NpHR, can inhibit neuronal activity in response to yellow light (~561 nm) (Chow et al., 2010). The most used opsin among BR is Archaerhodopsin-3 (Arch), which was discovered in the archaea *Halorubrum sodomense*. Arch, in contrast to the previous group, hyperpolarizes the cell membrane by pumping protons into the extracellular space, and moreover, with respect to NpHR, shows higher photocurrents and faster dynamics (~900 pA *in vitro*) (Chow et al., 2010). Recently, a new opsin derived from *Halorubrum* strain TP009 has been reported. This new opsin, named Arch T, has an increased ability to silence neuronal activity due to an enhanced sensitivity to light (Han et al., 2011).

Type I opsin provides the ability to manipulate neurons with high temporal resolution, but the spatial selectivity is achieved by the other two main components of optogenetics: molecular tools to target genetically identified subpopulation of cells, and optical methods to illuminate confined brain areas. Viral expression systems are widely used to convey opsin-coding sequences inside neuronal populations. This method has been shown to be successful in mice, rats and primates (Zhang et al., 2010). In rodents, it is possible to inject viruses into deep structures with relative minimal invasiveness. The two principal viruses used are adeno-associated viral vectors (AAVs) and lentiviruses, both of which can efficiently infect neuronal populations, leading to stable and long-term expression. However, since AAVs are not pathogenic by themselves, they are usually preferred to lentiviruses for safety reasons. Moreover, AAVs usually provoke a reduced immune response with respect to lentiviruses. Regulating the amount of virus and the location of the microinjection permits a certain degree of spatial confinement that can be further increased by linking the expression of the opsin under selective promoters. There are a wide range of AAV serotypes to choose from with distinct tropisms and various degrees of either anterograde or retrograde axonal transport ability. It is important to consider, however, that even if minimal, viral injection leads to a response from the immune system that can modify the regular physiological activity and lead to potential brain tissue damage at a local level. To further increase the level of expression and its spatial constraints, AAV transfection can be coupled with the Cre-loxP system described in the previous chapter.

Spatial selectivity can be improved on a different level by restricting the illumination to the area of interest. Different optical approaches have been used for this purpose, and for broader areas, simply focusing the light can suffice. In contrast, up to almost single-cell resolution can be achieved with either single-photon or two-photon patterned optical stimulation stimulation (Forli et al., 2018; Vaziri & Emiliani, 2012; Zhu, Fajardo, Shum, Zhang Schärer, & Friedrich, 2012). Moreover, optical fibres or endoscopes can be used to investigate areas located deep in the brain that are unreachable via direct light above the skull.

2 Rationale and aim

Whisker tactile information is generated in the follicles of the mouse snout and travels through the trigeminal ganglion, the brainstem, and the thalamus to reach the primary somatosensory cortex (Feldmeyer et al., 2013; C. C. H. Petersen, 2007). The canonical model posits that within this latter cortical region, thalamic afferents contact primarily layer IV neurons. In layer IV, sensory inputs are pre-processed and transferred to supragranular layer II/III, where they are integrated with other cortical and extracortical inputs (Feldmeyer, 2012). Despite the great amount of input it receives, layer II/III is characterized by sparse firing activity and unreliable sensory evoked responses, with a small fraction of highly active neurons accounting for the majority of the stimulus-evoked spikes (Barth & Poulet, 2012; de Kock et al., 2007; Kerr et al., 2007; Lefort et al., 2009; O'Connor, Peron, et al., 2010; C. C. H. Petersen & Crochet, 2013). These processes suggest that the large part of information integration and processing is performed at the subthreshold rather than at the suprathreshold level. Recent findings, however, suggest a more complex scenario for the processing of sensory information in primary sensory areas of the cortex compared with the one stated by the canonical model (Constantinople & Bruno, 2013). For example, thalamic fibres directly contact layer V neurons and send excitatory inputs to supragranular layer II/III (Constantinople & Bruno, 2013; Feldmeyer, 2012; Lefort et al., 2009; Meyer et al., 2010). How the information entering layer II/III from the multiple pathways is integrated at the subthreshold level is still unclear. To address this open question, this thesis work is focused on the information concerning specific features of the sensory stimulus that is broadcasted to layer II/III from one main thalamocortical layer, i.e., layer IV.

We performed *in vivo* patch-clamp recordings in layer II/III pyramidal cells during whisker stimulation in anaesthetized animals while optogenetically inhibiting layer IV principal cells during tactile sensation. We found that, during whisker deflection, layer IV optogenetic suppression did not completely block subthreshold sensory-evoked responses in layer II/III. Moreover, complete silencing of the barrel cortex by optogenetic stimulation of interneurons during whisker stimulation largely suppressed the subthreshold whisker response in supragranular layers. Finally, we found that layer IV activity was required for the direction tuning of layer II/III pyramidal cells. Based on these results, we propose a major revision of the canonical model, in which layer II/III receives sensory information from at least two main thalamocortical receiving layers, layer IV and

layer V. These two sensory pathways carry distinct information about the sensory stimulus with information about the stimulus direction travelling mostly through layer IV.

3 Materials and methods

3.1 Animals

Experimental protocols involving animals were approved by the IIT Animal Health Regulatory Committee and the National Council on Animal Care of the Italian Ministry of Health. The experiments were conducted in according to the guidelines of the National legislation and the European Communities Council Directive. The mouse lines Scnn-Cre (B6;C3-Tg(Scnn1a-cre)3Aibs/J, stock #009613) and PV-Cre (B6;129P2-Pvalb$^{tm1(cre)Arbr}$/J stock # 008069), were crossed with either the TdTom reporter line (B6;129S6-Gt(ROSA)26Sor$^{tm14(CAG-TdTomato)Hze}$/J, stock #007908) or with C57 (C57BL/6 J stock #000664). Scnn-Cre, PV-Cre and TdTom mouse lines were purchased from the Jackson Laboratory (Bar Harbor, USA), while the C57 mouse line was purchased from Charles River (Calco, IT). The experiments were performed in juvenile mice (4-10 weeks old, either sex) group housed in singled ventilated cages (maximum 5 animals/cage, divided by sex) and maintained under a 12:12 light-dark cycle with ad libitum access to food and water. Histological quantification of NpHR expression in the Scnn-Cre mouse line (Figure 25) was performed on 3 mice. 8 and 7 mice, respectively, were used for patch-clamp and juxtasomal recordings in Figure 26. For the experiments in Figure 27 we used 4 mice and 4 mice were used in the control experiments of Figure 28. The effect of cortical silencing (Figure 29) was observed in 3 mice. The data in Figure 30 was extracted from 6 mice. For the experiments in Figure 31, 4 mice were used.

3.2 Viral injections

The adeno-associated viruses (AAVs) AAV2.1EF1.dflox.hChR2(H134R)-mCherry.WPRE.hGH (Chr2), AAV1.EF1a.DIO.eNpHR3.0-eYFP.WPRE.hGH (NpHR), and AAV1.CAG.Flex.eGFP.WPRE.bGH (GFP) were purchased from the University of Pennsylvania Viral Vector Core (Philadelphia, USA). Stereotaxic injection was performed between postnatal day 0 (P0) and P2 in Scnn-Cre x TdTom, PV-Cre x TdTom and PV-Cre x C57 transgenic mice. Each pup was deeply anesthetized by hypothermia, kept at approximately 4°C, and immobilized in a customized stereotaxic apparatus. A small skin incision was performed along midline to expose the skull and a glass micropipette was lowered at stereotaxic coordinates of (with respect to bregma): 0 mm caudal, 1.5 mm lateral, and 0.25 mm depth. About 200–300 nl of virus suspension was injected slowly and the micropipette was held in place for 1 minute to prevent spilling of the virus during the retraction. Once the micropipette was removed, the skin was sutured and the pup was warmed under an infrared heating lamp until the recovery of normal body temperature and movements. The pup was then returned to its home cage.

3.3 Surgery

Mice were anesthetized with urethane (16.5%, 1.65 g/kg) intraperitoneal injection. The body temperature was constantly monitored with a rectal probe and kept at 36.5-37°C with a heating pad. The animals were maintained in a state of depth anesthesia for the duration of the surgery or until the end of the experiment. Depth of anesthesia was monitored by controlling the respiration rate, hear-beat frequency, eyelid reflex, reaction to tail and toes pinching, absence of vibrissae movements. In some experiments oxygen saturation was controlled by a pulse oxymeter (MouseOx, Starr Life Sciences Corp., Oakmont, PA, USA). Lidocaine solution (2%) was injected locally in the area of the surgery. The skin was cut to expose the skull and the area above the primary somatosensory cortex was thinned to allow intrinsic optical imaging (IOI) performed with a customized set-up to identify the cortical region where to perform the craniotomy. Before acquiring images for IOI, all but one whisker was trimmed in the contralateral whisker pad with respect to the virus injection site. Vibrissae were cut the day of the experiment to prevent sensory deprivation induced plasticity. Although we did not record electrical activity before or during the trimming, or we did not compare it with the activity after cutting the whisker, our protocol of acute whisker trimming should prevent major forms of long-term plasticity (Feldman & Brecht, 2005; Glazewski & Fox, 1996). The spared whisker was put inside a glass capillary tube glued to a piezoelectric bender actuator (Physik Instrumente, Milan, IT), the skull was illuminated with red light (630 ± 10 nm), and time series images were acquired with a camera (Hamamatsu, Milan, IT) for IOI. The whisker was then stimulated with a frequency of 18 Hz for 1.1 s at intervals of 20 s for a total of 40 trials. Camera frames were averaged over trials and a custom MATLAB script based on (Harrison, Sigler, & Murphy, 2009) was used to analyze the images. The region characterized by decreased reflectance relative to baseline identified the principal barrel corresponding to the stimulated spared whisker. Subsequently an image under green light (546 ± 10 nm) was acquired to reveal blood vessels which were used as spatial reference. A small craniotomy (< 1 mm^2) was performed over the area identified by IOI and HEPES-buffered artificial cerebrospinal fluid (aCSF) was used to keep the brain surface moist through the whole duration of the experiment.

3.4 Optical and whisker stimulation

To perform an optical stimulation, we used continuous-wave, solid-state laser sources to administer yellow light (λ = 594 nm) to mice injected with NpHR and blue light (λ = 488 nm or 491 nm) to mice injected with Chr2 (Cobolt, Vretenvägen, Sweden). Light stimuli lasted 1 s (light power 0.3 - 30 mW). In some experiments, inhibitory manipulation through activation of NpHR the light

stimulus ended with a ramp-like reduction in light power (ramp duration, 100 ms) to minimize the neural spiking rebound (Mahn, Prigge, Ron, Levy, & Yizhar, 2016). Light power was controlled with an acousto-optic modulator (R23080-3-LDT, Gooch & Housego PLC, Liminster, UK) and delivered to the sample through an optical fiber cable with a diameter of 940 µm and numerical aperture of 0.22 (QMMJ-3XF-UVVIS-940/1000-3-3, AMS Technologies, Milan, IT). The optical fibre cable was placed ~ 1 mm above the craniotomy. The intensity of the light was measured with a digital optical power metre (Thorlabs, Dachau, DE) placed proximally to the fibre tip. Before the experiment, the whisker was trimmed to a length of ~ 7 mm. Hold and release passive single whisker stimulations of 500 ms in duration and a deflection of ~ 2 mm were administered by means of a piezoelectric bender actuator (Physik Instrumente, Milan, IT). When whisker stimulation was coupled with optogenetic modulation, a delay of 100 ms between illumination and whisker stimulus onset was used. For the experiments shown in Figure 30, the piezoelectric actuator was connected to a manual metric rotation stage (MSRP01/M, Thorlabs) mounted on a flexible holder, allowing the deflection of the whisker at different angular directions. The whisker was pseudo-randomly deflected at angles of 0°, 45°, 90° and 315° with respect to the horizontal alignment of the whisker rows.

3.5 Patch-clamp recording

For patch-clamp intracellular recording, glass pipettes (Hilgenberg, Malsfeld, DE) were filled with internal solution containing in mM: K-gluconate 140, $MgCl_2$ 1, NaCl 8, Na_2ATP 2, NaGTP 0.5, HEPES 10, Tris-phosphocreatine 10 to pH 7.2 with KOH (all by Sigma-Aldrich). For electrophysiological recordings in layer II/III pyramidal cells, we used pipette with resistance of 3 to 6 MΩ, while for recordings in layer IV pipette resistance was in the range of 7-14 MΩ. Cells depth within the tissue was inferred by reading the depth of the glass pipette, respect to the pial surface, in the micromanipulators controller (Luigs & Neumann, Ratingen, DE) . The range of depths was 110-380 um for layer II/III cells and 410-500 for layer IV cells . In a small subset of experiments, layer IV principal cells were also identified post-hoc, using an internal solution containing biocytin (3 $mg*ml^{-1}$) (Sigma-Aldrich). In all experiments 30 consecutive acquisition (sweeps) were performed under each experimental condition and, for experiments in Figure 30, for each direction orientation. Data were collected using a Multiclamp 700B amplifier, acquired at 50 kHz and filtered at 10 kHz by a Digidata 1440 acquisition system (Axon instruments, Union City, CA, USA).

3.6 Two-photon targeted juxtasomal recordings

For two-photon targeted juxtasomal experiments, surgery was performed as described above, but the dura was removed with fine tip tweezers. The imaging setup was composed of: i) a Chameleon Discovery pulsed laser source (Coherent Italy, Milan, IT) tuned at λ 920, 980 or 1020 nm. The excitation power was measured at the focal plane of the objective with a power meter and set between 30 and 80 mW; ii) a laser scanning Ultima II scanhead (Bruker Italy, Milan, IT); iii) a 40× 0.80 NA objective (Olympus, Milan, IT); iv) two photomultiplier tubes for both green and red fluorescence collection (Hamamatsu, Milan, IT). For electrophysiological recordings, 5–7 MΩ glass pipettes were filled with Alexa Fluor 488 (concentration, 20 μM) at pH 7.4 added to aCSF solution. TdTomato-positive ($TdTomato^{+}$) neurons in layer IV were targeted while monitoring fluorescence of the glass pipette. When the electrode was in proximity of a targeted cell the positive pressure, that was applied to the pipette to prevent clogging, was released and negative pressure was used to achieve the juxtasomal configuration. Electrical signals were amplified and digitized as for the patch-clamp recordings described above.

3.7 Immunohistochemistry and confocal image acquisition

For morphological reconstruction of biocytin-filled layer IV recorded neurons, at the end of the experiments, the animals were perfused transcardially first with 0.01 M phosphate buffer (pH 7.4) (PBS) and then with 4% paraformaldehyde in PBS. The brains were post-fixed overnight at 4 °C, transferred to a solution of 30% sucrose in sodium chloride 0.9 g/100 ml for one day and sectioned (slice thickness, 200-300 μm) with a Thermo Fisher HM 450 sliding microtome (Bio-Optica, Milan, IT). The slices were then treated with 3% hydrogen peroxide in PBS for 20 minutes, permeabilized with 2% Triton X-100 in PBS at room temperature for one hour and then incubated overnight in 1% Triton X-100 and avidin-biotin HRP complex (ABC) (Vector Laboratories, Burlingame, CA, USA). After rinsing with PBS, the sections were incubated with 3, 3'-diaminobenzidine (DAB Peroxidase Substrate Kit, Vector Laboratories, Burlingame, CA, USA). When the neurons became visible, the slices were washed 3 times with PBS to stop the reaction. To identify different layers using fluorescence microscopy, the sections were incubated with 0.3% Hoechst in PBS at room temperature for 20 minutes. The sections were finally mounted on a glass slide with 1,4 diazobicyclo-(2,2,2)octane (DABCO) mounting medium and coverslipped. The Neurolucida software (MicroBrightField Williston, VT, USA) was used for morphological reconstruction.

For confocal image acquisition, fixed brains from Scnn-Cre x TdTom (age, 4-6 weeks) injected with AAV-transducing GFP were cut with a cryostat (Leica Microsystems, Milan, IT) to obtain coronal sections of 40 μm. The sections were incubated overnight in a solution containing 0.4% mouse anti-NeuN (Chemical International, West Melbourne, FL, USA), 0.01 M PBS (pH 7.4), 0.5% Triton X-100, and 1% normal serum of the same species as the secondary antibody. The next day, the sections were incubated at room temperature in goat anti-mouse Alexa 647 (1:800, A21236, Invitrogen, Carlsbad, CA, USA) secondary antibodies with 0.01 M PBS (pH 7.4) in 0.5% Triton X-100 for one hour.

For the cell count analysis shown in Figure 25, confocal z-stacks (512x512 pixels, 2 μm z steps, 40x magnification) of the barrel cortex were acquired using a Leica SP8 microscope (Leica SP5, Wetzlar, DE). Four consecutive sections were analysed in each mouse, imaging the whole thickness of the sections. The cells were counted manually using ImageJ (NIH, Bethesda, Maryland, MD, USA) with the grid and cell counter plugins (square area, 5000 μm^2). $NeuN^+$, $TdTomato^+$ and GFP^+ cells were counted in three randomly chosen squares placed inside a barrel. Cells that crossed the upper and right borders of the grid were included, while those that crossed the lower and left borders were excluded from the counts. Data were normalized to the total number of $NeuN^+$ cells and averaged across the sections for each animal. The mean values obtained across sections from one animal were averaged across animals.

3.8 Data analysis

For the intracellular recordings shown in Figure 26, we considered NpHR-positive neurons that showed, over an average of all stimulation sweeps, a clear net hyperpolarization of their membrane potential (> 3 times the standard deviation of the control membrane potential) upon yellow light illumination. For the juxtasomal recordings, we collected data only from neurons that showed red fluorescence. Clampfit 10.2 (Molecular Device, Sunnyvale, CA, USA) was used for analysis of the spike counts and membrane potential. In Figure 27-Figure 30, a MATLAB custom script (The MathWorks, Inc., Natick, MA, USA) was used for the analysis of the area below the membrane potential. The time period of the first 10 ms after the on and off set of the whisker stimulation was excluded from the analysis to avoid artefacts due to the piezoelectric actuator. Cells with a mean resting potential > -50 mV or a change in the resting membrane potential > 20 mV during the course of the experiment were excluded from the analysis. In Figure 31, whole-cell recordings were manually inspected, and only experiments with high and intense slow waves

dynamics in the majority of the sweeps were considered for the analysis. The resulting traces were analysed with a custom MATLAB script based on (Zucca et al., 2017) that efficiently detected periods of up or down states based on the membrane potential of the cells. For each electrophysiological sweep, we defined two regions (region duration, 1 s): the first corresponded to the period of light stimulation (light), and the second corresponded to the period before light onset (control). We defined the stimulation to be in an up or down state based on the membrane potential of the electrophysiological trace measured in a short (duration, 10 ms) time window before application of the stimulus.

3.9 Statistics

Data from each experiment were tested for normality with the Kolmogorov-Smirnov test. In case of normally distributed populations, the two-tailed Paired Student's t-Test or the one-way ANOVA with Bonferroni post-hoc test were used to confront, respectively, two or more data sets. For not normally distributed populations, the two-tailed Wilcoxon signed-rank test or the Friedman test with Dunn's Multiple Comparison post-hoc test were used to compare, respectively, two or more data sets. Unless stated otherwise, values are shown as mean ± s.e.m. with * indicating $p \leq 0.05$, ** indicating $p \leq 0.01$, *** indicating $p \leq 0.001$). Analysis was performed using OriginPro 9.1 (OriginLab Corporation, Northampton, MA, USA) and GraphPad Prism 5.01 (GraphPad Software, La Jolla, CA, USA).

4 Results

4.1 Expression of halorhodopsin in layer IV of the mouse barrel cortex

To casually investigate the information transfer from layer IV of the barrel cortex to the superficial layers during whisker-mediated somatosensation, we intracellularly recorded the response to single whisker deflection in layer II/III pyramidal neurons during optogenetic inhibition of layer IV. To restrict the expression of the inhibitory opsin NpHR selectively in layer IV excitatory neurons, we took advantage of the Scnn-Cre mouse line, which expresses Cre recombinase in the somatosensory cortex, preferentially in layer IV glutamatergic neurons of the sensory cortices (Madisen et al., 2010; Pluta et al., 2015). This line was bred with a Cre-dependent reporter strain conditionally expressing the red fluorescent protein TdTomato. Bigenic transgenic animals (Scnn x TdTom) were injected with Cre-dependent AAVs encoding eNpHR3.0-YFP (Figure 25 a). After 4-5 weeks, expression of the reporter was clearly visible in neurons located mainly in layer IV barrels (Figure 25 b-c). To quantify the AAV-mediated transgene expression efficacy under our experimental conditions, we acquired confocal images of fixed cortical sections. Cells expressing the opsin in the barrels were tightly packed, and the YFP fluorescence was localized to the membrane, as expected for opsin localization, making the precise estimation of a number of opsin-expressing cells unreliable. To overcome this problem, we injected Scnn x TdTom mice with the same AAV used for opsin expression but additionally carrying a construct coding for cytosolic GFP, and we quantified the percentage of infected GFP^+ cells in the barrel (Figure 25 d) (see Materials and Methods for details). Cytosolic GFP allowed the easy identification of infected cells based on the confocal acquisitions. We found that approximately 80% of the NeuN-positive cells, and therefore the majority of the excitatory cells (Ren, Aika, Heizmann, & Kosaka, 1992), within layer 4 barrels also expressed GFP (Figure 25 e). This result is in agreement with a previous work that characterized the expression of Cre recombinase in the Scnn-Cre mouse model (Pluta et al., 2015). In this work it was shown that, in histological preparations, Cre is expressed in the large majority of principal neurons of layer IV and that there is no co-localization between cells that express Cre and cells that express GAD67. This published result shows that recombination in Scnn-Cre mice occurs only in principal cells and not in interneurons.

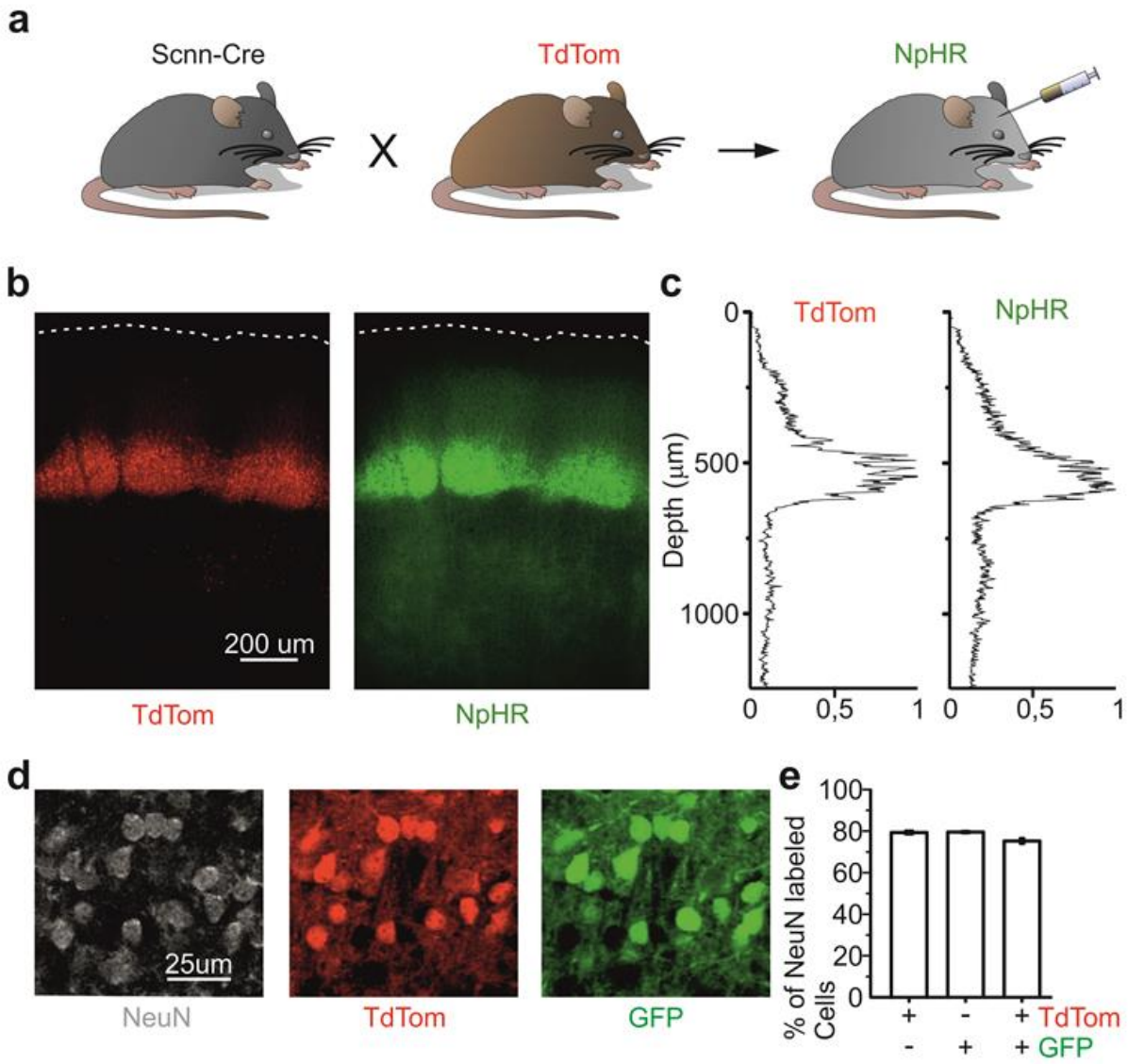

Figure 25. **Transgene expression in layer IV of the mouse barrel cortex. a**) Schematic representation of the experimental transgenic mouse model used. Offspring resulting from the crossing of Scnn-Cre mice with TdTom mice were injected with AAVs carrying the conditional Halorhodopsin construct (NpHR). **b**) Epifluorescence images of a coronal section showing either TdTomato (left) or NpHR-eYFP (right) expression in the barrel cortex. The white dotted line indicates the cortical surface. **c**) Normalized fluorescence expression profile of the images shown in **b** as a function of the cortical depth. **d**) Confocal images of a coronal section of a Scnn-Cre x TdTom mouse injected with AAVs carrying the conditional GFP construct. NeuN staining (left), TdTomato fluorescence (centre), and GFP fluorescence (right) in layer IV neurons are shown. **e**) Quantification of the percentage of NeuN-positive cells expressing TdTom (79%±1), GFP (80%±0.6) and the combination of the two proteins (75%±1.2) based on cell counting in confocal images. N = 36 fields of view from 3 mice, error bars represent s.e.m.

4.2 Optogenetic inhibition of layer IV excitatory neurons during whisker stimulation

We tested the functionality of the inhibitory opsin NpHR in layer IV in response to whisker deflection by performing *in vivo* patch-clamp recordings from opsin-expressing neurons in anaesthetized mice (Figure 26). In our experimental configuration, we trimmed all but one whisker (usually C2) on the contralateral side with respect to the injected hemisphere. The spared vibrissa was passively bent by means of a piezoelectric actuator. The stimulation consisted of a step and hold (on phase) deflection lasting for 500 ms. At the end of the deflection, the whisker was reverted to its original position (off phase) (Figure 26 a). To localize the primary cortical sensory region responding to the stimulated spared whisker, IOI was performed at the beginning of the experiment. Once the responding region was identified, patch-clamp recordings were performed from layer IV neurons. We found that whisker deflection evoked membrane depolarization of layer IV excitatory cells, which, in some cases, produced the firing of action potentials (Figure 26 b, top). When the stimulus was paired with yellow light illumination, NpHR activation drove significant hyperpolarization of the membrane potential with respect to its value in the presence of the whisker stimulus alone (Figure 26 b, bottom and c). Membrane potential hyperpolarization was sustained for the whole duration of the illumination (Figure 26 b, bottom).

To verify whether NpHR activation could silence the action potential (AP) generation in layer IV, we performed *in vivo* two-photon targeted juxtasomal recordings from layer IV TdTomato^{+} cells expressing NpHR during whisker stimulation. As expected, whisker stimulation significantly increased the firing rate of the recorded cells with respect to the basal condition evaluated previously and after whisker stimulation (Figure 26 e, top and f). Importantly, yellow light illumination efficiently prevented the whisker-evoked increase in the spike rate (Figure 26 e, bottom and g). These results demonstrated that under our experimental conditions, we could effectively blunt the suprathreshold response of layer IV neurons to whisker deflection.

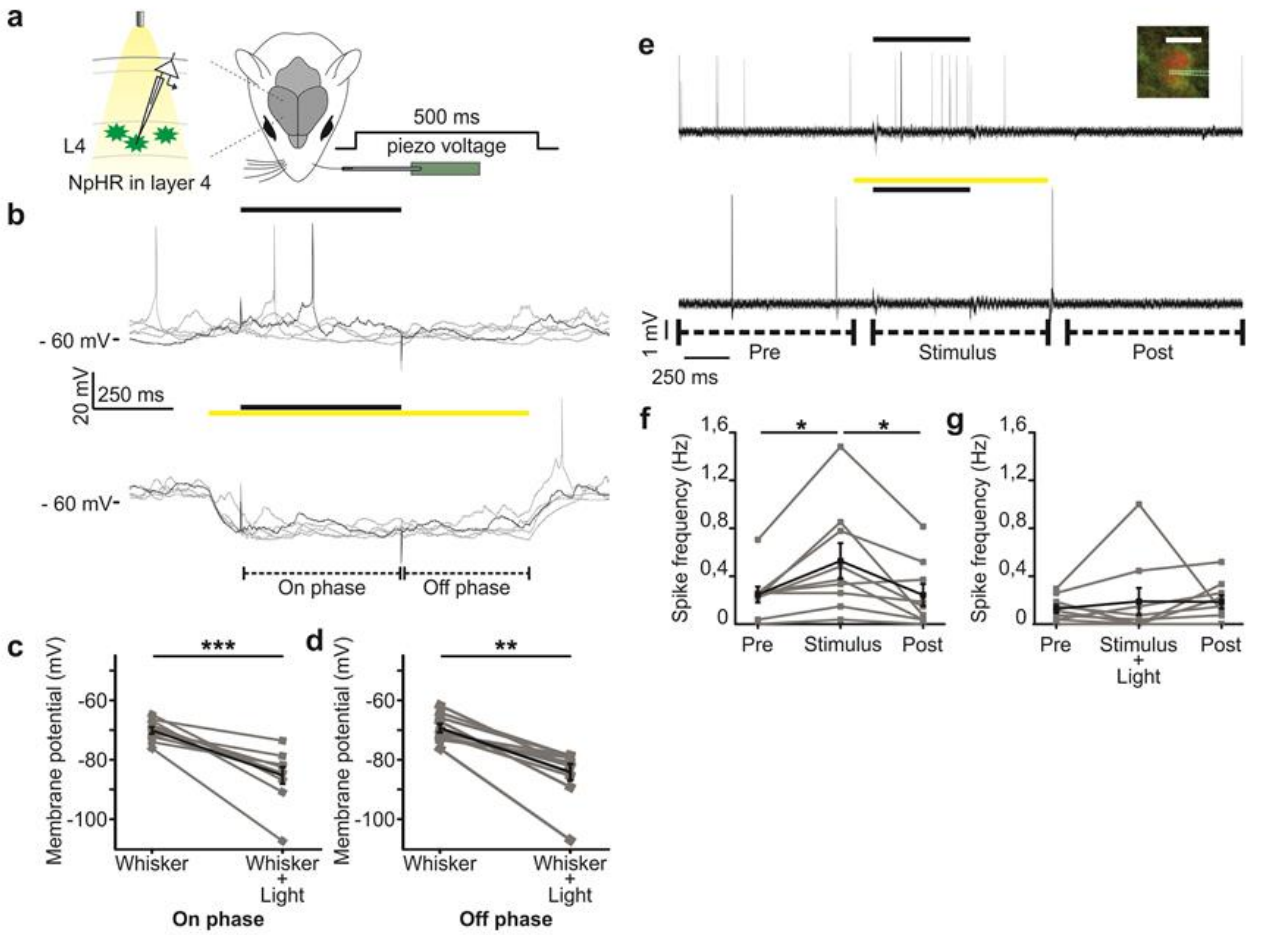

Figure 26. **NpHR activation in layer IV excitatory neurons during whisker stimulation *in vivo*. a**) Schematic representation of the experimental configuration for electrophysiological recordings in layer IV excitatory neurons expressing NpHR (green cells) in the barrel cortex. A single contralateral whisker was spared and stimulated using a glass capillary connected to a piezo actuator in anaesthetized mice. **b**) Representative traces of the membrane potential recorded in the whole-cell configuration from a layer IV NpHR$^+$ neuron during whisker stimulation in the absence (top) or presence of layer IV inhibition (bottom) *in vivo*. In this as well as in other figures, the black and the yellow bar represent the whisker stimulus and the optogenetic illumination, respectively. Whisker responses were divided into two categories: *On phase* (from 10 ms to 500 ms after the whisker stimulation onset, W-On) and *Off phase* (from 10 to 400 ms after the end of the deflection, W-Off). Five sweeps are presented for each condition. **c**) Membrane potential of NpHR$^+$ cells during the On Phase of the whisker stimulation in the absence (whisker) or presence of yellow light illumination (whisker + light) (N = 10 from 8 mice, paired Student's t-test, p = 2E-4). **d**) Same as in **c** but for the Off phase of the whisker response (N = 10 from 8 mice, Wilcoxon signed-rank test, p = 2E-3). **e**) Representative traces of two-photon guided juxtasomal recordings from a layer IV cell expressing NpHR and TdTomato during whisker stimulation in the absence (top) or presence of layer IV inhibition (bottom). Time windows before (Pre), during (Stimulus) and after (Post) stimulation are displayed below the traces. Five sweeps are presented for each condition. Inset: Two-photon image showing the juxtasomally recorded cell. Scale bar, 10 µm. White (dotted) lines indicate the glass pipette. **F**) Spike frequency of layer IV neurons during the Pre, Stimulus and Post time windows (N = 9 from 7 mice, Friedman test, p = 4E-3 with Dunn's post doc correction). **G**): Same as in **f** but during NpHR activation (N = 9 from 7 mice, Friedman test, p = 0.2E-1 with Dunn's post doc correction). In this as well in the other figures, grey lines indicate single

experiments, while the black line represents the average and s.e.m. of the entire dataset. *, $p \leq 0.05$; **, $p \leq 0.01$; ***, $p \leq 0.001$.

4.3 Layer IV inhibition does not abolish the layer II/III response to a whisker deflection

To measure the contribution of the granular layer to shape the response of superficial layer II/III, we recorded whisker-evoked subthreshold responses in layer II/III neurons under control conditions and during optogenetic inhibition of layer IV principal cells. Using the same experimental conditions displayed in Figure 26, we performed whole-cell current-clamp recordings from layer II/III pyramidal neurons (Figure 27 a). We found that under control conditions, whisker stimulation evoked a prolonged membrane potential depolarization in supragranular pyramidal cells (Figure 27 b, top). Importantly, the whisker-evoked response was significantly reduced during optogenetic suppression of layer IV using yellow light illumination (Figure 27b, bottom). We divided the whisker-evoked response measured in layer II/III cells into three different temporal windows: *i)* the early phase, from 10 ms to 100 ms after whisker deflection onset; *ii)* the late phase, from 100 ms to 500 ms; *iii)* the off phase, from 10 ms to 400 ms after the end of whisker stimulation (Figure 27 c). The early phase was typically characterized by a transient depolarized peak in the membrane potential, while the late phase was characterized by a slowly decreasing membrane potential depolarization (Figure 27 c, red line). To quantify the effect of layer IV suppression on whisker responses, we computed the area below the mean membrane potential in the different temporal windows, considering the first 10 ms before the whisker stimulus onset as the baseline. We found that optogenetic suppression of layer IV decreased the area underneath the membrane potential during the late and off-phase with no significant difference in the early phase (Figure 27 d). To control for potential side effects of light illumination on the cellular response, we repeated the same experiments in Scnn x TdTom mice that were not injected with the AAVs and thus did not express any opsin (Figure 28 a). We observed no effects of light on the membrane potential of layer II/III neurons in these experiments, demonstrating that optogenetic illumination *per se* did not significantly perturb the electrical activities of layer II/III neurons (Figure 28 d). These results demonstrate that layer IV strongly influences the layer II/III response to whisker deflection, as expected based on previous work (see introduction for a summary of those previous studies). However, these findings unexpectedly revealed that layer IV suppression did not

completely abolish whisker-evoked depolarization in layer II/III pyramidal cells, suggesting the existence of other input pathways to layer II/III.

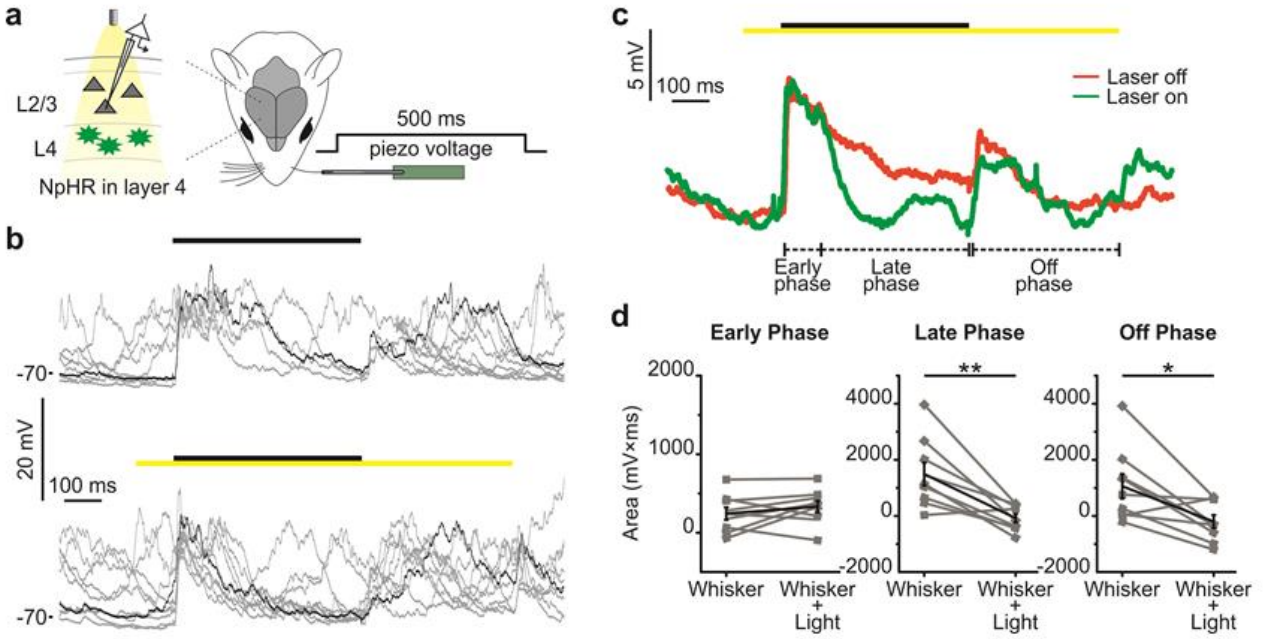

Figure 27. **Optogenetic inhibition of excitatory layer IV neurons decreases but does not suppress the subthreshold response to whisker deflection in layer II/III pyramidal cells. a**) Schematic representation of the experimental configuration for intracellular recordings in layer II/III pyramidal neurons during single whisker stimulation and optogenetic silencing of layer IV in anaesthetized mice. Scnn^{+} cells expressing NpHR in layer IV are coloured in green, and layer II/III principal cells are shown as grey triangles. **b**) Representative traces showing the membrane potential of a layer II/III pyramidal neuron during whisker stimulation in the absence (top) and presence (bottom) of optogenetic stimulation. Ten sweeps are presented for each condition. **c**) Average membrane potential of 30 sweeps in the absence (red) and presence (green) of layer IV photoinhibition for the cell shown in **b**. Early phase, 10 ms to 100 ms after the beginning of whisker stimulation; late phase, 100 ms to 500 ms after the beginning of whisker stimulation; off phase, 10 ms to 400 ms after the end of whisker stimulation. **d**) Area under the whisker-evoked depolarization in layer II/III pyramidal neurons during whisker stimulation in the absence (Whisker) and presence of layer IV inhibition (Whisker + Light) for the early (left), late (center), and off (right) temporal windows (paired student's t-test, N = 9 from 4 mice; early phase p = 0.27; late phase p = 3E-3; off phase p = 0.1E-1).

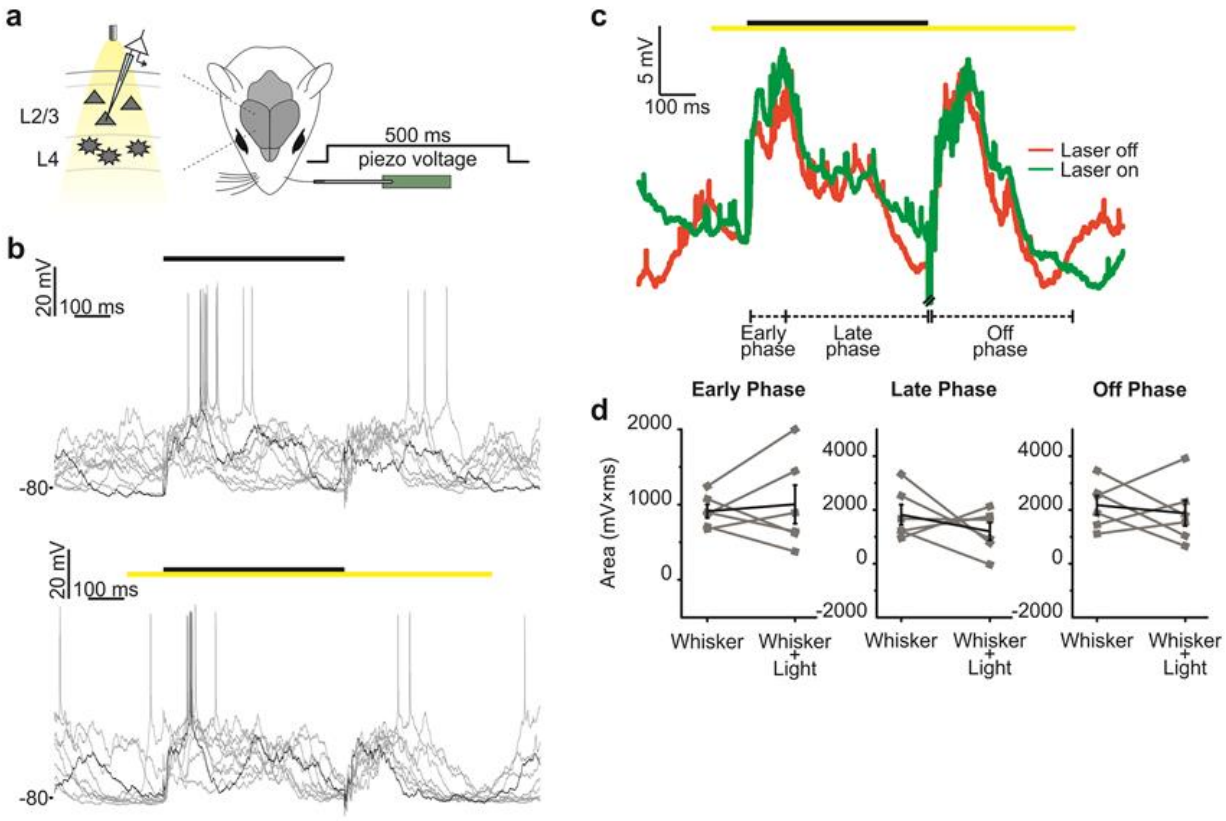

Figure 28. **Optical stimulation has no effect in mice that do not express opsins. a**) Schematic representation of the experimental setup for intracellular recordings in layer II/III pyramidal neurons in anaesthetized mice in which neither layer II/III cells nor layer IV cells expressed light-sensitive opsins. **b**) Representative traces showing the membrane potential of a layer II/III cell during whisker stimulation in the absence (top) and presence (bottom) of light stimulation. Ten sweeps are shown for each condition. **c**) Average membrane potential in the absence (red) and presence (green) of light stimulation for the cell shown in b. Early, late, and off temporal windows are indicated below the traces. **d**) Area under the mean whisker-evoked depolarization in layer II/III pyramidal neurons in the absence (Whisker) and presence (Whisker + Light) of light stimulation for the early (left), late (centre), and off phase (right) temporal windows (N = 6 from 4 mice, paired student's t-test, early phase p = 0.68; late phase p = 0.34; off phase p = 0.61).

4.4 Cortical silencing through the activation of local fast spiking interneurons suppresses whisker-evoked responses in layer II/III

To understand whether the whisker-evoked response of layer II/III neurons, which was resistant to layer IV photoinhibition, was of cortical or extracortical origin, we optogenetically silenced cortical activity by photoactivating fast-spiking parvalbumin (PV)-positive interneurons expressing channelrhodopsin 2 (Lien & Scanziani, 2013) (ChR2, see Materials and Methods) (Figure 29 a). ChR2 was expressed selectively in PV cells by injecting AAVs transduced with a floxed ChR2

construct into PV-Cre transgenic mice as described in previous work (Mariotti et al., 2018; Sessolo et al., 2015; Zucca et al., 2017). The area corresponding to the principal whisker and the surrounding columns were illuminated with blue light (duration, 1 s), and whole-cell patch clamp recordings from layer II/III pyramidal neurons were obtained during stimulation of the principal whisker in the presence and absence of ChR2 activation. We found that optogenetic stimulation of PV cells nearly abolished the whisker response in layer II/III principal neurons (Figure 29 b and c). In all three temporal windows (early, late, and off phases), the membrane potential depolarization elicited by whisker stimulation was significantly reduced (Figure 29 c and d). The nearly complete suppression of the whisker-evoked response in layer II/III by optogenetic activation of cortical PV interneurons suggested that most of the inputs responsible for layer II/III depolarization upon whisker deflection were of local cortical origin rather than long-range direct monosynaptic inputs onto layer II/III from other brain regions.

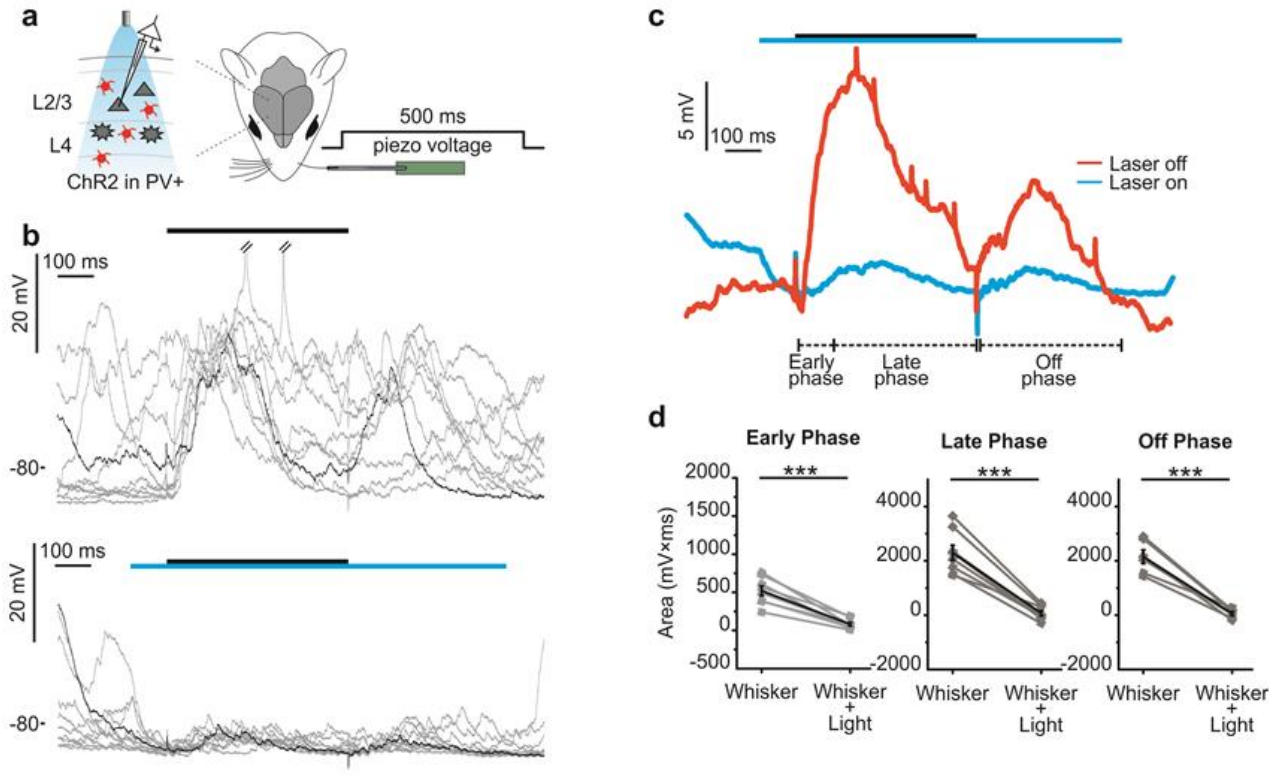

Figure 29. **Cortical silencing through optogenetic activation of PV-interneurons suppresses whisker-evoked responses in layer II/III principal neurons. A**) Schematic representation of the experimental configuration, in which intracellular recordings in layer II/III pyramidal neurons were performed during whisker stimulation in anaesthetized mice. Local cortical activity was suppressed via optogenetic stimulation of ChR2-expressing PV-positive (PV+) interneurons. PV cells expressing ChR2 are depicted in red, and layer II/III principal cells are illustrated with grey triangles. **b**) Representative traces showing the

membrane potential of layer II/III neurons during whisker stimulation in the absence (top) and presence (bottom) of PV cell photoactivation (the blue bar represents blue light illumination). Ten sweeps are presented for each experimental condition. **c**) Average membrane potential in the absence (red) and presence (blue) of layer IV inhibition for the cell shown in **b**. **d**) Area under the whisker-evoked depolarization in layer II/III pyramidal neurons during whisker stimulation in the absence (Whisker) and presence of PV photoactivation (Whisker + Light) for the early (left), late (center), and off (right) phases (N = 8 for early and late phase, N = 6 for off phase from 3 mice, paired student's t-test, early phase p = 2E-4; late phase p = 3E-5; off phase p = 3E-4).

4.5 Layer IV modulates the subthreshold orientation tuning of superficial pyramidal cells

To test the possibility that the layer IV-sensitive and the layer IV-insensitive response in layer II/III carry different information about the sensory stimulus, we next investigated whether the orientation selectivity of supragranular pyramidal cells was affected by layer IV photoinhibition. For this aim, we performed whole-cell current clamp recordings from layer II/III pyramidal neurons while deflecting the principal whisker in four different angular directions (Figure 30 a) under control conditions and during optogenetic suppression of layer IV. As reported in previous studies (Brecht & Sakmann, 2002), under control conditions in each recorded cell, the amplitude of the post synaptic potential during whisker stimulation varied as a function of the direction of whisker deflection. We ranked as I (preferred) the direction that evoked the highest response and as IV (non-preferred) the direction that evoked the lowest response. Intermediate directions were ranked as II and III on the basis of the amplitude of the response (with class II comprising responses of larger amplitude in comparison to class III,Figure 30 a). When the stimulus was presented in the preferred direction, layer IV photoinhibition significantly decreased the area below the membrane potential in the early, late, and off phases (Figure 30 b). Most importantly, when optogenetic inhibition of layer IV was performed for the class II and III directions, we found no significant difference in the average membrane depolarization. For the least preferred direction (class IV), layer IV inhibition increased the early phase response with no effect on the late and off phases. Based on these results, we computed the orientation selectivity index (OSI) based on the mean value of the area below the membrane potential for the preferred (P) and non-preferred (N) direction. The OSI was defined as follows:

$$(P-N)/(P+N)$$

We found that layer IV photoinhibition significantly decreased the OSI for the early and late phases, while no significant effect was observed for the off phase (Table 1). Altogether, these results demonstrated that the orientation selectivity in layer II/III was mostly mediated by layer IV.

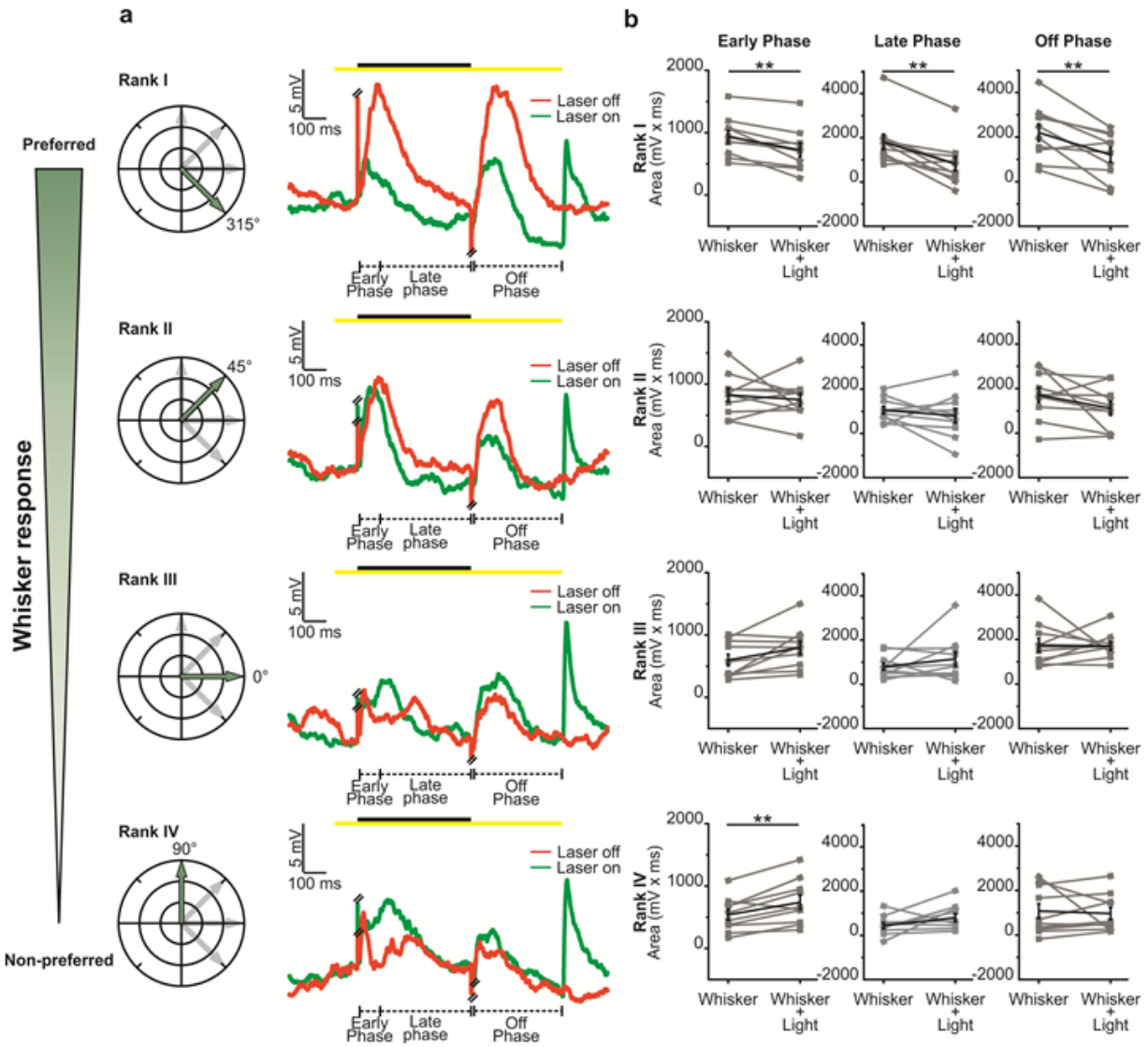

Figure 30. **Orientation-dependent effect of layer IV optogenetic inhibition on the subthreshold whisker responses in layer II/III pyramidal neurons. a**) Average membrane potential of layer II/III neurons in the absence (red) and presence (green) of layer IV inhibition during whisker stimulation in anaesthetized mice. For each neuron, a single whisker was stimulated in four different angular directions with respect to the rostral-caudal axis (polar plots on the left) and, based on the amplitude of the evoked response, directions were ranked as follows (from top to bottom): preferred (I), second best preferred (II), third best preferred (III), and non-preferred (IV). Corresponding responses from a representative neuron are shown on the right, and piezo artefacts were truncated for presentation purposes. **b**) The area under the sensory-evoked depolarization for layer II/III cells during whisker stimulation in the absence (Whisker) and presence of layer IV inhibition (Whisker + Light). Responses were grouped according to direction rank (I to IV, from top to bottom) and divided into the early (left), late (center), and off (right) phases (N = 10 from 6 mice; I: early

phase paired student's t-test p = 2E-3, late phase p = 4E-3, off phase paired student's t-test p = 5E-3; IV: early phase paired student's t-test p = 5E-3)

Orientation selectivity index (OSI)				
	Early Phase	**Late Phase**	**Early + Late**	**Off Phase**
Whisker	0.2563 ±0.0524	0.7128 ±0,1389	0.4886 ±0,0652	0.3875 ±0,1376
Whisker + Light	-0.0489 ±0,0354	-0.2529 ±0,2774	-0.1373 ±0,1487	0.3612 ±0,4195

Table 1. **Effect of layer IV inhibition on the orientation selectivity index of layer II/III principal cells.** Average ± s.e.m of OSI during whisker stimulation and whisker stimulation paired with layer IV photoinhibition. Data were calculated from the cells shown in Figure 30. Early Phase paired student's t-test p = 4E-4; Late Phase wilcoxon signed rank test p = 1E-2; Early Phase + Late Phase paired student's t-test p = 5E-3; Off Phase wilcoxon signed rank test p = 0.49.

4.6 Layer IV inhibition does not alter spontaneous activity in layer II/III cortical neurons

Cortical networks are spontaneously active. Indeed, even in the absence of incoming sensory inputs, cortical circuits display several classes of large-scale spontaneous network dynamics (Luczak, Bartho, Marguet, Buzsaki, & Harris, 2007; Steriade, Timofeev, & Grenier, 2001). One such example is slow oscillation, the dominant cortical rhythm observed during deep stages of NREM sleep and under several types of anaesthesia (Contreras & Steriade, 1995; Crunelli, Lörincz, Errington, & Hughes, 2012; Steriade, Nunez, & Amzica, 1993a). This oscillation is characterized by the rhythmic alternation (0.2 - 1 Hz) of silent (down) and active (up) network states, which can be captured in the membrane potential of cortical neurons as depolarized and hyperpolarized states, respectively. Thalamic inputs are known to strongly regulate the slow oscillation frequency and sensory stimulation or direct electrical stimulation of the thalamus to trigger cortical up state generation (Contreras & Steriade, 1995; Lemieux, Chauvette, & Timofeev, 2015; Sheroziya & Timofeev, 2014; Slezia, Hangya, Ulbert, & Acsady, 2011). However, whether the thalamic effect on cortical slow oscillation is mediated through layer IV (one of the main thalamo-recipient cortical layers) is currently unknown. To test this hypothesis, we inhibited layer IV principal cells using

optogenetics (stimulus duration, 1 s) during spontaneous activity in anaesthetized mice. For this analysis, we considered only recordings that displayed clear up and down state dynamics in the membrane potential of cortical neurons (see Methods), and we used a custom algorithm based on (Zucca et al., 2017) to automatically detect up and down states. Surprisingly, we observed no effect of the photoinhibition of layer IV on the average membrane potential of cortical neurons in the supragranular layer during light illumination, either when stimulation occurred during an ongoing up state or during an ongoing down state (Figure 31 b, g). The up and down state duration (Figure 31 c, h), as well as the total time spent by the neuron in the up or down states (Figure 31 d-e, j-k), were similarly unaffected. These results suggest that thalamic modulation of cortical up and down state dynamics are largely dependent on circuits other than layer IV.

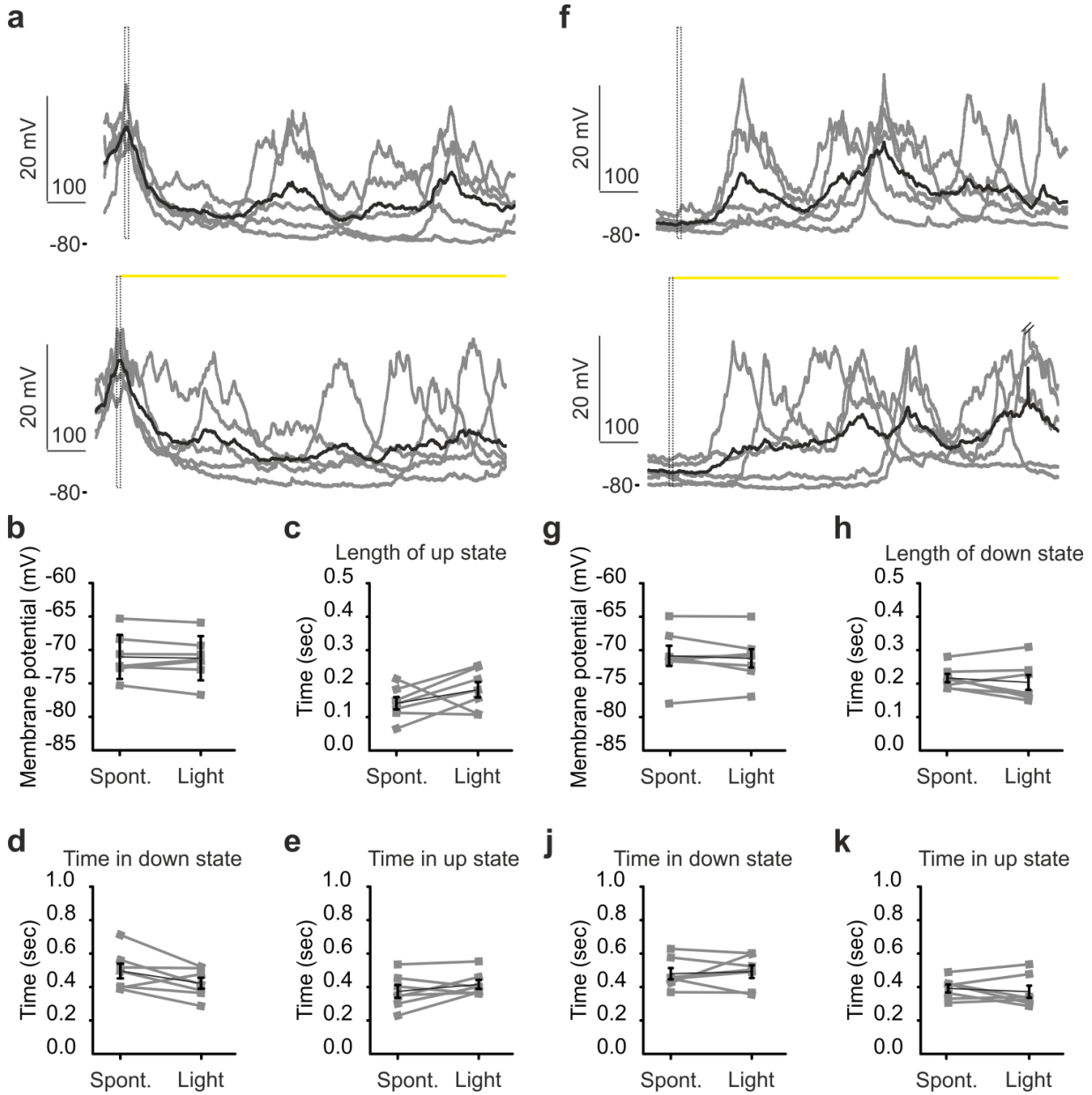

Figure 31. **No significant effect of optogenetic inhibition of layer IV on the spontaneous activity recorded in layer 2/3 pyramidal cells. a**) Representative traces of the spontaneous activity of layer II/III principal cells. In the lower part, yellow light was applied for 1 s. Sweeps were selected based on the presence of an up state in a time window of 10 ms (dotted box) prior to optogenetic stimulation (yellow line). Five sweeps (grey line) and their averages (black line) are shown. **b**) Membrane potential during spontaneous activity (Spont) and light stimulation (Light) in sweeps presenting an up state before the optogenetic stimulation (n = 7 in 4 mice, paired t-test: N.S.). **c**) Duration of the up state for the sweeps considered in **b** (paired t test**:** N.S.). **d**) Total time in the down state for the sweeps considered in **b** (paired t-test**:** N.S.)**. e**) Total time in the down state for the sweeps used in **b** (paired t test**:** N.S.). **f**) The same as in **a** but for sweeps showing a down state in a time window of 10 ms (dotted box) before the region of interest. **g**) The same as in b but for sweeps presenting a down state in the temporal window of 10 ms before the region of interest (n = 7 in 4 mice, paired t-test: N.S.). **h**) Mean duration of the down state for the sweeps considered in **g** (paired t test**:** N.S.). **j-k**) The same as in d and e, respectively, but for the sweeps considered in **g** (Wilcoxon signed-rank test: N.S for both **j** and **k**).

5 Discussion

Understanding the encoding of a physical stimulus into electric signals and how these electrical signals flow across circuits is a first fundamental step to identify the cellular mechanisms underlying the processing of sensory perception (Panzeri et al., 2017). In the superficial layers of S1, sensory inputs ascending from different pathways (lemniscal, paralemniscal and extra lemniscal) merge together and are superimposed with spontaneous activity (C. C. H. Petersen, Hahn, Mehta, Grinvald, & Sakmann, 2003; Sachdev, Ebner, & Wilson, 2004). The canonical model posits that sensory information across sensory modalities is processed in a serial manner from layer IV to layer II/III and then to deeper laminae, layer V and VI (Douglas & Martin, 2004; Gilbert & Wiesel, 1979). However, more recent work implies a more complex model for the processing of sensory information (Constantinople & Bruno, 2013; Pluta et al., 2015). For example, layer V has been shown to be directly contacted by thalamic excitatory inputs (Constantinople & Bruno, 2013) and layer V excitatory neurons have been shown to form excitatory synapses on layer II/III principal neurons (Lefort et al., 2009; Shepherd, 2005). Thus, a new model has been proposed for the processing of sensory information in S1 in which sensory information is processed by two parallel pathways layer IV-layer II/III and layer V-Layer II/III (Lübke & Feldmeyer, 2007; Shepherd, 2005). In this new model, layer II/III is an "integrative layer" where the inputs of layer IV and layer V merge together. Whether these two parallel pathways carry the same or rather different sensory information is currently unknown.

To start testing this hypothesis, we combined optogenetic manipulations targeted to layer IV excitatory neurons with two-photon targeted juxtasomal recordings and blind patch-clamp recordings in mice *in vivo*. Interestingly, we found that layer IV optogenetic suppression did not completely abolish sensory-evoked responses in layer II/III. More specifically, we observed a significant decrease in the late phase of the whisker response while the early part of the sensory-evoked post synaptic potential was unaffected. Importantly, we found that the effect of layer IV suppression on layer II/III responses depended on the angular direction of the whisker stimulation. When the layer IV inhibition was performed during the stimulation of the most responsive whisker direction, a reduction in the subthreshold response of all the phases of the whisker response was observed. In contrast, when layer IV was inhibited during stimulation of the least preferred

whisker direction we observed a significant and paradoxical increase in the early part of layer II/III responses. These results suggest that layer II/III excitatory neurons receive direction-tuned information from layer IV and that layer II/III receive direction-untuned information from circuits other than layer IV. This is in line with the observation that layer IV cells display strong whisker direction selectivity in their response (Brecht & Sakmann, 2002; Randy M. Bruno & Simons, 2002; Simons & Carvell, 1989b) and that deeper laminae, especially layer V which has been shown to send excitatory inputs to layer II/III (Lefort et al., 2009), display much lower whisker direction selectivity in their spiking response.

Our conclusion on the effect of optogenetic suppression of layer IV on layer II/III activity relies on the assumption that the optogenetic manipulation specifically and effectively affected layer IV principal cells. We have made important control experiments to confirm this. First, we found that the inhibitory opsin halorhodopsin was specifically expressed in the vast majority of layer IV excitatory neurons (Figure 25)(see also Pluta et al., 2015). Thus, although we cannot completely exclude it, it is unlikely that the layer II/III response unaffected by optogenetic suppression of layer IV was due to the firing activity of few layer IV cells which did not express the opsin. Second, we controlled that the opsins was functional and that it efficiently suppressed the increase in firing rate induced in layer IV neurons by whisker stimulation (Figure 26). Third, to exclude the possibility that the response of layer II/III cells located above one barrel could be due to layer IV activity in a neighboring barrel through horizontal layer II/III-layer II/III connectivity we used a large fiber optic (fiber diameter, 0.94 mm) positioned approximately 1 mm above the pia and with a numerical aperture of 0.22. Under these experimental conditions light is delivered in an area of $> 3\ mm^2$.

An alternative interpretation of the results discussed above is that the layer II/III response which is unaffected by the optogenetic suppression of layer IV is due to direct input of untuned thalamic fibers (for example those of the paralemniscal pathway) onto layer II/III neurons. However, we found that optogenetic activation of cortical PV interneurons (Lien & Scanziani, 2013) completely suppressed layer II/III responses, suggesting that the response elicited in layer II/III by the whisker input completely relied on the cortical rather than extracortical inputs. This conclusion is based on the assumption that potential thalamic-driven postsynaptic potential remain visible in the

presence of shunting inhibition due to the GABA release and the consequent decrease in input resistance of principal cell upon PV cell optogenetic activation. This assumption has been considered realistic in many previous studies investigating thalamic inputs to cortical cells (L. Li, Li, Zhou, Tao, & Zhang, 2013; Y. Li, Ibrahim, Liu, Zhang, & Tao, 2013; Lien & Scanziani, 2013; Malina, Mohar, Rappaport, & Lampl, 2016) although we cannot completely exclude that in our condition a weak direct thalamic drive could be present.

Previous work demonstrated the impact of layer IV photoinhibition on the suprathreshold response of cortical layer II/III cells (Pluta et al., 2015). They found that suppression of layer IV resulted in the decrease of the *suprathreshold* response of layer II/III. We extended that study to investigate the effect of layer IV inhibition on the *subthreshold* response of layer II/III. This is important because subthreshold responses to whisker inputs, especially in layer II/III, are much more reliable compared to spiking responses (Brecht et al., 2003; Crochet & Petersen, 2006; Crochet et al., 2011; C P J de Kock et al., 2007; O ’connor et al., 2010; Poulet & Petersen, 2008; Sachidhanandam et al., 2013) and they allow monitoring the summation of distinct post synaptic potentials. Indeed, our results allowed us to demonstrate that layer IV relays whisker orientation-tuned information to layer II/III and that layer II/III receives whisker orientation-untuned information from other cortical excitatory inputs. This latter excitatory pathway is still to be identified.

One limitation of the results described in this thesis is that all experiments were performed in anesthetized animals. While anesthesia allows precise control of the properties of the stimulus delivered to the whiskers and to monitor and maintain the state of the animals under controlled conditions, anesthesia may significantly interfere with network dynamics and does not allow studying the whisker system during natural whisking. Thus, it is important to extend the results described herein in the awake mouse preparation. Experiments are currently ongoing in the laboratory to achieve this goal (Figure 32). However, in this context it is important to mention that it may be difficult to test our hypothesis in the awake condition because previous work reported significant reduction in the firing activity of opsins positive cells only in a fraction of the layer IV excitatory neurons in awake mice (Minamisawa, Kwon, Chevée, Brown, & O’Connor, 2018; Pluta et

al., 2015). This may be due to the increased activity level that is usually observed in the awake condition compared to the anesthetized regime (Greenberg, Houweling, & Kerr, 2008; Steriade et al., 2001).

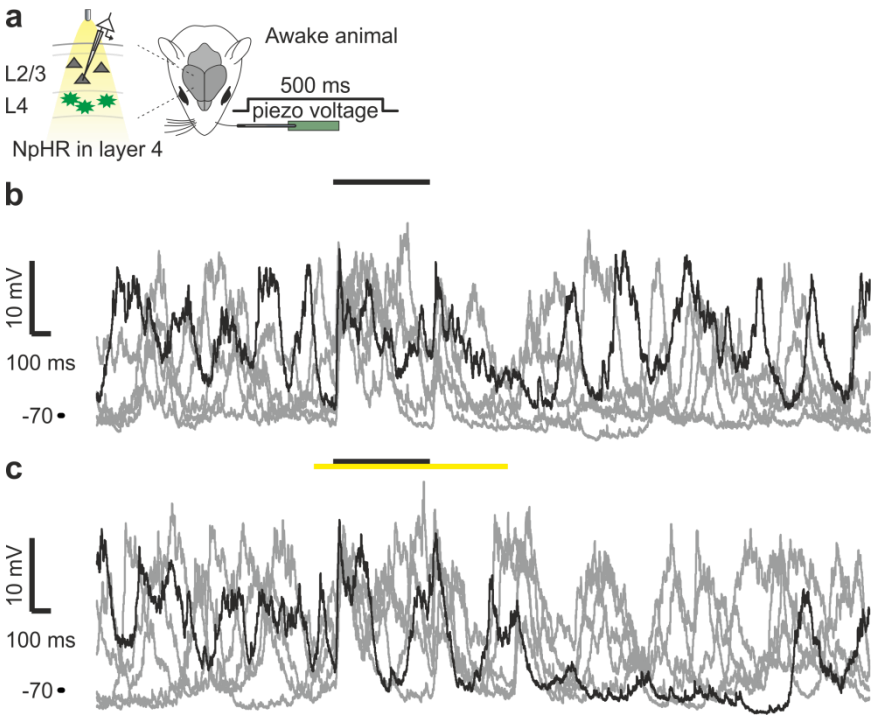

Figure 32. **Optogenetic inhibition of layer IV principal cells in awake head restrained mice.** **a**) Scheme of the experimental configuration. **b-c**) Intracellular recordings from a layer II/III principal cell during whisker stimulation (**b**) and whisker stimulation paired with layer IV optogenetic inhibition (**c**) in an awake mouse. Five consecutive sweeps are shown for each condition.

Cortical circuits involved in the processing of sensory information are active even in the absence of sensory inputs. Major components of these spontaneous dynamics are slow-wave oscillations which represents the dominant cortical rhythm observed during quite wakefulness, deep stages of NREM sleep, and under several types of anaesthesia (Luczak et al., 2007; Steriade, Contreras, Curro Dossi, & Nunez, 1993; Steriade, Nunez, et al., 1993a; Steriade, Nunez, & Amzica, 1993b). These oscillations are characterized by the rhythmic alternation (0.2 - 1 Hz) of silent (down) and active (up) network states which can be captured in the LFP signal as depth-positive and depth-negative waves, respectively (Saleem, Chadderton, Apergis-Schoute, Harris, & Schultz, 2010). Down and up states are observed in the cortex and in many subcortical regions, including the thalamus, and they are believed to be crucial in the regulation of several processes, such as memory consolidation, sensory responses, and synaptic plasticity (Crochet, Chauvette, Boucetta,

& Timofeev, 2005; Haider, Duque, Hasenstaub, Yu, & McCormick, 2007; Marshall, Helgadóttir, Mölle, & Born, 2006; C. C. H. Petersen et al., 2003; Reig, Zerlaut, Vergara, Destexhe, & Sanchez-Vives, 2015). During up states, most types of cortical neurons display depolarized membrane potential and, in some cases, action potential firing. In contrast, down states are characterized by hyperpolarized membrane potential and no action potential firing in most cortical cells, including virtually all principal cells (Chauvette, Crochet, Volgushev, & Timofeev, 2011; Timofeev, Grenier, & Steriade, 2001). Slow oscillations are observed in isolated cortical slices in vitro (Sanchez-Vives & McCormick, 2000) or in isolated cortical slab in vivo (Timofeev, Grenier, Bazhenov, Sejnowski, & Steriade, 2000). Moreover, slow oscillations have been shown to originate from deep layer V laminae and then propagate to upper layers (Beltramo et al., 2013; Chauvette, Volgushev, & Timofeev, 2010). However, sensory input has also been shown to effectively trigger up state generation. In our experiments we had the opportunity to test the hypothesis that sensory input triggers up state generation through activation of layer IV. However, we found no effect of layer IV photoinhibition on *subthreshold* spontaneous activity in layer II/III, a result in agreement with previous reports describing the *suprathreshold* response of layer II/III during optogenetic suppression of layer IV in awake mice (Pluta et al., 2015). This result suggests that sensory inputs may trigger up state transitions in the cortex through direct activation of layer V principal cells (Beltramo et al., 2013; Constantinople & Bruno, 2013).

Our results on the effect of layer IV inhibition of whisker-evoked responses in layer II/III are in stark contrast with the sequential activation model proposed by the canonical pathway (Douglas & Martin, 2004; Gilbert & Wiesel, 1979). Rather our work fits well with more recent data suggesting a more complex flow of sensory information across the layers of the barrel cortex. According to recent proposals (Constantinople & Bruno, 2013) upper layers (II/III and IV) and lower layers (V and VI) may form two distinct processing units. Our data partially support this view and show that layer II/III received whisker orientation-tuned inputs from layer IV and may receive whisker orientation-untuned inputs from deeper laminae (e.g., layer V). In this framework, layer II/III acts as an “integrative layer” where orientation-tuned and orientation-untuned inputs converge. Future experiments involving the silencing of large number of layer V and layer VI cells during whisker stimulation will be necessary to fully test this model.

More specifically, in order to test the hypothesis that deep laminae (layer V and layer VI) send sensory information to layer II/III we will need to selectively target and silence the majority of principal cell in those deep layers, as we did for layer IV in this thesis work. At the moment of writing this thesis, mouse lines whose expression is confined to either layer V or layer VI only target a fraction of the total excitatory cells in the targeted layer (Gerfen et al., 2013; J. A. Harris et al., 2014). To give few examples, the Rbp4-Cre mouse line which is commonly used to modulate layer V pyramidal cells in the somatosensory cortex expresses in < 30% of the total excitatory cell in layer V (Beltramo et al., 2013). Among transgenic lines that target selectively layer VI principal cells, the Ntsr1-Cre mouse line is the one with the wider expression and yet it expresses in only 64% of the total excitatory neurons with in layer VI (Gong et al., 2007; Kim, Matney, Blankenship, Hestrin, & Brown, 2014; Olsen, Bortone, Adesnik, & Scanziani, 2012). Moreover in the visual cortex of Ntsr1-Cre mice only a subpopulation of excitatory layer VI neurons (those that project both intracortically and to the thalamus) expresses the Cre (Bortone, Olsen, & Scanziani, 2014). This implies that, in both these mouse lines, optogenetic inhibitory modulation off the type used in this thesis work for layer IV would not interfere with the activity of a substantial number of target neurons, making the interpretation of any possible results difficult. Once a mouse line for the specific and extended expression of Cre in infragranular principal cells will be developed a new series of experiments will become at reach. This will include the generation of double transgenic animals in wich Cre is expressed extensively in one layer (e.g., layer IV) and Flip is expressed extensively in another layer (e.g., layer V). With such a tool, one would be able to investigate the effect of the modulation of layer V onto superficial layer in the presence or absence of layer IV optogenetic suppression to test for potential “non-linear” interactions between these two converging pathways.

6 Bibliography

Abraira, V. E., & Ginty, D. D. (2013). The sensory neurons of touch. *Neuron*, *79*(4), 618–639. https://doi.org/10.1016/j.neuron.2013.07.051

Adesnik, H., Bruns, W., Taniguchi, H., Huang, Z. J., & Scanziani, M. (2012). A neural circuit for spatial summation in visual cortex. *Nature*, *490*(7419), 226–230. https://doi.org/10.1038/nature11526

Andermann, M. L., & Moore, C. I. (2006). A somatotopic map of vibrissa motion direction within a barrel column. *Nature Neuroscience*, *9*(4), 543–551. https://doi.org/10.1038/nn1671

Andrew Hires, S., Gutnisky, D. A., Yu, J., O'Connor, D. H., & Svoboda, K. (2015). Low-noise encoding of active touch by layer 4 in the somatosensory cortex. *ELife*, *4*, 1–18. https://doi.org/10.7554/eLife.06619

Arabzadeh, E., Petersen, R. S., & Diamond, M. E. (2003). Encoding of whisker vibration by rat barrel cortex neurons: implications for texture discrimination. *The Journal of Neuroscience : The Official Journal of the Society for Neuroscience*, *23*(27), 9146–9154. https://doi.org/23/27/9146 [pii]

Arabzadeh, E., Zorzin, E., & Diamond, M. E. (2005). Neuronal Encoding of Texture in the Whisker Sensory Pathway. *PLoS Biology*, *3*(1), e17. https://doi.org/10.1371/journal.pbio.0030017

Armstrong-James, M., Fox, K., & Das-Gupta, A. (1992). Flow of excitation within rat barrel cortex on striking a single vibrissa. *Journal of Neurophysiology*, *68*(4), 1345–1358.

Aronoff, R., Matyas, F., Mateo, C., Ciron, C., Schneider, B., & Petersen, C. C. H. (2010). Long-range connectivity of mouse primary somatosensory barrel cortex. *European Journal of Neuroscience*, *31*(12), 2221–2233. https://doi.org/10.1111/j.1460-9568.2010.07264.x

Avermann, M., Tomm, C., Mateo, C., Gerstner, W., & Petersen, C. C. H. (2012). Microcircuits of excitatory and inhibitory neurons in layer 2/3 of mouse barrel cortex. *Journal of Neurophysiology*, *107*(11), 3116–3134. https://doi.org/10.1152/jn.00917.2011

Bale, M. R., Davies, K., Freeman, O. J., Ince, R. A. A., & Petersen, R. S. (2013). Low-Dimensional Sensory Feature Representation by Trigeminal Primary Afferents. *Journal of Neuroscience*,

33(29), 12003–12012. https://doi.org/10.1523/JNEUROSCI.0925-13.2013

Bale, M. R., & Maravall, M. (2018). Organization of Sensory Feature Selectivity in the Whisker System. *Neuroscience*, *368*, 70–80. https://doi.org/10.1016/j.neuroscience.2017.09.014

Bale, M. R., & Petersen, R. S. (2009). Transformation in the Neural Code for Whisker Deflection Direction Along the Lemniscal Pathway. *Journal of Neurophysiology*, *102*(5), 2771–2780. https://doi.org/10.1152/jn.00636.2009

Barth, A. L., & Poulet, J. F. A. (2012). Experimental evidence for sparse firing in the neocortex. *Trends in Neurosciences*. https://doi.org/10.1016/j.tins.2012.03.008

Beierlein, M., Gibson, J. R., & Connors, B. W. (2003). Two Dynamically Distinct Inhibitory Networks in Layer 4 of the Neocortex. *Journal of Neurophysiology*, *90*(5), 2987–3000. https://doi.org/10.1152/jn.00283.2003

Beltramo, R., D'Urso, G., Dal Maschio, M., Farisello, P., Bovetti, S., Clovis, Y., … Fellin, T. (2013). Layer-specific excitatory circuits differentially control recurrent network dynamics in the neocortex. *Nature Medicine*, *16*(2), 1–10. https://doi.org/10.1038/nn.3306

Berndt, A., Lee, S. Y., Ramakrishnan, C., & Deisseroth, K. (2014). Structure-guided transformation of channelrhodopsin into a light-activated chloride channel. *Science (New York, N.Y.)*, *344*(6182), 420–424. https://doi.org/10.1126/science.1252367

Bickford, M. E. (2016). Thalamic Circuit Diversity: Modulation of the Driver/Modulator Framework. *Frontiers in Neural Circuits*, *9*, 86. https://doi.org/10.3389/fncir.2015.00086

Blatow, M., Rozov, A., Katona, I., Hormuzdi, S. G., Meyer, A. H., Whittington, M. A., … Monyer, H. (2003). A novel network of multipolar bursting interneurons generates theta frequency oscillations in neocortex. *Neuron*, *38*(5), 805–817.

Bortone, D. S., Olsen, S. R., & Scanziani, M. (2014). Translaminar Inhibitory Cells Recruited by Layer 6 Corticothalamic Neurons Suppress Visual Cortex. *Neuron*, *82*(2), 474–485. https://doi.org/10.1016/J.NEURON.2014.02.021

Boyden, E. S. (2011). A history of optogenetics: the development of tools for controlling brain circuits with light. *F1000 Biology Reports*, *3*, 11. https://doi.org/10.3410/B3-11

Boyden, E. S., Zhang, F., Bamberg, E., Nagel, G., & Deisseroth, K. (2005). Millisecond-timescale, genetically targeted optical control of neural activity. *Nature Neuroscience*, *8*(9), 1263–1268. https://doi.org/10.1038/nn1525

Branda, C. S., & Dymecki, S. M. (2004). Talking about a revolution: The impact of site-specific recombinases on genetic analyses in mice. *Developmental Cell*, *6*(1), 7–28. https://doi.org/10.1016/S1534-5807(03)00399-X

Brecht, M., Roth, A., & Sakmann, B. (2003). Dynamic Receptive Fields of Reconstructed Pyramidal Cells in Layers 3 and 2 of Rat Somatosensory Barrel Cortex. *The Journal of Physiology*, *553*(1), 243–265. https://doi.org/10.1113/jphysiol.2003.044222

Brecht, M., & Sakmann, B. (2002). Dynamic representation of whisker deflection by synaptic potentials in spiny stellate and pyramidal cells in the barrels and septa of layer 4 rat somatosensory cortex. *The Journal of Physiology*, *543*(Pt 1), 49–70. https://doi.org/10.1113/jphysiol.2002.018465

Bruno, R. M., Khatri, V., Land, P. W., & Simons, D. J. (2003). Thalamocortical Angular Tuning Domains within Individual Barrels of Rat Somatosensory Cortex. *The Journal of Neuroscience*, *23*(29), 9565–9574. https://doi.org/10.1523/JNEUROSCI.23-29-09565.2003

Bruno, R. M., & Sakmann, B. (2006). Cortex Is Driven by Weak but Synchronously Active Thalamocortical Synapses. *Science*, *312*(5780), 1622–1627. https://doi.org/10.1126/science.1124593

Bruno, R. M., & Simons, D. J. (2002). Feedforward mechanisms of excitatory and inhibitory cortical receptive fields. *J Neurosci*, *22*(24), 10966–10975. https://doi.org/22/24/10966 [pii]

Bureau, I., Von Paul, F. Saint, & Svoboda, K. (2006). Interdigitated paralemniscal and lemniscal pathways in the mouse barrel cortex. *PLoS Biology*, *4*(12), 2361–2371. https://doi.org/10.1371/journal.pbio.0040382

Carey, L. M., Lamp, G., & Turville, M. (2016). The State-of-the-Science on Somatosensory Function and Its Impact on Daily Life in Adults and Older Adults, and Following Stroke: A Scoping Review. *OTJR : Occupation, Participation and Health*. https://doi.org/10.1177/1539449216643941

Carpenter, J. G. (1892). Mental aberration attending hypertrophic rhinitis, with sub-acute otitis media: Read in the Section of Laryngology and Otology, at the Forty-third annual meeting of the American Medical Association, held at Detroit, Mich., June, 1892. *Journal of the American Medical Association*, *XIX*(19), 539–542. https://doi.org/10.1001/jama.1892.02420190003001a

Carvell, G. E., & Simons, D. J. (1987). Thalamic and corticocortical connections of the second somatic sensory area of the mouse. *The Journal of Comparative Neurology*, *265*(3), 409–427. https://doi.org/10.1002/cne.902650309

Cauli, B., Audinat, E., Lambolez, B., Angulo, M. C., Ropert, N., Tsuzuki, K., … Rossier, J. (1997). Molecular and physiological diversity of cortical nonpyramidal cells. *The Journal of Neuroscience*, *17*(10), 3894–3906. https://doi.org/https://doi.org/10.1523/JNEUROSCI.17-10-03894.1997

Chauvette, S., Crochet, S., Volgushev, M., & Timofeev, I. (2011). Properties of Slow Oscillation during Slow-Wave Sleep and Anesthesia in Cats. *Journal of Neuroscience*, *31*(42), 14998–15008. https://doi.org/10.1523/JNEUROSCI.2339-11.2011

Chauvette, S., Volgushev, M., & Timofeev, I. (2010). Origin of active states in local neocortical networks during slow sleep oscillation. *Cerebral Cortex (New York, N.Y. : 1991)*, *20*(11), 2660–2674. https://doi.org/10.1093/cercor/bhq009

Chen, J. L., Carta, S., Soldado-Magraner, J., Schneider, B. L., & Helmchen, F. (2013). Behaviour-dependent recruitment of long-range projection neurons in somatosensory cortex. *Nature*, *499*(7458), 336–340. https://doi.org/10.1038/nature12236

Chen, J. L., Margolis, D. J., Stankov, A., Sumanovski, L. T., Schneider, B. L., & Helmchen, F. (2015). Pathway-specific reorganization of projection neurons in somatosensory cortex during learning. *Nature Neuroscience*, *18*(8), 1101–1108. https://doi.org/10.1038/nn.4046

Chen, J. L., Voigt, F. F., Javadzadeh, M., Krueppel, R., & Helmchen, F. (2016). Long-range population dynamics of anatomically defined neocortical networks. *ELife*, *5*(MAY2016), 1–26. https://doi.org/10.7554/eLife.14679

Chmielowska, J., Carvell, G. E., & Simons, D. J. (1989). Spatial organization of thalamocortical and

corticothalamic projection systems in the rat SmI barrel cortex. *The Journal of Comparative Neurology*, *285*(3), 325–338. https://doi.org/10.1002/cne.902850304

Chow, B. Y., Han, X., Bernstein, J. G., Monahan, P. E., & Boyden, E. S. (2011). Light-Activated Ion Pumps and Channels for Temporally Precise Optical Control of Activity in Genetically Targeted Neurons. In *Neuromethods* (Vol. 67, pp. 305–338). https://doi.org/10.1007/7657_2011_10

Chow, B. Y., Han, X., Dobry, A. S., Qian, X., Chuong, A. S., Li, M., … Boyden, E. S. (2010). High-performance genetically targetable optical neural silencing by light-driven proton pumps. *Nature*, *463*(7277), 98–102. https://doi.org/10.1038/nature08652

Clancy, K. B., Schnepel, P., Rao, A. T., & Feldman, D. E. (2015). Structure of a Single Whisker Representation in Layer 2 of Mouse Somatosensory Cortex. *Journal of Neuroscience*, *35*(9), 3946–3958. https://doi.org/10.1523/JNEUROSCI.3887-14.2015

Constantinople, C. M., & Bruno, R. M. (2013). Deep Cortical Layers Are Activated Directly by Thalamus. *Science*, *340*(6140), 1591–1594. https://doi.org/10.1126/science.1236425

Contreras, D., & Steriade, M. (1995). Cellular basis of EEG slow rhythms: corticothalamic relationships. *Journal of Neuroscience*, *15*(1), 604–622. https://doi.org/10.1021/jo502028g

Cosentino, C., Alberio, L., Gazzarrini, S., Aquila, M., Romano, E., Cermenati, S., … Moroni, A. (2015). Engineering of a light-gated potassium channel. *Science*, *348*(6235), 707–710. https://doi.org/10.1126/science.aaa2787

Crochet, S., Chauvette, S., Boucetta, S., & Timofeev, I. (2005). Modulation of synaptic transmission in neocortex by network activities. *European Journal of Neuroscience*, *21*(4), 1030–1044. https://doi.org/10.1111/j.1460-9568.2005.03932.x

Crochet, S., & Petersen, C. C. H. (2006). Correlating whisker behavior with membrane potential in barrel cortex of awake mice. *Nature Neuroscience*, *9*(5), 608–610. https://doi.org/10.1038/nn1690

Crochet, S., Poulet, J. F. A., Kremer, Y., & Petersen, C. C. H. (2011). Synaptic Mechanisms Underlying Sparse Coding of Active Touch. *Neuron*, *69*(6), 1160–1175. https://doi.org/10.1016/j.neuron.2011.02.022

Crunelli, V., Lörincz, M. L., Errington, A. C., & Hughes, S. W. (2012). Activity of cortical and thalamic

neurons during the slow (. *Pflugers Archiv : European Journal of Physiology*, *463*(1), 73–88. https://doi.org/10.1007/s00424-011-1011-9

Dal Maschio, M., Beltramo, R., De Stasi, A. M., & Fellin, T. (2012). Two-photon calcium imaging in the intact brain. *Advances in Experimental Medicine and Biology*, *740*, 83–102. https://doi.org/10.1007/978-94-007-2888-2_4

de Kock, C. P. J., Bruno, R. M., Spors, H., & Sakmann, B. (2007). Layer- and cell-type-specific suprathreshold stimulus representation in rat primary somatosensory cortex. *The Journal of Physiology*, *581*(1), 139–154. https://doi.org/10.1113/jphysiol.2006.124321

de Kock, C. P. J., & Sakmann, B. (2009). Spiking in primary somatosensory cortex during natural whisking in awake head-restrained rats is cell-type specific. *Proceedings of the National Academy of Sciences of the United States of America*, *106*(38), 16446–16450. https://doi.org/10.1073/pnas.0904143106

Dehay, C., & Kennedy, H. (2007). Cell-cycle control and cortical development. *Nature Reviews Neuroscience*, *8*(6), 438–450. https://doi.org/10.1038/nrn2097

Deisseroth, K., Feng, G., Majewska, A. K., Miesenbock, G., Ting, A., & Schnitzer, M. J. (2006). Next-Generation Optical Technologies for Illuminating Genetically Targeted Brain Circuits. *Journal of Neuroscience*, *26*(41), 10380–10386. https://doi.org/10.1523/JNEUROSCI.3863-06.2006

Delmas, P., Hao, J., & Rodat-Despoix, L. (2011). Molecular mechanisms of mechanotransduction in mammalian sensory neurons. *Nature Reviews Neuroscience*, *12*(3), 139–153. https://doi.org/10.1038/nrn2993

Denk, W., Strickler, J. H., Watt, ;, & Webb, W. (1990). *Two-Photon Laser Scanning Fluorescence Microscopy*. *New Series* (Vol. 248).

Denk, W., & Svoboda, K. (1997). Photon upmanship: why multiphoton imaging is more than a gimmick. *Neuron*, *18*(3), 351–357. https://doi.org/10.1016/S0896-6273(00)81237-4

Diamond, M. E., & Arabzadeh, E. (2013). Whisker sensory system – From receptor to decision. *Progress in Neurobiology*, *103*, 28–40. https://doi.org/10.1016/j.pneurobio.2012.05.013

Diamond, M. E., von Heimendahl, M., Knutsen, P. M., Kleinfeld, D., & Ahissar, E. (2008). “Where” and “what” in the whisker sensorimotor system. *Nature Reviews Neuroscience*, *9*(8), 601–

612. https://doi.org/10.1038/nrn2411

Douglas, R. J., Koch, C., Mahowald, M., Martin, K., & Suarez, H. (1995). Recurrent excitation in neocortical circuits. *Science*, *269*(5226), 981–985. https://doi.org/10.1126/science.7638624

Douglas, R. J., & Martin, K. A. C. (2004). NEURONAL CIRCUITS OF THE NEOCORTEX. *Annual Review of Neuroscience*, *27*(1), 419–451. https://doi.org/10.1146/annurev.neuro.27.070203.144152

Druga, R. (2009). Neocortical inhibitory system. *Folia Biologica*, *55*(6), 201–217.

Estebanez, L., Férézou, I., Ego-Stengel, V., & Shulz, D. E. (2018). Representation of tactile scenes in the rodent barrel cortex. *Neuroscience*. https://doi.org/10.1016/j.neuroscience.2017.08.039

Feldman, D. E., & Brecht, M. (2005). Map Plasticity in Somatosensory Cortex. *Science*, *310*(5749), 810–815. https://doi.org/10.1126/science.1115807

Feldmeyer, D. (2012). Excitatory neuronal connectivity in the barrel cortex. *Frontiers in Neuroanatomy*, *6*(July), 24. https://doi.org/10.3389/fnana.2012.00024

Feldmeyer, D., Brecht, M., Helmchen, F., Petersen, C. C. H., Poulet, J. F. A., Staiger, J. F., … Schwarz, C. (2013). Barrel cortex function. *Progress in Neurobiology*, *103*, 3–27. https://doi.org/10.1016/j.pneurobio.2012.11.002

Feldmeyer, D., Egger, V., Lübke, J., & Sakmann, B. (1999). Reliable synaptic connections between pairs of excitatory layer 4 neurones within a single “barrel” of developing rat somatosensory cortex. *Journal of Physiology*, *521*(1), 169–190. https://doi.org/10.1111/j.1469-7793.1999.00169.x

Forli, A., Vecchia, D., Binini, N., Succol, F., Bovetti, S., Moretti, C., … Fellin, T. (2018). Two-Photon Bidirectional Control and Imaging of Neuronal Excitability with High Spatial Resolution In Vivo. *Cell Reports*, *22*(11), 3087–3098. https://doi.org/10.1016/j.celrep.2018.02.063

Gentet, L. J., Avermann, M., Matyas, F., Staiger, J. F., & Petersen, C. C. H. (2010). Membrane Potential Dynamics of GABAergic Neurons in the Barrel Cortex of Behaving Mice. *Neuron*, *65*(3), 422–435. https://doi.org/10.1016/j.neuron.2010.01.006

Gentet, L. J., Kremer, Y., Taniguchi, H., Huang, Z. J., Staiger, J. F., & Petersen, C. C. H. (2012). Unique functional properties of somatostatin-expressing GABAergic neurons in mouse barrel

cortex. *Nature Neuroscience*, *15*(4), 607–612. https://doi.org/10.1038/nn.3051

Gerfen, C. R., Paletzki, R., & Heintz, N. (2013). GENSAT BAC cre-recombinase driver lines to study the functional organization of cerebral cortical and basal ganglia circuits. *Neuron*, *80*(6), 1368–1383. https://doi.org/10.1016/j.neuron.2013.10.016

Gilbert, C. D., & Wiesel, T. N. (1979). Morphology and intracortical projections of functionally characterised neurones in the cat visual cortex. *Nature*, *280*(5718), 120–125. https://doi.org/10.1038/280120a0

Glazewski, S., & Fox, K. (1996). Time course of experience-dependent synaptic potentiation and depression in barrel cortex of adolescent rats. *Journal of Neurophysiology*, *75*(4), 1714–1729. https://doi.org/10.1152/jn.1996.75.4.1714

Gong, S., Doughty, M., Harbaugh, C. R., Cummins, A., Hatten, M. E., Heintz, N., & Gerfen, C. R. (2007). Targeting Cre Recombinase to Specific Neuron Populations with Bacterial Artificial Chromosome Constructs. *Journal of Neuroscience*, *27*(37), 9817–9823. https://doi.org/10.1523/JNEUROSCI.2707-07.2007

Goodwin, A. W., & Wheat, H. E. (2008). Physiological Responses of Sensory Afferents in Glabrous and Hairy Skin of Humans and Monkeys. *The Senses: A Comprehensive Reference*, 39–54. https://doi.org/10.1016/B978-012370880-9.00344-3

Göppert-Mayer, M. (1931). Über Elementarakte mit zwei Quantensprüngen. *Annalen Der Physik*, *401*(3), 273–294. https://doi.org/10.1002/andp.19314010303

Govorunova, E. G., Sineshchekov, O. A., Janz, R., Liu, X., & Spudich, J. L. (2015). Natural light-gated anion channels: A family of microbial rhodopsins for advanced optogenetics. *Science*, *349*(6248), 647–650. https://doi.org/10.1126/science.aaa7484

Gradinaru, V., Thompson, K. R., & Deisseroth, K. (2008). eNpHR: a Natronomonas halorhodopsin enhanced for optogenetic applications. *Brain Cell Biology*, *36*(1–4), 129–139. https://doi.org/10.1007/s11068-008-9027-6

Gradinaru, V., Thompson, K. R., Zhang, F., Mogri, M., Kay, K., Schneider, M. B., & Deisseroth, K. (2007). Targeting and Readout Strategies for Fast Optical Neural Control In Vitro and In Vivo. *Journal of Neuroscience*, *27*(52), 14231–14238. https://doi.org/10.1523/JNEUROSCI.3578-

07.2007

Gradinaru, V., Zhang, F., Ramakrishnan, C., Mattis, J., Prakash, R., Diester, I., … Deisseroth, K. (2010). Molecular and cellular approaches for diversifying and extending optogenetics. *Cell*, *141*(1), 154–165. https://doi.org/10.1016/j.cell.2010.02.037

Greenberg, D. S., Houweling, A. R., & Kerr, J. N. D. (2008). Population imaging of ongoing neuronal activity in the visual cortex of awake rats. *Nature Neuroscience*, *11*(7), 749–751. https://doi.org/10.1038/nn.2140

Haider, B., Duque, A., Hasenstaub, A. R., Yu, Y., & McCormick, D. A. (2007). Enhancement of visual responsiveness by spontaneous local network activity in vivo. *Journal of Neurophysiology*, *97*(6), 4186–4202. https://doi.org/10.1152/jn.01114.2006

Han, X., Chow, B. Y., Zhou, H., Klapoetke, N. C., Chuong, A., Rajimehr, R., … Boyden, E. S. (2011). A High-Light Sensitivity Optical Neural Silencer: Development and Application to Optogenetic Control of Non-Human Primate Cortex. *Frontiers in Systems Neuroscience*, *5*, 18. https://doi.org/10.3389/fnsys.2011.00018

Hao, J., Bonnet, C., Amsalem, M., Ruel, J., & Delmas, P. (2014). Transduction and encoding sensory information by skin mechanoreceptors. *Pflugers Archiv European Journal of Physiology*. https://doi.org/10.1007/s00424-014-1651-7

Harris, J. A., Hirokawa, K. E., Sorensen, S. A., Gu, H., Mills, M., Ng, L. L., … Zeng, H. (2014). Anatomical characterization of Cre driver mice for neural circuit mapping and manipulation. *Frontiers in Neural Circuits*, *8*(July). https://doi.org/10.3389/fncir.2014.00076

Harris, K. D., & Shepherd, G. M. G. (2015, February 27). The neocortical circuit: Themes and variations. *Nature Neuroscience*. Nature Publishing Group. https://doi.org/10.1038/nn.3917

Harrison, T. C., Sigler, A., & Murphy, T. H. (2009). Simple and cost-effective hardware and software for functional brain mapping using intrinsic optical signal imaging. *Journal of Neuroscience Methods*, *182*, 211–218. https://doi.org/10.1016/j.jneumeth.2009.06.021

Häusser, M., & Margrie, T. W. (2014). Two-photon targeted patching and electroporation in vivo. *Cold Spring Harbor Protocols*, *2014*(1), 78–85. https://doi.org/10.1101/pdb.prot080143

Helmchen, F., Gilad, A., & Chen, J. L. (2018). Neocortical Dynamics During Whisker-Based Sensory

Discrimination in Head-Restrained Mice. *Neuroscience*, *368*, 57–69. https://doi.org/10.1016/j.neuroscience.2017.09.003

Holmgren, C., Harkany, T., Svennenfors, B., & Zilberter, Y. (2003). Pyramidal cell communication within local networks in layer 2/3 of rat neocortex. *The Journal of Physiology*, *551*(1), 139–153. https://doi.org/10.1113/jphysiol.2003.044784

Ito, M. (1988). Response properties and topography of vibrissa-sensitive VPM neurons in the rat. *Journal of Neurophysiology*, *60*(4), 1181–1197. https://doi.org/10.1152/jn.1988.60.4.1181

Jones, E. G., & Diamond, I. T. (1995). *The Barrel Cortex of Rodents*. (E. G. Jones & I. T. Diamond, Eds.) (Vol. 11). Boston, MA: Springer US. https://doi.org/10.1007/978-1-4757-9616-2

Jones, L. M., Depireux, D. A., Simons, D. J., & Keller, A. (2004). Robust temporal coding in the trigeminal system. *Science*, *304*(5679), 1986–1989. https://doi.org/10.1126/science.1097779

Kaiser, W., & Garrett, C. G. B. (1961). Two-Photon Excitation in CaF2: Eu2+. *Physical Review Letters*, *7*(6), 229–231. https://doi.org/10.1103/PhysRevLett.7.229

Kapfer, C., Glickfeld, L. L., Atallah, B. V, & Scanziani, M. (2007). Supralinear increase of recurrent inhibition during sparse activity in the somatosensory cortex. *Nature Neuroscience*, *10*(6), 743–753. https://doi.org/10.1038/nn1909

Kawaguchi, Y., & Kubota, Y. (1997). GABAergic cell subtypes and their synaptic connections in rat frontal cortex. *Cerebral Cortex*, *7*(6), 476–486. https://doi.org/10.1093/cercor/7.6.476

Kerr, J. N. D., de Kock, C. P. J., Greenberg, D. S., Bruno, R. M., Sakmann, B., & Helmchen, F. (2007). Spatial Organization of Neuronal Population Responses in Layer 2/3 of Rat Barrel Cortex. *Journal of Neuroscience*, *27*(48), 13316–13328. https://doi.org/10.1523/JNEUROSCI.2210-07.2007

Kim, J., Matney, C. J., Blankenship, A., Hestrin, S., & Brown, S. P. (2014). Layer 6 corticothalamic neurons activate a cortical output layer, layer 5a. *The Journal of Neuroscience : The Official Journal of the Society for Neuroscience*, *34*(29), 9656–9664. https://doi.org/10.1523/JNEUROSCI.1325-14.2014

Kitamura, K., Judkewitz, B., Kano, M., Denk, W., & Häusser, M. (2008). Targeted patch-clamp recordings and single-cell electroporation of unlabeled neurons in vivo.

https://doi.org/10.1038/NMETH1150

Knutsen, P. M., & Ahissar, E. (2009). Orthogonal coding of object location. *Trends in Neurosciences*, *32*(2), 101–109. https://doi.org/10.1016/j.tins.2008.10.002

Koelbl, C., Helmstaedter, M., Lübke, J., & Feldmeyer, D. (2015). A barrel-related interneuron in layer 4 of rat somatosensory cortex with a high intrabarrel connectivity. *Cerebral Cortex (New York, N.Y. : 1991)*, *25*(3), 713–725. https://doi.org/10.1093/cercor/bht263

Komai, S., Denk, W., Osten, P., Brecht, M., & Margrie, T. W. (2006). Two-photon targeted patching (TPTP) in vivo. *Nature Protocols*, *1*(2), 647–652. https://doi.org/10.1038/nprot.2006.100

Koralek, K. A., Jensen, K. F., & Killackey, H. P. (1988). Evidence for two complementary patterns of thalamic input to the rat somatosensory cortex. *Brain Research*, *463*(2), 346–351. https://doi.org/10.1016/0006-8993(88)90408-8

Kremer, Y., Leger, J. F., Goodman, D., Brette, R., & Bourdieu, L. (2011). Late Emergence of the Vibrissa Direction Selectivity Map in the Rat Barrel Cortex. *Journal of Neuroscience*, *31*(29), 10689–10700. https://doi.org/10.1523/JNEUROSCI.6541-10.2011

Kremers, G.-J., Gilbert, S. G., Cranfill, P. J., Davidson, M. W., & Piston, D. W. (2011). Fluorescent proteins at a glance. *Journal of Cell Science*, *124*(Pt 2), 157–160. https://doi.org/10.1242/jcs.072744

Kubota, Y., Shigematsu, N., Karube, F., Sekigawa, A., Kato, S., Yamaguchi, N., … Kawaguchi, Y. (2011). Selective Coexpression of Multiple Chemical Markers Defines Discrete Populations of Neocortical GABAergic Neurons. *Cerebral Cortex*, *21*(8), 1803–1817. https://doi.org/10.1093/cercor/bhq252

Kwegyir-Afful, E. E., Marella, S., & Simons, D. J. (2008). Response properties of mouse trigeminal ganglion neurons. *Somatosensory and Motor Research*, *25*(4), 209–221. https://doi.org/10.1080/08990220802467612

Kwon, S. E., Tsytsarev, V., Erzurumlu, R. S., & O'Connor, D. H. (2018). Organization of Orientation-Specific Whisker Deflection Responses in Layer 2/3 of Mouse Somatosensory Cortex. *Neuroscience*, *368*, 46–56. https://doi.org/10.1016/j.neuroscience.2017.07.067

Kwon, S. E., Yang, H., Minamisawa, G., & O'Connor, D. H. (2016). Sensory and decision-related

activity propagate in a cortical feedback loop during touch perception. *Nature Neuroscience*, *19*(9), 1243–1249. https://doi.org/10.1038/nn.4356

Lam, Y.-W., & Sherman, S. M. (2010). Functional organization of the somatosensory cortical layer 6 feedback to the thalamus. *Cerebral Cortex (New York, N.Y. : 1991)*, *20*(1), 13–24. https://doi.org/10.1093/cercor/bhp077

Lefort, S., Tomm, C., Floyd Sarria, J.-C., & Petersen, C. C. H. (2009). The Excitatory Neuronal Network of the C2 Barrel Column in Mouse Primary Somatosensory Cortex. *Neuron*, *61*(2), 301–316. https://doi.org/10.1016/j.neuron.2008.12.020

Lemieux, M., Chauvette, S., & Timofeev, I. (2015). Neocortical inhibitory activities and long-range afferents contribute to the synchronous onset of silent states of the neocortical slow oscillation. *Journal of Neurophysiology*, *113*(3), 768–779. https://doi.org/10.1152/jn.00858.2013

Li, L., Li, Y., Zhou, M., Tao, H. W., & Zhang, L. I. (2013). Intracortical multiplication of thalamocortical signals in mouse auditory cortex. *Nature Neuroscience*, *16*(9), 1179–1181. https://doi.org/10.1038/nn.3493

Li, Y., Ibrahim, L. A., Liu, B., Zhang, L. I., & Tao, H. W. (2013). Linear transformation of thalamocortical input by intracortical excitation. *Nature Neuroscience*, *16*(9), 1324–1330. https://doi.org/10.1038/nn.3494

Lien, A. D., & Scanziani, M. (2013). Tuned thalamic excitation is amplified by visual cortical circuits. *Nature Neuroscience*, *16*(9), 1315–1323. https://doi.org/10.1038/nn.3488

Lin, C.-S., Nicolelis, M., Schneider, J., & Chapin, J. (1990). A major direct GABAergic pathway from zona incerta to neocortex. *Science*, *248*(4962), 1553–1556. https://doi.org/10.1126/science.2360049

Lin, J. Y., Knutsen, P. M., Muller, A., Kleinfeld, D., & Tsien, R. Y. (2013). ReaChR: a red-shifted variant of channelrhodopsin enables deep transcranial optogenetic excitation. *Nature Neuroscience*, *16*(10), 1499–1508. https://doi.org/10.1038/nn.3502

Lodato, S., & Arlotta, P. (2015). Generating neuronal diversity in the mammalian cerebral cortex. *Annual Review of Cell and Developmental Biology*, *31*, 699–720.

https://doi.org/10.1146/annurev-cellbio-100814-125353

Lu, S.-M., & Lin, R. C. S. (1993). Thalamic Afferents of the Rat Barrel Cortex: A Light-and Electron-Microscopic Study Using Phaseolus vulgaris Leucoagglutinin as an Anterograde Tracer. *Somatosensory & Motor Research*, *10*(1), 1–16. https://doi.org/10.3109/08990229309028819

Lübke, J., Egger, V., Sakmann, B., & Feldmeyer, D. (2000). Columnar Organization of Dendrites and Axons of Single and Synaptically Coupled Excitatory Spiny Neurons in Layer 4 of the Rat Barrel Cortex. *The Journal of Neuroscience*, *20*(14), 5300–5311. https://doi.org/10.1523/JNEUROSCI.20-14-05300.2000

Lübke, J., & Feldmeyer, D. (2007). Excitatory signal flow and connectivity in a cortical column: Focus on barrel cortex. *Brain Structure and Function*. https://doi.org/10.1007/s00429-007-0144-2

Luczak, A., Bartho, P., Marguet, S. L., Buzsaki, G., & Harris, K. D. (2007). Sequential structure of neocortical spontaneous activity in vivo. *Proceedings of the National Academy of Sciences*, *104*(1), 347–352. https://doi.org/10.1073/pnas.0605643104

Lumpkin, E. A., & Bautista, D. M. (2005). Feeling the pressure in mammalian somatosensation. https://doi.org/10.1016/j.conb.2005.06.005

Lumpkin, E. A., Marshall, K. L., & Nelson, A. M. (2010). The cell biology of touch. *Journal of Cell Biology*. https://doi.org/10.1083/jcb.201006074

Ma, P. M. (1991). The barrelettes--architectonic vibrissal representations in the brainstem trigeminal complex of the mouse. Normal structural organization. *The Journal of Comparative Neurology*, *309*(2), 161–199. https://doi.org/10.1002/cne.903090202

Madisen, L., Zwingman, T. A., Sunkin, S. M., Oh, S. W., Zariwala, H. A., Gu, H., … Zeng, H. (2010). A robust and high-throughput Cre reporting and characterization system for the whole mouse brain. *Nature Neuroscience*, *13*(1), 133–140. https://doi.org/10.1038/nn.2467

Mahn, M., Prigge, M., Ron, S., Levy, R., & Yizhar, O. (2016). Biophysical constraints of optogenetic inhibition at presynaptic terminals. *Nature Neuroscience*, *19*(4), 1–5. https://doi.org/10.1038/nn.4266

Malina, K. C., Mohar, B., Rappaport, A. N., & Lampl, I. (2016). Local and thalamic origins of ongoing

and sensory evoked cortical. *BiorXiv*, *7*, 1–11. https://doi.org/10.1101/058727

Mao, T., Kusefoglu, D., Hooks, B. M., Huber, D., Petreanu, L., & Svoboda, K. (2011). Long-Range Neuronal Circuits Underlying the Interaction between Sensory and Motor Cortex. *Neuron*, *72*(1), 111–123. https://doi.org/10.1016/j.neuron.2011.07.029

Maravall, M., Alenda, A., Bale, M. R., & Petersen, R. S. (2013). Transformation of Adaptation and Gain Rescaling along the Whisker Sensory Pathway. *PLoS ONE*, *8*(12), e82418. https://doi.org/10.1371/journal.pone.0082418

Maravall, M., Petersen, R. S., Fairhall, A. L., Arabzadeh, E., & Diamond, M. E. (2007). Shifts in Coding Properties and Maintenance of Information Transmission during Adaptation in Barrel Cortex. *PLoS Biology*, *5*(2), e19. https://doi.org/10.1371/journal.pbio.0050019

Mardinly, A. R., Oldenburg, I. A., & Pégard, N. C. (2018). Precise multimodal optical control of neural ensemble activity. *Nature Neuroscience*. https://doi.org/10.1038/s41593-018-0139-8

Mariotti, L., Losi, G., Lia, A., Melone, M., Chiavegato, A., Gómez-Gonzalo, M., … Carmignoto, G. (2018). Interneuron-specific signaling evokes distinctive somatostatin-mediated responses in adult cortical astrocytes. *Nature Communications*, *9*(1), 82. https://doi.org/10.1038/s41467-017-02642-6

Markram, H., Toledo-Rodriguez, M., Wang, Y., Gupta, A., Silberberg, G., & Wu, C. (2004). Interneurons of the neocortical inhibitory system. *Nature Reviews Neuroscience*, *5*(10), 793–807. https://doi.org/10.1038/nrn1519

Marshall, L., Helgadóttir, H., Mölle, M., & Born, J. (2006). Boosting slow oscillations during sleep potentiates memory. *Nature*, *444*(7119), 610–613. https://doi.org/10.1038/nature05278

McLellan, M. A., Rosenthal, N. A., & Pinto, A. R. (2017). Cre-loxP-Mediated Recombination: General Principles and Experimental Considerations. *Current Protocols in Mouse Biology*, *7*(1), 1–12. https://doi.org/10.1002/cpmo.22

Mehta, S. B., Whitmer, D., Figueroa, R., Williams, B. A., & Kleinfeld, D. (2007). Active Spatial Perception in the Vibrissa Scanning Sensorimotor System. *PLoS Biology*, *5*(2), e15. https://doi.org/10.1371/journal.pbio.0050015

Meyer, H. S., Wimmer, V. C., Oberlaender, M., de Kock, C. P. J., Sakmann, B., & Helmstaedter, M.

(2010). Number and laminar distribution of neurons in a thalamocortical projection column of rat vibrissal cortex. *Cerebral Cortex (New York, N.Y. : 1991)*, *20*(10), 2277–2286. https://doi.org/10.1093/cercor/bhq067

Minamisawa, G., Kwon, S. E., Chevée, M., Brown, S. P., & O'Connor, D. H. (2018). A Non-canonical Feedback Circuit for Rapid Interactions between Somatosensory Cortices. *Cell Reports*, pp. 2718–2731. https://doi.org/10.1016/j.celrep.2018.04.115

Minnery, B. S., Bruno, R. M., & Simons, D. J. (2003). Response Transformation and Receptive-Field Synthesis in the Lemniscal Trigeminothalamic Circuit. https://doi.org/10.1152/jn.00111.2003

Moore, C. I., Carlen, M., Knoblich, U., & Cardin, J. A. (2010). Neocortical interneurons: from diversity, strength. *Cell*, *142*(2), 189–193. https://doi.org/10.1016/j.cell.2010.07.005

Nagel, G., Szellas, T., Huhn, W., Kateriya, S., Adeishvili, N., Berthold, P., … Bamberg, E. (2003). Channelrhodopsin-2, a directly light-gated cation-selective membrane channel. *Proceedings of the National Academy of Sciences of the United States of America*, *100*(24), 13940–13945. https://doi.org/10.1073/pnas.1936192100

Narayanan, R. T., Udvary, D., & Oberlaender, M. (2017). Cell Type-Specific Structural Organization of the Six Layers in Rat Barrel Cortex. *Frontiers in Neuroanatomy*, *11*(October), 1–10. https://doi.org/10.3389/fnana.2017.00091

Nikbakht, N., Tafreshiha, A., Zoccolan, D., & Diamond, M. E. (2018). Supralinear and Supramodal Integration of Visual and Tactile Signals in Rats: Psychophysics and Neuronal Mechanisms. *Neuron*, *97*(3), 626–639.e8. https://doi.org/10.1016/j.neuron.2018.01.003

O'Connor, D. H., Clack, N. G., Huber, D., Komiyama, T., Myers, E. W., & Svoboda, K. (2010). Vibrissa-Based Object Localization in Head-Fixed Mice. *Journal of Neuroscience*, *30*(5), 1947–1967. https://doi.org/10.1523/JNEUROSCI.3762-09.2010

O'Connor, D. H., Hires, S. A., Guo, Z. V., Li, N., Yu, J., Sun, Q. Q., … Svoboda, K. (2013). Neural coding during active somatosensation revealed using illusory touch. *Nature Neuroscience*, *16*(7), 958–965. https://doi.org/10.1038/nn.3419

O'Connor, D. H., Huber, D., & Svoboda, K. (2009). Reverse engineering the mouse brain. *Nature*, *461*(7266), 923–929. https://doi.org/10.1038/nature08539

O'Connor, D. H., Peron, S. P., Huber, D., & Svoboda, K. (2010). Neural Activity in Barrel Cortex Underlying Vibrissa-Based Object Localization in Mice. *Neuron*, *67*(6), 1048–1061. https://doi.org/10.1016/j.neuron.2010.08.026

Oaklander, A. L., & Siegel, S. M. (2005). Cutaneous innervation: Form and function. *Journal of the American Academy of Dermatology*. https://doi.org/10.1016/j.jaad.2005.08.049

Oberlaender, M., de Kock, C. P. J., Bruno, R. M., Ramirez, A., Meyer, H. S., Dercksen, V. J., … Sakmann, B. (2012). Cell type-specific three-dimensional structure of thalamocortical circuits in a column of rat vibrissal cortex. *Cerebral Cortex*, *22*(10), 2375–2391. https://doi.org/10.1093/cercor/bhr317

Olsen, S. R., Bortone, D. S., Adesnik, H., & Scanziani, M. (2012). Gain control by layer six in cortical circuits of vision. *Nature*, *483*(7387), 47–52. https://doi.org/10.1038/nature10835

Omerbašić, D., Schuhmacher, L.-N., Bernal Sierra, Y.-A., Smith, E. S. J., & Lewin, G. R. (2015). ASICs and mammalian mechanoreceptor function. *Neuropharmacology*, *94*, 80–86. https://doi.org/10.1016/j.neuropharm.2014.12.007

Panzeri, S., Harvey, C. D., Piasini, E., Latham, P. E., & Fellin, T. (2017). Cracking the Neural Code for Sensory Perception by Combining Statistics, Intervention, and Behavior. *Neuron*, *93*(3), 491–507. https://doi.org/10.1016/j.neuron.2016.12.036

Peron, S. P., Freeman, J., Iyer, V., Guo, C., & Svoboda, K. (2015). A Cellular Resolution Map of Barrel Cortex Activity during Tactile Behavior. *Neuron*, *86*(3), 783–799. https://doi.org/10.1016/j.neuron.2015.03.027

Petersen, C. C. H. (2003, November 1). The barrel cortex - Integrating molecular, cellular and systems physiology. *Pflugers Archiv European Journal of Physiology*. https://doi.org/10.1007/s00424-003-1167-z

Petersen, C. C. H. (2007). The Functional Organization of the Barrel Cortex. *Neuron*, *56*(2), 339–355. https://doi.org/10.1016/j.neuron.2007.09.017

Petersen, C. C. H., & Crochet, S. (2013). Synaptic Computation and Sensory Processing in Neocortical Layer 2/3. *Neuron*, *78*(1), 28–48. https://doi.org/10.1016/j.neuron.2013.03.020

Petersen, C. C. H., Hahn, T. T. G., Mehta, M., Grinvald, A., & Sakmann, B. (2003). Interaction of

sensory responses with spontaneous depolarization in layer 2/3 barrel cortex. *Proceedings of the National Academy of Sciences*, *100*(23), 13638–13643. https://doi.org/10.1073/pnas.2235811100

Petersen, R. S., Panzeri, S., & Maravall, M. (2009, June 3). Neural coding and contextual influences in the whisker system. *Biological Cybernetics*. https://doi.org/10.1007/s00422-008-0290-5

Petreanu, L., Huber, D., Sobczyk, A., & Svoboda, K. (2007). Channelrhodopsin-2–assisted circuit mapping of long-range callosal projections. *Nature Neuroscience*, *10*(5), 663–668. https://doi.org/10.1038/nn1891

Petrof, I., Viaene, A. N., & Sherman, S. M. (2015). Properties of the primary somatosensory cortex projection to the primary motor cortex in the mouse. *Journal of Neurophysiology*, *113*(7), 2400–2407. https://doi.org/10.1152/jn.00949.2014

Pierret, T., Lavallée, P., & Deschênes, M. (2000). Parallel Streams for the Relay of Vibrissal Information through Thalamic Barreloids. *Journal of Neuroscience*, *20*(19), 7455–7462. https://doi.org/10.1523/JNEUROSCI.20-19-07455.2000

Pluta, S., Naka, A., Veit, J., Telian, G., Yao, L., Hakim, R., … Adesnik, H. (2015). A direct translaminar inhibitory circuit tunes cortical output. *Nature Publishing Group*, *18*(11). https://doi.org/10.1038/nn.4123

Polack, P.-O., Friedman, J., & Golshani, P. (2013). Cellular mechanisms of brain state–dependent gain modulation in visual cortex. *Nature Neuroscience*, *16*(9), 1331–1339. https://doi.org/10.1038/nn.3464

Poulet, J. F. A., & Petersen, C. C. H. (2008). Internal brain state regulates membrane potential synchrony in barrel cortex of behaving mice. *Nature*, *454*(7206), 881–885. https://doi.org/10.1038/nature07150

Prigge, M., Schneider, F., Tsunoda, S. P., Shilyansky, C., Wietek, J., Deisseroth, K., & Hegemann, P. (2012). Color-tuned channelrhodopsins for multiwavelength optogenetics. *The Journal of Biological Chemistry*, *287*(38), 31804–31812. https://doi.org/10.1074/jbc.M112.391185

Quiquempoix, M., Fayad, S. L., Boutourlinsky, K., Leresche, N., Lambert, R. C., & Bessaih, T. (2018). Layer 2/3 Pyramidal Neurons Control the Gain of Cortical Output. *Cell Reports*, *24*(11), 2799–

2807.e4. https://doi.org/10.1016/j.celrep.2018.08.038

Radnikow, G., & Feldmeyer, D. (2018). Layer- and Cell Type-Specific Modulation of Excitatory Neuronal Activity in the Neocortex. *Frontiers in Neuroanatomy*, *12*, 1. https://doi.org/10.3389/fnana.2018.00001

Reed-Geaghan, E. G., & Maricich, S. M. (2011). Peripheral somatosensation: a touch of genetics. *Current Opinion in Genetics & Development*, *21*(3), 240–248. https://doi.org/10.1016/j.gde.2010.12.009

Reig, R., Zerlaut, Y., Vergara, R., Destexhe, A., & Sanchez-Vives, M. V. (2015). Gain Modulation of Synaptic Inputs by Network State in Auditory Cortex In Vivo. *Journal of Neuroscience*, *35*(6), 2689–2702. https://doi.org/10.1523/JNEUROSCI.2004-14.2015

Ren, J. Q., Aika, Y., Heizmann, C. W., & Kosaka, T. (1992). Quantitative analysis of neurons and glial cells in the rat somatosensory cortex, with special reference to GABAergic neurons and parvalbumin-containing neurons. *Exp Brain Res*, *92*, 1–14.

Rudy, B., Fishell, G., Lee, S. H., & Hjerling-Leffler, J. (2011). Three groups of interneurons account for nearly 100% of neocortical GABAergic neurons. *Developmental Neurobiology*, *71*(1), 45–61. https://doi.org/10.1002/dneu.20853

Sachdev, R. N. S., Ebner, F. F., & Wilson, C. J. (2004). Effect of Subthreshold Up and Down States on the Whisker-Evoked Response in Somatosensory Cortex. *J Neurophysiol*, *92*, 3511–3521. https://doi.org/10.1152/jn.00347.2004

Sachidhanandam, S., Sreenivasan, V., Kyriakatos, A., Kremer, Y., & Petersen, C. C. H. (2013). Membrane potential correlates of sensory perception in mouse barrel cortex. *Nature Neuroscience*, *16*(11), 1671–1677. https://doi.org/10.1038/nn.3532

Saito, T., & Nakatsuji, N. (2001). Efficient Gene Transfer into the Embryonic Mouse Brain Using in Vivo Electroporation. *Developmental Biology*, *240*(1), 237–246. https://doi.org/10.1006/dbio.2001.0439

Saleem, A. ., Chadderton, P., Apergis-Schoute, J., Harris, K. D., & Schultz, S. R. (2010). Methods for predicting cortical UP and DOWN states from the phase of deep layer local field potentials. *Journal of Computational Neuroscience*, *29*(1–2), 49–62. https://doi.org/10.1007/s10827-010-

0228-5

Sanchez-Vives, M. V., & McCormick, D. A. (2000). Cellular and network mechanisms of rhythmic recurrent activity in neocortex. *Nature Neuroscience*, *3*(10), 1027–1034. https://doi.org/10.1038/79848

Sato, T. R., Gray, N. W., Mainen, Z. F., & Svoboda, K. (2007). The Functional Microarchitecture of the Mouse Barrel Cortex. *PLoS Biology*, *5*(7), e189. https://doi.org/10.1371/journal.pbio.0050189

Sato, T. R., & Svoboda, K. (2010). The Functional Properties of Barrel Cortex Neurons Projecting to the Primary Motor Cortex. *Journal of Neuroscience*, *30*(12), 4256–4260. https://doi.org/10.1523/JNEUROSCI.3774-09.2010

Schubert, D., Kötter, R., Zilles, K., Luhmann, H. J., & Staiger, J. F. (2003). Cell type-specific circuits of cortical layer IV spiny neurons. *J Neuroscience*, *23*(7), 2961–2970. https://doi.org/23/7/2961 [pii]

Sehara, K., & Kawasaki, H. (2011). Neuronal Circuits with Whisker-Related Patterns. *Molecular Neurobiology*, *43*(3), 155–162. https://doi.org/10.1007/s12035-011-8170-8

Sermet, B. S., Mayrhofer, J., Auffret, M., Oram, T., Yizhar, O., & Petersen, C. C. H. (2018). Layer, cell-type and pathway-specific thalamocortical input to mouse primary somatosensory barrel cortex.

Sessolo, M., Marcon, I., Bovetti, S., Losi, G., Cammarota, M., Ratto, G. M., … Carmignoto, G. (2015). Parvalbumin-Positive Inhibitory Interneurons Oppose Propagation But Favor Generation of Focal Epileptiform Activity. *Journal of Neuroscience*, *35*(26), 9544–9557. https://doi.org/10.1523/JNEUROSCI.5117-14.2015

Shepherd, G. M. G. (2005). Laminar and Columnar Organization of Ascending Excitatory Projections to Layer 2/3 Pyramidal Neurons in Rat Barrel Cortex. *Journal of Neuroscience*, *25*(24), 5670–5679. https://doi.org/10.1523/JNEUROSCI.1173-05.2005

Shepherd, G. M. G., Stepanyants, A., Bureau, I., Chklovskii, D., & Svoboda, K. (2005). Geometric and functional organization of cortical circuits. *Nature Neuroscience*, *8*(6), 782–790. https://doi.org/10.1038/nn1447

Sheroziya, M., & Timofeev, I. (2014). Global Intracellular Slow-Wave Dynamics of the Thalamocortical System. *Journal of Neuroscience*, *34*(26), 8875–8893. https://doi.org/10.1523/JNEUROSCI.4460-13.2014

Shipley, M. (1974). Response characteristics of single units in the rat's trigeminal nuclei to vibrissa displacements. *Journal of Neurophysiology*, *37*(1), 73–90.

Shoykhet, M., Doherty, D., & Simons, D. J. (2000). Coding of deflection velocity and amplitude by whisker primary afferent neurons: implications for higher level processing. *Somatosensory & Motor Research*, *17*(2), 171–180. https://doi.org/10.1080/08990220050020580

Simons, D. J. (1978). Response properties of vibrissa units in rat SI somatosensory neocortex. *Journal of Neurophysiology*, *41*(3), 798–820. https://doi.org/10.1152/jn.1978.41.3.798

Simons, D. J., & Carvell, G. E. (1989a). Thalamocortical response transformation in the rat vibrissa/barrel system. *Journal of Neurophysiology*, *61*(2), 311–330. https://doi.org/10.1152/jn.1989.61.2.311

Simons, D. J., & Carvell, G. E. (1989b). Thalamocortical response transformation in the rat vibrissa/barrel system. *Journal of Neurophysiology*, *61*(2), 311–330. https://doi.org/10.1152/jn.1989.61.2.311

Slezia, A., Hangya, B., Ulbert, I., & Acsady, L. (2011). Phase Advancement and Nucleus-Specific Timing of Thalamocortical Activity during Slow Cortical Oscillation. *Journal of Neuroscience*, *31*(2), 607–617. https://doi.org/10.1523/JNEUROSCI.3375-10.2011

Steriade, M., Contreras, D., Curro Dossi, R., & Nunez, A. (1993). The slow (< 1 Hz) oscillation in reticular thalamic and thalamocortical neurons: scenario of sleep rhythm generation in interacting thalamic and neocortical networks. *The Journal of Neuroscience*, *13*(8), 3284–3299. https://doi.org/10.1523/JNEUROSCI.13-08-03284.1993

Steriade, M., Nunez, A., & Amzica, F. (1993a). A novel slow (< 1 Hz) oscillation of neocortical neurons in vivo: depolarizing and hyperpolarizing components. *The Journal of Neuroscience*, *13*(8), 3252–3265. https://doi.org/https://doi.org/10.1523/JNEUROSCI.13-08-03252.1993

Steriade, M., Nunez, A., & Amzica, F. (1993b). Intracellular analysis of relations between the slow (< 1 Hz) neocortical oscillation and other sleep rhythms of the electroencephalogram. *The*

Journal of Neuroscience, *13*(8), 3266–3283. https://doi.org/https://doi.org/10.1523/JNEUROSCI.13-08-03266.1993

Steriade, M., Timofeev, I., & Grenier, F. (2001). Natural waking and sleep states: a view from inside neocortical neurons. *Journal of Neurophysiology*, *85*(5), 1969–1985. https://doi.org/10.1016/j.neuroimage.2009.03.074

Stuttgen, M. C., Ruter, J., & Schwarz, C. (2006). Two Psychophysical Channels of Whisker Deflection in Rats Align with Two Neuronal Classes of Primary Afferents. *Journal of Neuroscience*, *26*(30), 7933–7941. https://doi.org/10.1523/JNEUROSCI.1864-06.2006

Suter, B. A., & Shepherd, G. M. G. (2015). Reciprocal Interareal Connections to Corticospinal Neurons in Mouse M1 and S2. *Journal of Neuroscience*, *35*(7), 2959–2974. https://doi.org/10.1523/JNEUROSCI.4287-14.2015

Svoboda, K., & Yasuda, R. (2006). Principles of Two-Photon Excitation Microscopy and Its Applications to Neuroscience. *Neuron*, *50*(6), 823–839. https://doi.org/10.1016/j.neuron.2006.05.019

Taniguchi, H., He, M., Wu, P., Kim, S., Paik, R., Sugino, K., … Huang, Z. J. (2011). A Resource of Cre Driver Lines for Genetic Targeting of GABAergic Neurons in Cerebral Cortex. *Neuron*, *71*(6), 995–1013. https://doi.org/10.1016/j.neuron.2011.07.026

Tao, C., Zhang, G., Xiong, Y., & Zhou, Y. (2015). Functional dissection of synaptic circuits: in vivo patch-clamp recording in neuroscience. *Frontiers in Neural Circuits*, *9*, 23. https://doi.org/10.3389/fncir.2015.00023

Taylor, S., McLean, B., Falkmer, T., Carey, L., Girdler, S., Elliott, C., & Blair, E. (2016). Does somatosensation change with age in children and adolescents? A systematic review. *Child: Care, Health and Development*, *42*(6), 809–824. https://doi.org/10.1111/cch.12375

Temereanca, S., & Simons, D. J. (2003). Local field potentials and the encoding of whisker deflections by population firing synchrony in thalamic barreloids. *Journal of Neurophysiology*, *89*(4), 2137–2145. https://doi.org/10.1152/jn.00582.2002

Timofeev, I., Grenier, F., Bazhenov, M., Sejnowski, T. J., & Steriade, M. (2000). Origin of slow cortical oscillations in deafferented cortical slabs. *Cerebral Cortex (New York, N.Y. : 1991)*,

10(12), 1185–1199.

Timofeev, I., Grenier, F., & Steriade, M. (2001). Disfacilitation and active inhibition in the neocortex during the natural sleep-wake cycle: An intracellular study. *Proceedings of the National Academy of Sciences*, *98*(4), 1924–1929. https://doi.org/10.1073/pnas.98.4.1924

Timofeeva, E., Mérette, C., Émond, C., Lavallée, P., & Deschênes, M. (2003). A Map of Angular Tuning Preference in Thalamic Barreloids. *The Journal of Neuroscience*, *23*(33), 10717–10723. https://doi.org/10.1523/JNEUROSCI.23-33-10717.2003

Vaziri, A., & Emiliani, V. (2012). Reshaping the optical dimension in optogenetics. *Current Opinion in Neurobiology*, *22*(1), 128–137. https://doi.org/10.1016/J.CONB.2011.11.011

Veinante, P., & Deschênes, M. (1999). Single- and multi-whisker channels in the ascending projections from the principal trigeminal nucleus in the rat. *The Journal of Neuroscience*, *19*(12), 5085–5095.

Waterston, R. H., Lindblad-Toh, K., Birney, E., Rogers, J., Abril, J. F., Agarwal, P., … Lander, E. S. (2002). Initial sequencing and comparative analysis of the mouse genome. *Nature*, *420*(6915), 520–562. https://doi.org/10.1038/nature01262

Welker, E., & Van der Loos, H. (1986). Quantitative correlation between barrel-field size and the sensory innervation of the whiskerpad: a comparative study in six strains of mice bred for different patterns of mystacial vibrissae. *The Journal of Neuroscience*, *6*(11), 3355–3373. https://doi.org/https://doi.org/10.1523/JNEUROSCI.06-11-03355.1986

Wietek, J., Wiegert, J. S., Adeishvili, N., Schneider, F., Watanabe, H., Tsunoda, S. P., … Hegemann, P. (2014). Conversion of Channelrhodopsin into a Light-Gated Chloride Channel. *Science*, *344*(6182), 409–412. https://doi.org/10.1126/science.1249375

Wilent, W. B., & Contreras, D. (2005). Dynamics of excitation and inhibition underlying stimulus selectivity in rat somatosensory cortex. *Nature Neuroscience*, *8*(10), 1364–1370. https://doi.org/10.1038/nn1545

Woolsey, T. A., & Van der Loos, H. (1970). The structural organization of layer IV in the somatosensory region (S I) of mouse cerebral cortex. The description of a cortical field composed of discrete cytoarchitectonic units. *Brain Research*, *17*(2), 205–242.

https://doi.org/10.1016/0006-8993(70)90079-X

Xu, H., Jeong, H. Y., Tremblay, R., & Rudy, B. (2013). Neocortical Somatostatin-Expressing GABAergic Interneurons Disinhibit the Thalamorecipient Layer 4. *Neuron*, *77*(1), 155–167. https://doi.org/10.1016/j.neuron.2012.11.004

Yamashita, T., Pala, A., Pedrido, L., Kremer, Y., Welker, E., & Petersen, C. C. H. (2013). Membrane potential dynamics of neocortical projection neurons driving target-specific signals. *Neuron*, *80*(6), 1477–1490. https://doi.org/10.1016/j.neuron.2013.10.059

Yizhar, O., Fenno, L. E., Davidson, T. J., Mogri, M., & Deisseroth, K. (2011). Optogenetics in Neural Systems. *Neuron*, *71*(1), 9–34. https://doi.org/10.1016/j.neuron.2011.06.004

Yu, J., Gutnisky, D. A., Hires, S. A., & Svoboda, K. (2016). Layer 4 fast-spiking interneurons filter thalamocortical signals during active somatosensation. *Nature Neuroscience*, *19*(October), 1–14. https://doi.org/10.1038/nn.4412

Yuste, R., & Simons, D. J. (1997). Barrels in the desert: The Sde Boker workshop on neocortical circuits. In *Neuron* (Vol. 19, pp. 231–237). Cell Press. https://doi.org/10.1016/S0896-6273(00)80935-6

Zhang, F., Gradinaru, V., Adamantidis, A. R., Durand, R., Airan, R. D., de Lecea, L., & Deisseroth, K. (2010). Optogenetic interrogation of neural circuits: technology for probing mammalian brain structures. *Nature Protocols*, *5*(3), 439–456. https://doi.org/10.1038/nprot.2009.226

Zhang, F., Prigge, M., Beyrière, F., Tsunoda, S. P., Mattis, J., Yizhar, O., … Deisseroth, K. (2008). Red-shifted optogenetic excitation: a tool for fast neural control derived from Volvox carteri. *Nature Neuroscience*, *11*(6), 631–633. https://doi.org/10.1038/nn.2120

Zhang, F., Vierock, J., Yizhar, O., Fenno, L. E., Tsunoda, S., Kianianmomeni, A., … Deisseroth, K. (2011). The microbial opsin family of optogenetic tools. *Cell*, *147*(7), 1446–1457. https://doi.org/10.1016/j.cell.2011.12.004

Zhang, F., Wang, L.-P., Boyden, E. S., & Deisseroth, K. (2006). Channelrhodopsin-2 and optical control of excitable cells. *Nature Methods*, *3*(10), 785–792. https://doi.org/10.1038/nmeth936

Zhang, F., Wang, L. P., Brauner, M., Liewald, J. F., Kay, K., Watzke, N., … Deisseroth, K. (2007).

Multimodal fast optical interrogation of neural circuitry. *Nature*, *446*(7136), 633–639. https://doi.org/10.1038/nature05744

Zhu, P., Fajardo, O., Shum, J., Zhang Schärer, Y.-P., & Friedrich, R. W. (2012). High-resolution optical control of spatiotemporal neuronal activity patterns in zebrafish using a digital micromirror device. *Nature Protocols*, *7*(7), 1410–1425. https://doi.org/10.1038/nprot.2012.072

Zucca, S., D'Urso, G., Pasquale, V., Vecchia, D., Pica, G., Bovetti, S., … Fellin, T. (2017). An inhibitory gate for state transition in cortex. *ELife*, *6*, e26177. https://doi.org/10.7554/eLife.26177.001

Zucker, E., & Welker, W. I. (1969). Coding of somatic sensory input by vibrissae neurons in the rat's trigeminal ganglion. *Brain Research*, *12*(1), 138–156. https://doi.org/10.1016/0006-8993(69)90061-4

Zuo, Y., Safaai, H., Notaro, G., Mazzoni, A., Panzeri, S., & Diamond, M. E. (2015). Complementary Contributions of Spike Timing and Spike Rate to Perceptual Decisions in Rat S1 and S2 Cortex. *Current Biology*, *25*(3), 357–363. https://doi.org/10.1016/J.CUB.2014.11.065

7 Acknowledgments

Firstly, I would like to thank my mentor Tommaso Fellin, who entrusted me and believed on me throughout the years. Tommaso gave me the opportunity to pursue my passions in a stimulating and interdisciplinary environment. He improved my critical thinking and scientific vision both technically and theoretically. I am heartily grateful to Tommaso for the role he had and still has in my personal and academic growth. Secondly, I have found in Tommaso's group both a competent team and a supportive family. I would like to thank them all not only for the formative discussions and their help, but also for the time we shared in working and non-working hours. In particular, I would like to express my gratitude to Stefano Zucca and Angelo Forli for "introducing" me to electrophysiology and for their contribution to the project that became the subject of my thesis. Dania Vecchia deserves a special mention: in addition to her critical reading of this thesis, she has been supporting and helping me on a daily basis since the start of my PhD. Finally, I would like to thank my family and my girlfriend for the support during all these years.